INVESTIGATIONS ON THE KINETICS OF REDUCTION OF FERRIC OXIDE WITH GRAPHITE

A Thesis Submitted
In Partial Fulfilment of the Requirements
for the Degree of
DOCTOR OF PHILOSOPHY

By
MANAYATHE CHACKO ABRAHAM

to the

DEPARTMENT OF METALLURGICAL ENGINEERING
INDIAN INSTITUTE OF TECHNOLOGY KANPUR
OCTOBER, 1976

ME-1976-D-ABR-INV

CERTIFICATE

Certified that this work on "Investigations on the Kinetics of Reduction of Ferric Oxide With Graphite" has been carried out under my supervision and that it has not been submitted elsewhere for a degree.

A Ghosh

(A. Ghosh)
Professor
Department of Metallurgical Engineeri
Indian Institute of Technology,
Kanpur.

ACKNOWLEDGEMENTS

The author is thankful to Professor A. Ghosh for suggesting the problem, inspiring guidance and the valuable discussions he had with him.

He is thankful to Professor K.P. Gupta, Dr. H.S. Ray, Dr. T.A. Ramanarayanan, Professor E.C. Subbarao and Professor A.K. Biswas for providing with some of the materials and equipments.

The author wishes to acknowledge the help received from Mr. V.P. Gupta and Mr. Rajani in the fabrication of the apparatus.

The help and cooperation received from Messrs B. Sharma, V.N. Sharma, R.K. Prasad, K.P. Mukherji, Vishwanath Singh, A. Sharma, Ram Avtar and other members of the staff are sincerely acknowledged.

He is thankful to the B.A.R.C., Bombay for analysing the graphite ash sample.

The author wishes to express his thanks for the help received from Mr. D.P. Mazumdar, Dr. S.P. Mehrotra and Mr. N.B. Ballal in connection with the computer work.

The sincere help of Mr. M. Kuriakose during the calculations and Mr. S. Bhattacharya and Mr. R.K. Das in doing part of the proof reading are acknowledged.

The author is thankful to Mrs. Sally Abraham for rewriting part of the manuscript.

It is a pleasure to acknowledge the patient and excellent typing of Mr. R.N. Srivastava.

He wishes to thank Mr. A. Ganguli for doing the tracing.

The author is thankful to the Principal and the authorities of Regional Engineering College, Durgapur for sponsoring him under the Quality Improvement Programme and the Ministry of Education, Government of India for awarding the fellowship. He is thankful to Professor S.C. Das Gupta and his colleagues in the Department of Metallurgical Engineering, Regional Engineering College, Durgapur for willing to release him for the completion of the work.

The goodwill, inspiration and help of many friends and relatives whose names are not included here were a great asset in completing the work.

He is grateful to Jesus who was a constant source of strength.

CONTENTS

LIST OF TABLES

LIST OF FIGURES

LIST OF SYMBOLS

A = Capillary constant

C = Concentration, gm.moles/cc

d = Internal diameter of alumina crucible, cm.

d_p = Diameter of pellet, cm.

D = Diffusivity, $cm^2/sec.$

D_e = Effective diffusivity, $cm^2/sec.$

E = EMF, volts

f = Fractional reduction

F = Faraday's number = 23,060

$\dot{F}$ = Normalised rate of reaction, sec^{-1}

ΔG^o = Standard free energy of reaction, cals/gm. mole

Δh = Difference in the levels of flowmeter fluid, cm.

I_2, I_3 = Ratios of reaction rate constants

J_{iz} = Flux of the i^{th} species in the z direction, $gm.moles/sec.cm^2$

k = Rate constant

k_i = Intrinsic rate constant for gasification reaction, gm-mole/gm-c.min.

K_e = Equilibrium constant

l = Distance of separation between oxide pellet and graphite powder, cm

L = Thickness of oxide pellet, cm.

M = Molecular weight, gms/mole

$\dot{n}$ = Rate of reaction, moles/sec.

p_{CO}, p_{CO_2} = Partial pressure of CO and CO_2 respectively, atm.

P = Total pressure, atm.

$\dot{Q}$ = Volumetric flow rate, cc/sec.

r_p = Partial reaction rate per unit mass of oxide, gm.mole O/sec. (gm. of oxide)

r_S = Rate of reaction at the surface, gm.mole O/sec. (gm. of oxide)

R = Universal gas constant, cc.atm./gm.mole °K or cals/gm.moles °K

t = Time, sec.

T = Temperature, °K

V = Volume, cc.

W = Weight, gm.

$\dot{W}$ = Rate of change of mass, gm/sec.

W = Cumulative weight loss, gm.

X_i = Mole fraction of species i

Greek Symbols

γ = Ratio of rate at any stage to rate at the steady state

ε = Porosity of the reacting bed

η = Effectiveness factor

μ = Viscosity, poise

ν = Stoichiometric coefficient

ρ = Density, gm/cc.

τ = Tortuosity factor

ϕ = Rate parameter

ϕ_L = Dimensionless modulus

σ = Lennard Jones parameter, Angstrom

Ω = Dimensionless function of the temperature and of the intermolecular potential field

Subscript

c = Carbon

Expt. = Experimental

Calc. = Calculated

o = Oxygen

S = Surface

Superscript

e = Equilibrium

ex = Exit

1 = Graphite surface

o = Oxide surface

SYNOPSIS

INVESTIGATIONS ON THE KINETICS OF REDUCTION
OF FERRIC OXIDE WITH GRAPHITE
A Thesis Submitted
In Partial Fulfilment of the Requirements
for the Degree of
DOCTOR OF PHILOSOPHY
by
MANAYATHE CHACKO ABRAHAM
to the
Department of Metallurgical Engineering
Indian Institute of Technology, Kanpur
October 1976

Reduction of iron oxides and ores by carbon is a key metallurgical reaction. The principal reaction in the rotary kiln process is reduction of iron oxide by carbon. Direct reduction of iron oxide by carbon is of interest also in the iron making in blast furnaces and electric smelting furnaces. Therefore an understanding of the kinetics and mechanism of reduction of iron oxides by carbon is important. The present thesis is concerned with it. Conditions prevailing in the rotary kiln process of sponge iron making have been kept in mind in the formulation of the problem, because it is being considered as one of the important processes in India.

Theoretical considerations and experimental findings point out that reduction of iron oxides and ores by carbon proceed via the gas phase, wherever the latter is

present. The overall reaction is a coupling of the following two component reactions, viz.

Gasification of carbon: $C(s) + CO_2(g) = 2CO(g)$

and reduction of iron oxides:

$$mFe_xO_y(s) + CO(g) = nFe_zO_w(s) + CO_2(g)$$

Most of the studies on the rate and mechanism of reduction have been done with powder mixtures of iron oxide/ore and carbon/coke. They have found that the gasification reaction is controlling the rate of the overall process. Some investigators have also pointed out that the reduction takes place in stages (i.e. $Fe_2O_3 \rightarrow Fe_3O_4 \rightarrow Fe_xO \rightarrow Fe$). They observed a marked increase in the rate of reduction in the last stage and attributed this to the catalysing effect of reduced iron on the gasification reaction. However in the rotary kiln process of sponge iron making the ore is in the form of pellet or lump, the reductants are comparatively finer and the packing is loose. This assemblage differs appreciably from the compact mixture of powders studied so far in the laboratories by other investigators.

The present work is a fundamental study but directed towards better understanding of the rotary kiln process of sponge iron making. It was thus decided to separate the two reactants viz. iron oxide and carbon as well as to take

the oxide in the form of pellet. The principal series of investigation was concerned with reaction of Fe_2O_3 pellets primarily porous and some dense with electrode graphite powder. Graphite powders were kept in an alumina crucible on top of which rested the pellet with a hole at the centre. The hole at the centre through which a 0.75 mm i.d. alumina tube was introduced was the only outlet for the product gases of reaction. The pellet and the graphite were sealed from all sides except the surfaces facing each other. Temperature of reaction was varied from 870°C to 1007°C and distance of separation between pellet and graphite varied from 0.0 to 1.6 cm.

The product gas ($CO + CO_2$) was continuously monitored in-situ with the help of a calcia-stabilized zirconia EMF cell. Rate of evolution of product gas was measured with a precision capillary flowmeter. A computer programme was made to calculate instantaneous carbon and oxygen loss rates, gas composition and cumulative carbon and oxygen losses at intervals of time. The agreement of the final cumulative carbon and oxygen losses respectively with weight losses of graphite and the oxide, measured at the end of the experiment was within 5 to 10 pct. This is considered as quite satisfactory.

Auxilliary investigations were carried out to verify the literature findings as well as to help in the interpretation of the main results. -325 mesh size particles of ferric oxide were mixed with -200 + 230 mesh graphite particles and reaction rates were studied with pressing and without pressing. Experiments with mixtures of micro-pellets of oxide and graphite powder were also carried out. The reactivity of graphite powder was estimated in CO_2 and in mixtures of CO and CO_2. Finally the partially reduced pellets were examined to identify the different phases present. This indicated porous pellet type reduction.

Variation of gas composition with progress of reduction indicated stagewise reduction. The instantaneous rate versus percent reduction curves were divided into four regions for the sake of explanation. Region III was a steady state one corresponding to $Fe_xO \rightarrow Fe$ reduction. Experimental results were interpreted mainly with the help of this region.

Activation energy for the overall reaction was found to be 75 kcal/mole. This indicated that the reaction was controlled by the gasification of carbon. High activation energy also confirmed the absence of catalysis. The distance of separation between the two reactants was found to have influence on the rate in region III. As the reactants were brought nearer the rate increased.

Theoretical analysis were carried out for mass transfer in the oxide pellet, in the graphite bed and in the intervening gas space. The difference in the composition of gas across the gas space was found to be about 8 percent when the distance of separation between the surfaces of oxide pellet and the graphite layer was 1.6 cm. This indicated that transfer of CO molecules from the graphite surface to the pellet surface and transfer of CO_2 in the opposite direction were also partially controlling the rate of reaction. The increase of rate with decrease in the distance of separation between the oxide pellet and the graphite bed could thus be explained.

Mass transfer of CO and CO_2 inside the porous oxide pellet is an example of mass transfer in porous solid accompanied by chemical reaction in the pores. The chemical reaction, viz.

$$Fe_xO + CO = xFe + CO_2$$

was assumed as a first order reversible one and the empirical rate equation obtained by Bicknese and Clarke for reduction of fine particles of wustite was employed in order to calculate the effectiveness factor (η). Making a few assumptions, the exit gas compositions could be calculated. These agreed well with the experimentally determined values. It was found that mass transfer in the pellet also partially controlled the rate.

Mass transfer inside the bed of graphite also comes under the category of mass transfer inside porous solid accompanied by chemical reaction. However, in contrast with the reduction of iron oxide, the gasification reaction obeys Langmuir-Hinshelwood rate equation. Following the procedure of Roberts and Satterfield, effectiveness factors (η) were calculated. Calculations are not reliable because they are very sensitive to certain parameters whose values are not known accurately. Values of η were found to be less than one indicating also partial rate control by mass transfer inside the graphite layer. However the values of η are approximately the same at various temperatures. Therefore partial control by mass transfer did not lower the value of activation energy obtained at the steady state significantly.

The instantaneous rate versus percent reduction curves showed a sharp peak at about 20 percent reduction followed by a steady state after about 30 percent reduction. The shape was qualitatively explained by variation of rate of gasification with change in CO/CO_2 ratio. Extrapolation formulae from literature were employed for this purpose. One of the equation used for extrapolation was given by Rao et al and some others and is as follows.

$$\text{Rate of gasification} = \frac{I_3 k_i p_{CO_2}}{1 + I_2 p_{CO} + I_3 p_{CO_2}} \quad , \quad sec^{-1}$$

k_i = Intrinsic rate constant, gm.mole/gm.sec.

I_2 and I_3 are ratios of rate constants. The values of k_i, I_2 and I_3 were obtained from literature for a particular temperature.

The other extrapolation formulae was taken from Turkdogan et al and is given below

$$\text{Rate} = \frac{\phi_1 [(p_{CO_2}) - (p^e_{CO_2})]}{(1 + p_{CO}/\phi_{CO})\, 60} \quad , \quad \text{sec}^{-1}$$

ϕ_1 and ϕ_{CO} are rate parameters dependent on temperature only. The values of ϕ_1 and ϕ_{CO} were calculated for charcoal, metallurgical coke and graphite using values given in literature.

There was quantitative disagreement between the experimental rates and calculated rates of gasification. The reason for the same seems to be primarily due to the errors in extrapolation of reactivity data in pure CO_2 to that in a CO-rich gas.

Experiments with dense pellets exhibited a lower rate of reaction. This is presumably due to a greater mass transfer resistance inside the oxide pellet. The investigations on mixtures of iron oxide powder and graphite powder exhibited two peaks. The second peak corresponded to $Fe_xO \longrightarrow Fe$ stage of reduction. This observation is in agreement with literature findings. The rate in this stage was an order of magnitude greater than that for the

pellet-graphite system. Comparison of rate obtained with powder mixture, oxide micro-pellet-graphite powder mixture and oxide pellet-graphite powder in separation showed that the rate in the second stage (region III) increased with increasing contact between the reactants. This may be attributed to catalysis by reduced iron as well as less mass transfer resistance. However it seems that the volume of the gas space has an effect on rate in the first stage of reduction. If the volume was more the rate in this stage was also found to be more. No explanation could be found for this.

On the basis of the various findings of this investigation as well as informations available on the fundamentals of reduction of iron oxides by carbon, certain qualitative predictions have been made about the rate and mechanism of reduction in the rotary kiln process of sponge iron making.

CHAPTER 1

INTRODUCTION

Reduction of iron oxides and ores by carbon is a key metallurgical reaction. It was postulated in the nineteenth century that both indirect and direct reductions were taking place inside an iron blast furnace. The former was meant to denote reduction by carbon monoxide, and the latter stood for reduction of iron oxides directly by carbon as follows,

$$FeO + C = Fe + CO \qquad (1-1)$$

taking place principally in the lower portion of the stack.

Blast furnaces produce liquid impure iron and is the principal iron making apparatus. However, 'sponge iron' is becoming increasingly popular now. All countries are setting up sponge iron plants, and India is no exception.

Sponge iron is the porous metallic iron obtained by reduction of iron ore in the solid state. The metallization is usually 85-95%. The reasons behind the growing popularity of sponge iron are several.[1] The important ones are listed below.

(1) Blast furnace operates on coke made from coking coal. Shortage of coking coal is a World wide phenomena. In India the reserves are limited to about

4600 m.t.[2]. Sponge-iron can be made using other types of reductants.

(2) High capital cost and long gestation period of integrated iron and steel plants led to licensing and setting up of mini steel plants, which use electric arc furnaces. Shortage of scrap for electric-arc steelmaking is visualised. Sponge-iron can be used as a substitute for scrap. This will make the mini steel plants less dependent on scrap.

(3) Sponge-iron - electric arc route of steelmaking is cheaper than Blast Furnace - Basic Oxygen Furnace route at smaller plant size.[3]

(4) Coking coal availability is localized. Ironmaking can be dispersed only by going for sponge iron.

India is rich in non-coking coal. Petroleum and natural gas resources in the country are extremely limited. Thus the choice is to go for a technology of sponge iron-making based on non-coking coal. This can be achieved in two ways.

(1) One possibility is to gasify the coal and use the gas for reduction. This may become costly as the process involves two steps.

(2) The other alternative is to employ coal directly as a solid reductant.

Realizing the importance of sponge iron, the National Metallurgical Laboratory set up pilot plant of the

rotary kiln process which uses solid reductant directly. The rotary kiln process can take in all kinds of coal breeze that would be available at the mine site at throw away price giving enormous cost advantage.

The trials at the National Metallurgical Laboratory[4] with a 0.9 meter diameter and 10.7 meter long rotary kiln using high grade iron ores and pellets and non-coking coal has shown promising results. A degree of metallization higher than 90% could be achieved by them. They could use green pellets and the report shows that the pellets did not suffer degradation during reduction. The fuel oil input for maintaining the kiln temperature could be entirely curtailed by proper operational techniques such as coal throwing from the discharge end.

The Indian Iron and Steel Company, Burnpur, has developed and patented[5] a process of making sponge iron in a rotary kiln. In this process 12 mm iron ore fines are reduced in a rotary kiln using low grade non-metallurgical coals or coke breeze as a reductant. Trials made with a 0.6 m dia,8 m. long rotary kiln has shown that over 90% metallization with about 95% iron recovery could be obtained.

The National Committee of Science and Technology has recommended research and development work on a large scale on sponge iron making using indigeneous non-coking coals.[6] They also emphasized the rotary kiln process primarily and have recommended setting up of semi-commercial

units of 200-300 tons per day capacity. To author's knowledge[7], a few semi-commercial rotary kiln units for sponge iron manufacture are being set up in India now.

The principal reaction in the rotary kiln process is reduction of iron oxide by carbon. As mentioned earlier, the direct reduction of iron oxide by carbon is of interest in the blast furnace method also. Therefore an understanding of the kinetics and mechanism of the reduction of iron oxides by carbon is important. The present thesis is concerned with it. Conditions prevailing in rotary kiln have been kept in mind in the formulation of the problem.

Some work on the rate and mechanism of reduction have been done with compacted powder mixtures of iron oxide and carbon.[8] However the ore is in the form of pellet or lump in a rotary kiln and the packing is loose. Moreover, reduced iron in contact with carbon seems to have a catalyzing effect on the reaction. This complicated the interpretation of results on powder mixture. It can be avoided only by experimenting on iron oxide and carbon in separation. No useful information is available in the literature regarding the effect of distance of separation between oxide and carbon on the kinetics of reduction.

It was thus decided that the two reactants viz., iron oxide and carbon should be separated if the reactions are to be understood properly. Also the oxide should be in the pellet form. It was further decided to conduct

auxilliary investigations to evolve a comprehensive picture of this reaction.

1-1 TRUE DIRECT REDUCTION VERSUS REDUCTION VIA GASEOUS MEDIUM

Kinetically, a solid-solid reaction is expected to be much slower compared to a gas-solid one for two reasons. First of all, the solid-solid contact area is much smaller compared to gas-solid contact area. Secondly, solid-state diffusion is much slower compared to mass transfer in gases. Therefore, it was recognized even in early days that the overall reaction is perhaps taking place in two stages, viz.

Reduction of iron oxides, which can be generalized as follows:

$$nFe_xO_y(S) + CO(g) = nFe_zO_w(S) + CO_2(g) \qquad (1\text{-}2)$$

and, gasification of carbon:

$$C(S) + CO_2(g) = 2CO(g) \qquad (1\text{-}3)$$

Reaction (1-2) can be any one of the following:

$$3Fe_2O_3(S) + CO(g) = 2Fe_3O_4(S) + CO_2(g) \qquad (1\text{-}4)$$

$$Fe_3O_4(S) + CO(g) = 3FeO(S) + CO_2(g) \qquad (1\text{-}5)$$

$$FeO(S) + CO(g) = Fe(S) + CO_2(g) \qquad (1\text{-}6)$$

It should be noted that wustite is non-stoichiometric. Hence equation (1-5) and (1-6) are simplifications.

Several investigators[9-12] attempted to measure the rates of true "direct" reduction, viz., the solid-solid reaction between iron oxide and carbon by continuous evacuation of the chamber in the overall temperature range of 700 to 1150°C and pressure range of 5×10^{-4} -10^{-2} torr. They assumed that the gas phase were substantially eliminated by evacuation and hence the rates they obtained represented those of solid-solid reaction. Fig. 1.1 compares these experimental data with those obtained by Rao[8], who employed inert gas flushing.

It may be concluded from Figure 1.1 that the rates under inert gas flushing were even smaller compared to some of those obtained under evacuated conditions. Therefore as such there is no experimental proof to support the theoretical expectation that the rate of the solid-solid reaction should be much slower than that of the gas-solid reaction in this case. However, in these experiments fine iron oxide were mixed with powdered graphite and pressed into pellet. Although the chamber was evacuated the pressure inside the fine pores of the pellets were likely to be appreciable because flow of CO and CO_2 from the interior of the pellet to the chamber would require a substantial pressure difference. The following sample calculation reveals it.

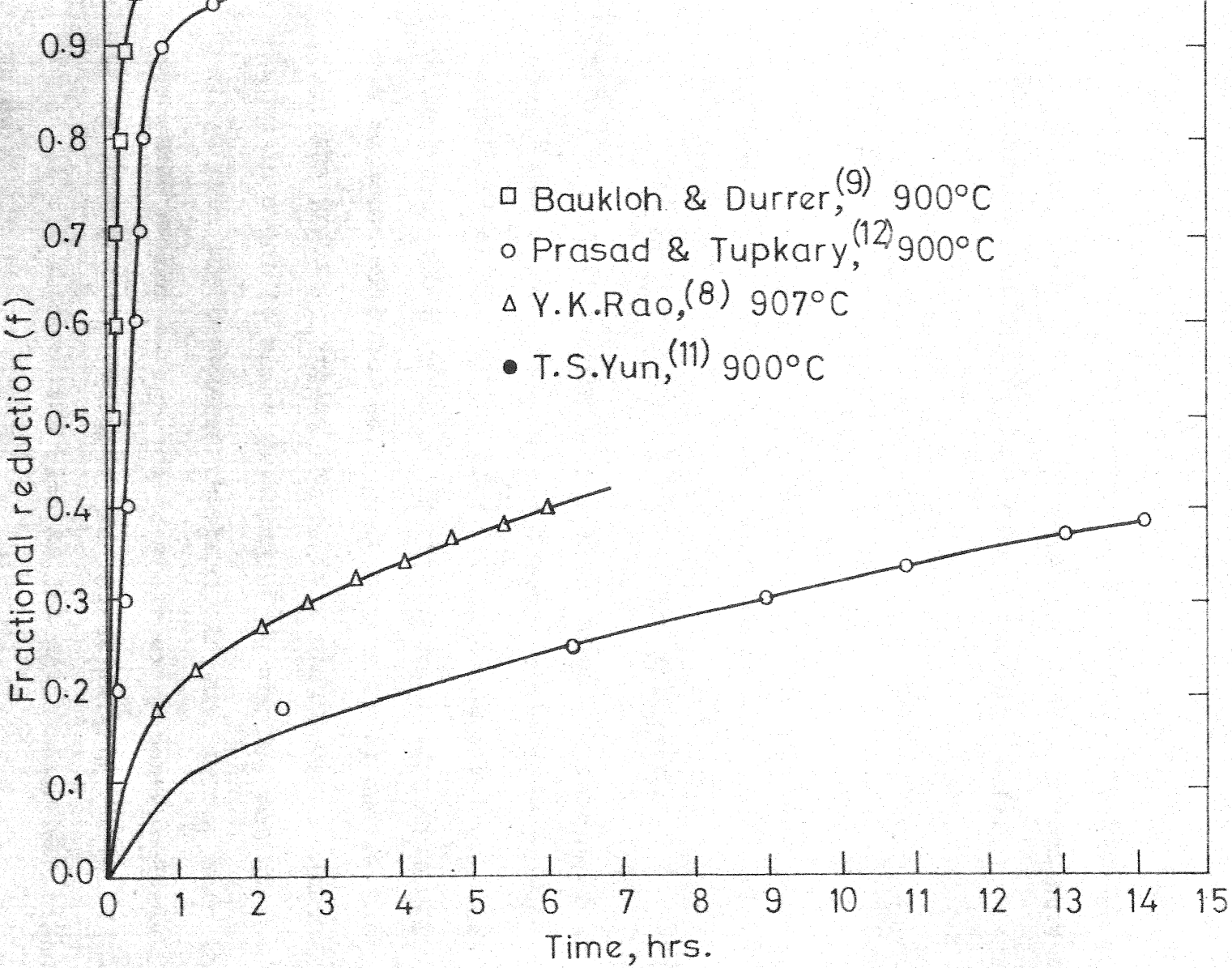

FIG. 1.1 FRACTIONAL REDUCTION Vs. TIME FOR CARBON REDUCTION

The flow of gas through a pore is "molecular" or "Knudsen", when the mean free path is larger than the pore diameter. This condition was very well met in the tiny pores of pellets under a reduced pressure. The through put of gas per unit time (U) through such a cylindrical pore may be expressed by the following relationship (1-7):

$$p\dot{V} = U = C\,(p_1 - p_2) \qquad (1\text{-}7)$$

where, $\dot{V}$ is the volumetric flow rate in c.c./sec. at pressure p; $(p_1 - p_2)$ is the difference in pressure across the tube; C is known as the conductance and is given by:

$$C = 3{,}810\ \sqrt{T/M}\ .\ D^3/1 \quad \text{c.c./sec.} \qquad (1\text{-}8)$$

where T is temperature in °K, M is molecular weight of the gas, D and 1 are diameter and length of the pore in cm. Assuming that the pellet size is approximately 1 cm. the diameter of the pore to be of the order of 10 micron, it can be shown with the help of equations (1-7) and (1-8) that the pressure inside the pellets should be at least 10 mm in order to allow flushing of CO and CO_2 out of the pellet into the evacuated chamber. If that is so, then the gas phase cannot be ignored in their experiments. Hence it is very doubtful whether the investigations[9-12] could at all measure the rate of the solid-solid reactions as such.

On the other hand, it may be stated here itself that there are a number of evidence in support of the contention that the overall reduction takes place via reactions (1-2) and (1-3), whenever a gaseous medium is present. These will be evident from the discussions in the following sections. Here a mention may be made of the experiments by Baldwin[14], who passed nitrogen over a heated bed of iron oxide and coke, and found that the rate of removal of oxygen decreased as the flow rate was increased. The possible explanation is that nitrogen was flushing out CO and CO_2 formed, thus diluting their concentrations and decreasing the rates of gas-solid reactions. This could not have happened if the reaction was a solid-solid one.

Since it seems to be fairly well established as will be evident later that the carbon reduction takes place via reactions (1-2) and (1-3) in the presence of a gaseous environment, such as in industrial processes, the kinetic features of the two component reactions (eqn. (1-2) and (1-3)) will be presented first and then the carbon reduction shall be taken up.

1-2 KINETICS OF REDUCTION OF IRON OXIDES BY CARBON MONOXIDES

Numerous fundamental investigations have been carried out in the past two decades on the kinetics of reduction of iron oxides by hydrogen[15-17]. In comparison

much less data are available on reduction by CO due to the problem associated with deposition of carbon through the reaction: $2CO(g) = CO_2(g) + C(S)$ during investigation.

Table 1.1 presents the important experimental conditions of some fundamental investigations of the kinetics of reduction of iron oxides by CO[18-24].

It should be noted that some of the investigators studied the reduction kinetics of FeO. Both single pellet-cum-thermobalance technique[19,22,24] as well as packed bed systems were employed[20,21]. The particle size ranged anywhere from a fraction of a millimeter to 4 centimeter. The temperature ranged from 700°C to 1300°C and both CO as well as mixtures of CO and CO_2 were employed. However it must be emphasized here that all these are somewhat scattered studies. There is a definite need for comprehensive investigations in this area.

At low flow rates of CO or CO-CO_2 mixture the rates of reduction were found to be dependent on the gas flow rate and increased with increasing flow rate[20-22], till there was no more influence. At this stage, reagent starvation as well as mass transfer in the gas phase has insignificant influence on the reduction rate.

For reduction of iron oxides and ores by hydrogen, the equation:

$$1 - (1 - f)^{1/3} = Kt \qquad (1-9)$$

TABLE 1.1

Experimental Conditions for Investigation on Kinetics of Reduction by Carbon Monoxide

Reference	Material	Particle Size (dia)	Porosity	Gas Composition	Temp. range (°C)	Technique	Activation Energy kcal/mole
1. Smith and McKewan[19]	Hematite ore (pellets)	1.5-1.9 cm	Voids fraction 0.21	Pure CO	760-1120	Single pellet; Thermobalance	Porous pellet= 8.5 Dense pellet= 8.0
2. Khalafalla et al[20]	a)Magnetite pellets of ore	-6+8 mesh	-	70% CO 30% CO_2	1000 1300	Packed bed; gas analysis	13.0
	b)Magnetite particles	"	-	"	"	"	45.0
3. Bicknese & Clark[21]	FeO prepared from pure Fe_2O_3 & Fe	-12+16 mesh	Surface area 0.0177-0.0213 m^2/gm	1.9 mole N_2 for 1 mole of CO	1145	Packed bed; thermobalance	13.9
4. Kawasaki et al[23]	Fe_2O_3 prepared from pure Fe	1.5-4.4 cm spheres	Voids fraction 0.31	Pure CO	700-1200	Single layer of pellets; thermobalance	-
5. Khalafalla & Weston[24]	Wustite from pure Fe_2O_3	-4+5 mesh spheres	-	Pure CO	1000	Packed bed; gas analysis	-

has been found to be widely obeyed, especially in the middle ranges of the reduction curves[25]. Here f denotes fractional reduction ($\frac{\%\ \text{reduction}}{100}$), t is time from beginning of reduction and K is a constant. McKewan[26] interpreted it in terms of rate-control by slow chemical reaction at the Fe-Fe_xO interface. However, it was shown later by Warner[27] as well as Olsson and McKewan[28] that mass transfer steps are also fairly slow and the reduction is a case of mixed control kinetics. Spitzer, Manning and Philbrook[29,30] later analytically proved that equation (1-9) is expected to be approximately obeyed in iron oxide reduction even if all transport steps as well as the chemical reaction step simultaneously control the rate. Also it appears to be immaterial whether the pellet is porous or dense as long as topochemical pattern of reduction is maintained. According to Ross[31] it has been found to be obeyed even when the reduction is completely internal.

Therefore, it is worth while to examine whether equation (1-9) is obeyed by CO reduction or not. Fig. 1.2 shows the data of some workers plotted this way.

From the straight line plot it can be said that equation (1-9) is generally valid even for CO reduction of iron oxides.

For chemical control, K of eqn. (1-9) should be inversely proportional to the diameter (d_p) (in general, size) of the specimen. This was observed in some cases[18],

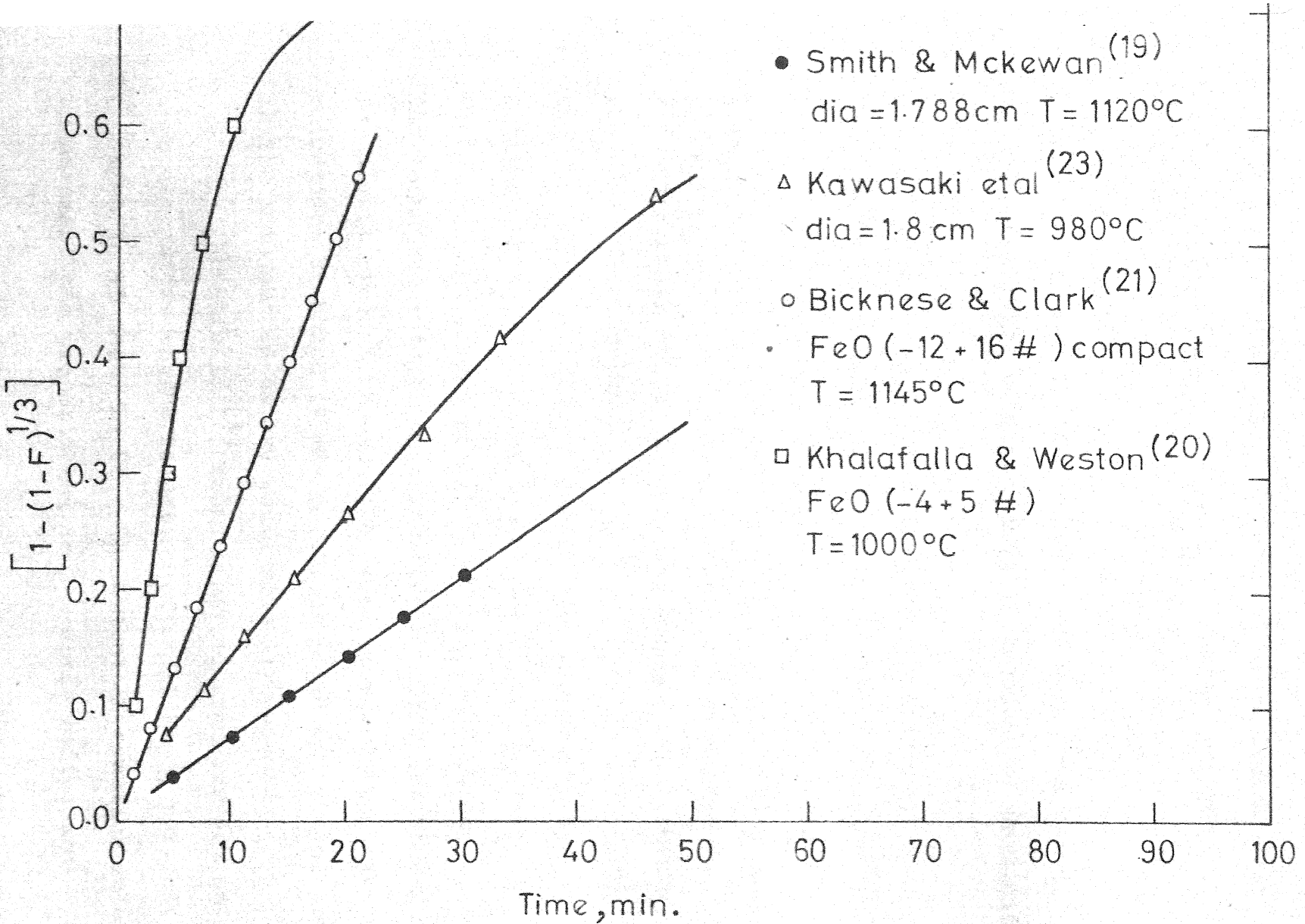

FIG. 1·2 $\left[1-(1-F)^{1/3}\right]$ Vs. Time For CO - REDUCTION

but Bickenese and Clarke[21] found it to be independent of d_p. Microstructural observations revealed completely internal reduction due to porousness and smallness of the particles. In such a case individual grains of the particles have access to gas and themselves behave as tiny particles, thereby making the reduction rate independent of particle size.

For hydrogen reduction also experimental data[17] point out that time for certain fractional reduction is independent of d_p for completely internal reduction, proportional to d_p for limiting mixed control and proportional to d_p^2 for diffusion in porous iron. To which case a situation shall belong to depends, amongst other things, on the size of the pellet.

This conclusion can be strengthened by noting the findings of the following investigations. Kawasaki et al[23] employed large porous pellets of Fe_2O_3 (dia 1.8 cm - 4.2 cm), and found the rate to be controlled by diffusion through the porous product layer. They also observed stagewise reduction, although it was not accompanied by typical breaks in the rate curves as one would normally expect.

Khalafalla[24] found a marked promoter action of impurity oxides on the reduction of small Fe_2O_3 particles (-4 mesh to +5 mesh) by CO. The extent of reaction rate enhancement was proportional to the ionic radius and

electronic charge of the promoter additive. This points out to chemical control.

Walker and Carpenter[22] found that addition of CO_2 to CO decreased the rate of reduction of Fe_2O_3 remarkably. Bickenese and Clarke[21], in their experiments on reduction of synthetic and natural FeO, using N_2 and CO mixture found this to contain an appreciable percentage of CO_2 and, therefore, considered its likely influence. They could fit their rate data with the following equation:

$$[1 - (1 - f)^{1/3}]/t = [4.3 \exp(-\frac{13800}{RT})] \times [\frac{C_e - C}{C_e}] \qquad (1\text{-}10)$$

where C is the concentration of CO_2 at the metal-oxide interface and C_e is the concentration of CO_2 at equilibrium with Fe_xO and iron. Compliance with equation (1-10) implied that reaction (1-5) is a first order, reversible one. Chufarov et al[32] found CO_2 to have quite a retarding effect on reduction of Fe_3O_4 and FeO by CO and expressed the influence of gas composition as:

$$\text{rate} = K\, p_{CO}/p_{CO_2}^{n} \qquad (1\text{-}11)$$

This type of equation is to be found if CO_2 is preferentially adsorbed at the surface of the oxide thus blocking the number of bare surface sites. Further investigation is required in this area.

Activation energy of the reduction process has been obtained in two ways. In the first approach, a rate equation like equation (1-9) or (1-10) has been derived and then the constant K has been expressed as an Arrhenius-type equation, as exemplified by equation (1-10). Alternatively, the rates have been determined from the slopes of the pct. reduction vs. time plots at constant f at various temperatures and the temperature dependence of the rate fitted with Arrhenius-type equation. The values of activation energy were variously found as 8.5 K.cal/mole[19], 13.9 K.cal/mole[21], 33-50 K.cal/mole[20]. Khalafalla[20] found an unusually large activation energy (33-50 K.cal/mole) for reduction of coarse and crystalline FeO and Fe_3O_4. He attributed it to a large negative heat of adsorption of CO on the oxide surface. However, they could not adequately substantiate this point.

It is recognized that the reduction process is complex. Such complexity arises from various sources. The product layer is porous and the diffusion process through the pores is influenced by the pore texture, which again depends on many factors. In addition, considerable swelling of pellets, even to the extent of 10 times the original volume[33] has been observed. Cracking during reduction, especially in dense specimens, recrystallization of reduced iron layer and presence of unreduced oxide islands add to

the complexity further. No wonder that the temperature dependence of reaction rate as well as occurrence of rate maxima and minima as found by various investigators are full of controversy[15]. However, experiments under controlled conditions have shown[19,24] that reduction by CO is 5 to 7 times slower as compared to that by H_2.

1-3 KINETIC ASPECTS OF GASIFICATION OF CARBON BY CARBON DIOXIDE

Because of the importance of this reaction, there have been numerous investigations over the past several decades, and investigators arrived at many divergent conclusions. Therefore, this brief review will be based on some recent analysis on the subject[34-39].

Cokes, carbon and synthetic graphites are highly porous with pores ranging from about 10 Å to several microns in diameter. The kinetic steps involved are gas film diffusion, diffusion through pores and chemical reaction at gas-solid interface. It has been established that the chemical reaction is exclusively rate controlling below 1100°C, if the size of the graphite particle is not too large (diameter less than 1 cm.). Such a conclusion has been arrived at from evidences, such as high activation energy (80-90 K.cal/mole), and strong influence of solid and gaseous impurities even in trace quantities. For chemical reaction control, the entire internal pore surface

area should be active and the rate of loss of carbon should be proportional to the volume of the particle. Turkdogan et al[36] found it to be valid for particle diameter less than 1 cm.

By the very method of manufacture, carbon comes out with infinite spectrum of structural imperfections and surface defects. Again some solid inorganic materials, moisture, H_2 etc. catalyze or inhibit the reaction strongly even if they are present in ppm. level. Regarding rate and mechanism of this reaction these were the sources of discrepancies in the past. Most authors[34-38] have found that the rate of the reaction can be represented by an equation of the form:

$$\text{rate} = \frac{K_1 \, p_{CO_2}}{1 + K_2 \, p_{CO} + K_3 \, p_{CO_2}} \qquad (1\text{-}12)$$

The first step in the reaction is the formation of a surface oxide, C(O), on an active free site (C_f) at the surface:

$$CO_2(g) + C_f \underset{k-1}{\overset{k_1}{\rightleftharpoons}} C(O) + CO(g) \qquad (1\text{-}13)$$

The second step is the breakdown of the surface oxide to form gaseous CO leaving a new active site behind:

$$C(O) \underset{m-2}{\overset{k_2}{\rightleftharpoons}} CO(g) + C_f \qquad (1\text{-}14)$$

Treatments of non-catalyzed reactions are modifications of Langmuir-Hinshelwood mechanism of surface reaction. Two mechanisms have been proposed to account for the inhibiting action of CO. In one mechanism, CO is assumed to adsorb reversibly on the active sites blocking them off. In the second mechanism, adsorption of CO has been assumed to be negligible and the retardation is stated to be caused by the reversible nature of reaction (1-13). The latter is more supported now-a-days because amongst other evidences the chemisorption of CO has been shown to be negligible[37]. The mechanism, proposed by Turkdogan and co-workers[36], who explained the inhibiting action of CO in terms of chemisorption of CO, is at variance with the above.

A number of other rate equations have been proposed[34] giving different order of dependence on p_{CO_2} and p_{CO}. For example, Turkdogan and co-workers[36] found the following:

(a) rate $\propto p_{CO_2}^{1/2}$ in absence of CO

(b) rate $\propto (p_{CO_2} - p^e_{CO_2})$ at smaller values of p_{CO_2} in presence of CO, and

(c) rate $\propto (p_{CO_2} - p^e_{CO_2})^{1/2}$ at larger values of p_{CO_2} in presence of CO. It can be seen that these are not too different if the equation (1-12) is suitably simplified. Rao and Jalan[38] have harmonized the apparently divergent conclusions and have shown the validity of equation (1-12). It

may be pointed out here that the rate decreases enormously with increase of percentage of CO in the gas. The rate of gasification with pure CO_2 at 1 atm. has been found to be two orders of magnitude compared to a gas of 90%CO-10%CO_2 at 900°C.[37]

For an equation, such as (1-12), there can be no simple activation energy. However such energies have been determined by investigators employing simple rate equations. The value is mostly between 80-90 K.cal/mole at 850-1100°C[34] for pure graphite. In the presence of catalyst it has been found to be as low as 15 K.cal/mole.[39]

Specially relevant to sponge iron making is the marked catalytic effect of metallic Fe even at very low concentrations. This has been reported by a number of investigators.[34,36] The rate has been found to be enhanced even by a factor of 300 for graphite.[34] The activation energy also goes down considerably. Walker and co-workers[35] carried out magnetic susceptibility studies and found that iron is an effective catalyst only when it is present as metallic iron, mixed with a little FeO. Oxidation to Fe_3O_4 and Fe_2O_3 destroys the catalyst action. However, it can be again regenerated in a reducing atmosphere. The explanation put forward contends that oxygen transfer at the graphite surface is enhanced by alternate oxidation of Fe and reduction of FeO. The catalytic activity is helped by

mobility of oxygen on the metal surface. Ni and Co also exhibit similar catalytic action.

The time-dependence of gasification rate is a complex phenomenon. The size of the particle shrinks. Pores get more and more enlarged. New pores open up as a result of which the pore surface area can increase even by a factor of 20.[34] The impurities start concentrating on the surface as a result of "burn-off" of carbon. Therefore, the rate measurements ought to be done during the initial period only. Turkdogan and co-workers[36] found that the rate of weight loss was constant during the first 20 pct. of gasification and was proportional to the initial weight. Therefore, specific rate constant may be written as:

$$K = (dw/dt)/W_o \qquad (1\text{-}15)$$

where Wo is the initial weight.

Lastly, in many cases such as large particles and tiny pores, high temperature etc. pore diffusion may be partially controlling the reaction rate and cannot be ignored.[38] This would be indicated if rate is proportional to square of diameter and would in effect lower the activation energy considerably.

1-4 EXPERIMENTS ON REDUCTION OF IRON OXIDES BY CARBON IN GASEOUS ENVIRONMENT

Several studies had been done in the past, but the ones of fundamental importance are mostly of recent origin and have been conducted by taking intimate mixtures of iron oxide and carbon particles[8,21,40,41]. Just from the weight loss of such a specimen it is not possible to find out the fractional reduction directly, since the weight loss is due to loss of oxygen and carbon both. Rao[8] attempted to separate these two theoretically with the help of the rate equation for solution loss reaction proposed by Turkdogan et al.[42] However, the approach suffered from some objectionable assumptions, notably constancy of gas composition with respect to time. On the other hand, Bickenese and Clarke[21] as well as Otsuka and Kunii[40] measured the quantities of gases evolved in conjunction with weight loss measurement. Ghosh and Tiwari[41] determined percentages of iron and carbon in the product. All investigators employed pure Fe_2O_3 and C, except for Ghosh and Tiwari, who worked with Gua hematite iron ore and South Indian lignite coke.

Otsuka and Kunii[40] found a change in rate at approximately 33 pct. reduction, which corresponds to the FeO stage (Fig. 1.3). They also measured quantities of CO and CO_2 evolved as a function of time by flushing with nitrogen and using gas chromatograph. The change in gas composition as reduction proceeds is shown against

composition in equilibrium with various oxide mixtures (Fig. 1.4). It is evident that the gas was not reducing enough to allow formation of metallic Fe at the early stage.

The first stage was accompanied by a high activation energy (55-75 K.cal/mole). From this it was concluded that the rate-controlling step was the gasification reaction (equation (1-3)). As mentioned before activation energy values obtained by various investigations of the latter reaction[34-39] differed and ranged between 80-90 K.cal/mole for uncatalysed reaction and down to 15 K.cal/mole for strongly catalysed reaction. Even the high activation energy definitely points out that the rate-controlling step is gasification, because the activation energy for CO reduction of oxides is much lower (13 K.cal/mole).

Further evidence were obtained by Otsuka and Kunii[40] in support of rate-control by gasification reaction for the 1st stage of reduction. The rate increased when the particle size of carbon was less. Similarly the rate was independent of the particle size of Fe_2O_3.

On the other hand, the second stage was characterized by a low activation energy (15-23.5 K.cal/mole). The rate increased when the particle size of Fe_2O_3 was decreased. From the above observations it would appear that in the second stage ($FeO \longrightarrow Fe$) the rat[illegible] was controlled

there were evidence against this conclusion as noted below:

(a) The actual gas composition (Fig. 1.4) was very close to that corresponding to FeO/Fe equilibrium.

(b) Lower particle size of carbon also enhanced rates.

Therefore, Otsuka and Kunii proposed that the rate in the second stage was accelerated in the presence of metallic Fe which has been found to be a good catalyst for the gasification reaction[34-36]. Their contention derives further support from the following observations:

(a) The rate at the second stage was accelerated if the rate of the gasification reaction was accelerated too, inspite of the fact that CO content of the gas was higher. This points out to catalysis.

(b) An increase in pelletizing pressure increased the rate in the second stage presumably due to better contact of metallic Fe with graphite and better catalytic action. This was held as the explanation for the enhancement of rate by lowering the particle size of Fe_2O_3, since that could lead to better contact.

(c) When the particle size of both Fe_2O_3 and C were simultaneously altered there was no change in rate.

The lowering of activation energy was very large (approx. 40 K.cal). However there are instances of such lowering due to impurity effects[39].

Rao[8] also found a high activation energy of the overall reaction. Lowering of particle size of carbon

enhanced the rate. In addition the presence of SiO_2 in the mixture enhanced the rate and FeS retarded it. It is known that these two compounds behave the same way for the gasification reaction (1-3). Hence it was concluded that the rate of overall reaction was controlled by that of the gasification reaction.

Ghosh and Tiwari[41] in their studies on Gua iron ore found all phases, viz. Fe_2O_3, Fe_3O_4, FeO, Fe to be present in the partially reduced pellets. Activation energy was determined as 18.7 K.cal/mole between 56-91 pct. reduction. Although the authors inferred a slow reduction step from this, it has to be recognized that this feature has similarity with the second stage of Otsuka and Kunii[40] and may be a case of Fe-catalyzed gasification reaction.

From the above studies as well as the work of Baldwin[14] there seems to be no doubt that the rate of carbothermic reduction is controlled by the rate of the gasification reaction (eqn.(1-3)). The catalytic effect of metallic Fe is also very likely. However the studies have been made only with powdered mixtures of oxide and carbon in intimate contacts and suffer from the following uncertainties:

(1) Ill-defined size and geometry.

(2) Unknown factors such as catalytic effect of Fe on gasification reaction.

Moreover such studies cannot predict rates for situations where the ore size is much larger than the size of the reductant. Bickenese and Clarke[21] did find some influence of the size of the oxide on the rate. Mathematical description of such an assembly (powdered mixture) poses a problem too. Therefore, at best qualitative informations only can be obtained from such studies.

Bones, Reeves and Saunders[43] found that during CO reduction of iron oxides, carbon was deposited within the pores and interstices of ore granules and it was confirmed by later workers.[44] This can conceivably be imagined in the mixed pellets as well since metallic Fe is a good catalyst for it.[45] This effect can substantially alter the detailed interpretations of experimental data. It is not out of place here that care is to be exercised to examine its influence on carbon monoxide reduction too.

1-5 METHODS OF MEASUREMENT

The indices of instantaneous reaction rate were chosen as:

1. Rate of removal of oxygen from the ore/oxide
2. Rate of gasification of carbon.

It was planned to determine both of these with the help of the following measurements.

1. Measurement of the gas evolution rate at intervals of time during the course of the reaction by sensitive capillary flowmeter.

2. Determination of the composition of the gas evolving at intervals of time during the course of the reaction with the help of a solid electrolyte oxygen sensor.

The gas that comes out of the reaction chamber would consist of CO and CO_2.

$$\dot{Q} = \dot{Q}_{CO} + \dot{Q}_{CO_2} \tag{1-16}$$

where $\dot{Q}_{CO}$, $\dot{Q}_{CO_2}$ and $\dot{Q}$ are volumetric flow rates of CO, CO_2 and total gas respectively.

Hence knowing $\dot{Q}$ and gas composition, $\dot{Q}_{CO}$ and $\dot{Q}_{CO_2}$ can be estimated separately. From stoichiometry

$$\dot{W}_O = 16(\dot{Q}_{CO} + 2\dot{Q}_{CO_2})\,(\text{Conversion factor}) \tag{1-17}$$

$$\dot{W}_C = 12(\dot{Q}_{CO} + \dot{Q}_{CO_2})\,(\text{Conversion factor}) \tag{1-18}$$

where $\dot{W}_O$ and $\dot{W}_C$ denote rate of weight loss of oxygen and carbon respectively.

1-5.1 Determination of Gas Composition by Solid Electrolyte Oxygen Sensor

The conventional methods of determining gas composition are by using a gas chromatograph or an orsat apparatus. However recently a very versatile and accurate method has been evolved, which utilizes a solid oxide

electrolyte cell. As this is much more rapid and hence convenient for determining gas compositions instantaneously it was decided to use the same for the present investigation. Many reviews are available on this topic.[46-49] Only a brief presentation of the principles of the method will be given below.

A solid electrolyte cell is a galvanic cell consisting of a cathode at one end and an anode at the other with a ceramic solid electrolyte in between. The galvanic cell must be so designed as to eliminate all the side reactions. The emf (E) of such a cell can be related to the free energy change ' G' of the reaction of interest by the relationship:

$$\Delta G = - ZFE \qquad (1\text{-}19)$$

where Z = number of Faradays of electricity to be passed across the cell to effect the reaction and F is a Faraday. The conduction of electricity across the electrolyte must be all ionic. The presence of even a small electronic contribution to the conductivity will give rise to internal short-circuiting. This will disturb the thermodynamic equilibrium existing at the electrode-electrolyte interface.

Calcia-stabilized zirconia (CSZ) has almost 100 pct. ionic conductivity at the operating temperatures of common interest. The oxygen ion is the conducting species.

1-5.1. Principle

The solid electrolyte cell used for measuring the oxygen potential in the gas phase may be written as follows:

Pt, Sample gas	Solid oxide electrolyte	Reference gas, Pt
P_{O_2}, μ_{O_2}	(O^{2-})	$P^{o}_{O_2}$, $\mu^{o}_{O_2}$

The emf of the cell is

$$E = -\frac{\Delta G}{2F} = -(\mu_{O_2} - \mu^{o}_{O_2})/4F \qquad (1\text{-}20)$$

$$= \frac{RT}{4F} \ln P^{o}_{O_2}/P_{O_2} \qquad (1\text{-}21)$$

Here, μ_{O_2} means the chemical potential of oxygen and P_{O_2} is the partial pressure of oxygen. R and T are respectively the Universal gas constant and the absolute temperature. Superscript o indicates the reference state. If the oxygen in gases behave nonidealy the pressure terms must be replaced by fugacities.

1-5.1.2 Estimation of Gas Composition from p_{O_2} Measurement

The oxygen sensor determines oxygen potential (μ_{O_2}) or p_{O_2}. If the gas mixture is that of CO and CO_2, then

$$p_{O_2} = \frac{1}{K_c} \cdot (P_{CO_2}/P_{CO})^2 \qquad (1\text{-}22)$$

where K_c is the equilibrium constant for the reaction:

$$2CO(g) + O_2(g) = 2CO_2(g)$$

The highest oxygen concentration through dissociation of CO_2 is about 4×10^{-6} at 1500°K. p_{O_2} is still lower at lower temperature. Therefore the mixture can be considered to contain only CO and CO_2.

The p_{O_2} measured by the sensor at constant CO_2/CO ratio would depend on the measurement temperature, because K_c is a function of temperature.

1-5.1.3 Advantages and Limitations of the Oxygen Sensor

A. Advantages

(1) Emf response of a S.E. cell is usually specific, rapid and continuous.

(2) Emf measurement can be made directly in or with the system to be investigated without disturbing the system at large.

(3) A single sensor can often cover wide ranges of oxygen potential and temperature.

(4) Sensor output (i.e. the cell voltage) is amenable to high precision measurement.

(5) The meter draws very little current and, therefore, hardly disturbs the system.

(6) It is versatile and, in principle, applicable to any phase for oxygen analysis since it measures oxygen potential specifically.

B. Limitations

(1) If the electrolyte has electronic conductivity this will lead to transfer of oxygen from high p_{O_2} to low p_{O_2} side. The error due to this is more serious at high temperature than at low temperature.

(2) The sensor cannot be used below a certain temperature.

(3) The solid electrolyte tube is very sensitive to thermal shocks.

1-6 PLAN OF THE WORK

The literature review reported in Sections 1-1 to 1-5 reveal that some fundamental work on powder mixtures of iron oxide and carbon have been carried out. These studies do not sufficiently reveal the kinetics of the actual reactions taking place in a rotary kiln where the ore is in the form of pellets. Also due to the catalyzing effect of iron on the gasification reaction, it is difficult to predict the influence of the individual reaction stages on the overall rate from these studies. Therefore it was decided:

(1) to investigate the reaction rate between Fe oxide pellet and carbon powder to simulate rotary kiln.

a. to separate the oxide pellet and carbon physically.

b. to study the influence of distance of separation as well as temperature and porosity of the pellet on reaction rate.

(2) Since for proper interpretation, instantaneous carbon loss rate, oxygen loss rate as well as gas compositions during the course of reaction are desirable, it was decided to employ capillary flow meter and oxygen sensor for measurement (see Section 1-6).

(3) In order to arrive at percentage reduction and to cross check with experimental weight loss, it was planned to resort to numerical integration of instantaneous rates using digital computer.

(4) Since it is a fundamental study, it was decided to employ pure Fe_2O_3 and pure graphite for this purpose.

(5) In order to make the investigation more comprehensive and for better correlation, the following, auxilliary investigations were also planned.

a. determination of graphite reactivity

b. rate determination using powder mixtures of oxide and carbon

c. examination of partially reduced pellets.

On the basis of the above considerations, it was decided to do the following:

(1) To design and fabricate a reaction cell assembly with available materials to contain Fe_2O_3 pellet and graphite powder at controlled but variable distances of separation. The cell is to be a closed one with a tiny opening only in order to prevent interference from surroundings.

(2) To study reaction kinetics of Fe_2O_3 powder and graphite powder mixture as well as to determine graphite reactivity.

(3) To set up solid electrolyte cell assembly and sensitive flowmeters for measurement of rates.

(4) To study the reaction kinetics of porous and dense pellets of Fe_2O_3 with graphite kept in separation at different temperatures and distances of separation.

(5) To study the reaction kinetics of powder mixtures of Fe_2O_3 and graphite as well as mixture of micro-pellets of Fe_2O_3 and graphite powder at different temperatures.

(6) To study the gasification reaction of graphite with pure CO_2 as well as mixture of CO and CO_2 at different temperatures.

(7) To make a computer programme; for calculation of gas composition and instantaneous rates from the data on emf and flow measurements, as well as to determine the integrated weight loss.

(8) To interpret the data thus obtained.

CHAPTER 2

APPARATUS

The present investigation included three sets of experiments. The principal set concerned with study of the reaction kinetics between Fe_2O_3 pellet and graphite powder. The apparatus for this study had provision for varying the distance of separation between the oxide pellet and graphite. Experiments on powder mixture of Fe_2O_3 and graphite as well as pellet-graphite mixture were conducted in a different apparatus. Graphite reactivity was determined first by employing the former set up and then employing the latter one.

2-1 APPARATUS FOR STUDYING REACTION KINETICS BETWEEN Fe_2O_3 PELLET AND GRAPHITE POWDER

The set up used has facility for controlling the distance of separation between the oxide pellet and graphite powder and is shown schematically in Fig. 2.1. It consists of a furnace, reaction chamber, reaction cell and a solid electrolyte tube.

2-1.1 Furnace

A Kanthal-wound vertical furnace of 50 cm. length was used for heating the reaction chamber. The temperature of the furnace was controlled by a Leeds and Northrup

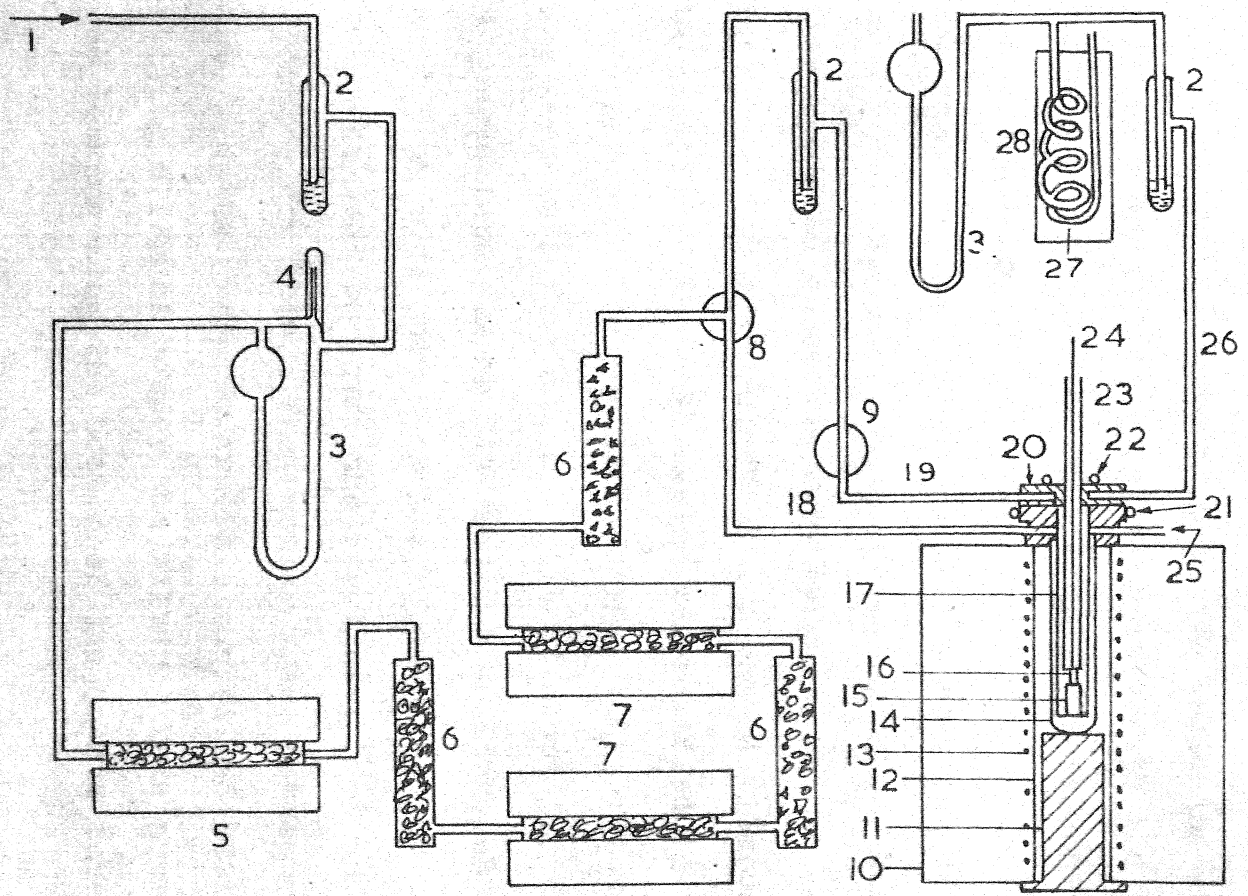

1 Tank nitrogen
2 Bubbler
3 Manometer
4 Capillary
5 Copper gauze furnace
6 $CaCl_2$ tower
7 BTS furnace
8 3-Way stop cock
9 2-Way stop cock
10 Reaction furnace
11 Brick support
12 Mullite tube
13 Furnace winding
14 Silica tube
15 Reaction cell
16 Alumina support
17 Reaction chamber
18,19 Gas inlet
20 Brass flange
21 Cooling coil
22 CSZ tube
23 Pt-lead wire
25,26 Gas outlet
27 Fine capilary
28 Thermos flask

FIG. 2·1 EXPERIMENTAL SET UP FOR PELLET-GRAPHITE REACTION

model 6260 Electromax solid state controller actuated by a Pt/Pt-10 pct Rh thermocouple. A constant temperature zone of about 5 cm length could be obtained at the centre of the furnace.

2-1.2 Reaction Chamber

A few trials were made in the beginning with a small crucible containing graphite powder with the Fe_2O_3 pellet placed on top of the crucible. This arrangement suffered from two main disadvantages.

(1) The reaction chamber enclosing the reaction cell consisted of a 5 cm i.d. and 30 cm long quartz tube. Because of this the dead space was very large.

(2) Provision for measurement of gas composition could not be provided. The cell design was modified to reduce the dead space in the reaction chamber. The reaction cell was kept in a graphite crucible of about 3.6 cm i.d. A quartz tube, 22 cm i.d. and 3.6 cm long, was joined to a 5 mm i.d. and 40 cm long quartz tube by blowing. This was used to cover the reactants, kept in the graphite crucible. The annular space between the quartz tube and the graphite crucible was filled with a low melting alloy of copper and silver. This prevented the gas leaking from the bottom of the quartz tube.

The main disadvantage with this arrangement was that the gas composition could not be determined instantaneously using a solid electrolyte tube.

The next attempt was made with a 30 cm long fused quartz tube closed at one end. The tube was fixed on to a brass flange using silicone sealant. The arrangement of the graphite powder and iron oxide pellet remained the same as before. A 12 mm o.d. CSZ tube was introduced from the top for instantaneous measurement of gas composition. The rate of gas evolution was determined at intervals using a sensitive capillary flow meter.

The main drawback with this set up was the frequent breakage of the quartz tube because of devitrification and the large empty space of the reaction tube. Thus it was decided to use an inconal tube closed at one end as the reaction chamber. Also the reaction cell was modified so that the product gases escaped through a small outlet. One problem with inconel could have been carbon deposition. But it was found to be negligible in subsequent trials.

Fig. 2.2 shows the details of the reaction chamber. It consists of a 22 mm o.d., 19 mm i.d. and 26 cm long Inconel tube. One end of this tube was closed with a 3 mm thick inconel plate by argon arc welding. The bottom portion of the tube was chamfered and the plate was force-fitted into the tube so that about 2 mm of the plate was inside

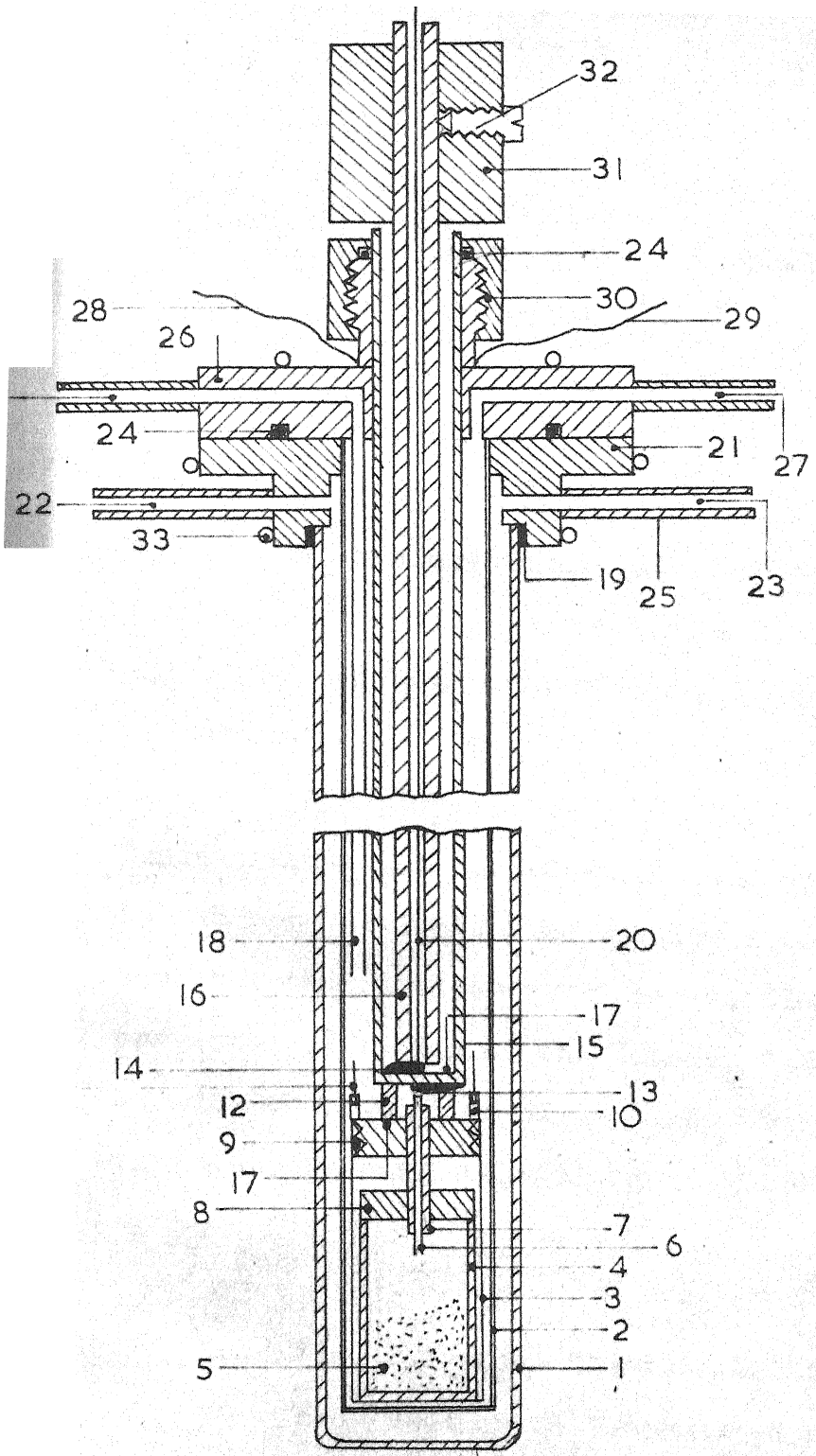

1 Silica tube
2 Inconel chamber
3 Inconel cell
4 Alumina crucible
5 Graphite powder
6 Alumina tube
7 Alumina tube
8 Fe_2O_3 pellet
9 Lid of cell
10 Inconel hook
11 Nichrome wire
12 Alumina tube
13 Thermocouple bead
14 Platinum bead
15 CSZ tube
16 Alumina sheath
17 Platinum coating
18 S.S.tube
19 Silicone sealant
20 Platinum wire
21 Brass flange
22 Gas inlet hole
23 Gas outlet hole
24 'O' rings
25 Copper tube
26 Nitrogen inlet
27 Nitrogen outlet
28 Platinum wire
29 Pt–10%Rh. wire
30 Tubing coupling
31 Dead weight
32 Screw hole
33 Cooling coil

FIG. 2·2 REACTION CHAMBER WITH CSZ TUBE AND REACTION CELL (Pellet – Graphite System)

the tube. This ensured complete sealing of the whole thickness of the tube during arc welding and prevented any chance of leakage. The other end of the tube was brazed onto a water-cooled brass flange. The inlet and outlet for the gases were provided by drilling holes through the top flange. Purified N_2 gas was taken to the bottom of the reaction chamber by means of a 2 mm i.d. stainless steel tube. The outlet gas was taken out through a bubbler containing di-butyl phthalate.

The Inconel reaction chamber was surrounded by a fused quartz tube closed at one end and fixed on to the flange by silicone sealant. The annular space between the Inconel tube and the fused quartz tube was flushed with N_2. This prevented oxidation of the Inconel tube at high temperature as well as leakage of oxygen into the reaction chamber by diffusion through the walls of the Inconel tube.

2-1.3 Reaction Cell

Fig. 2.2 shows the details of the reaction cell.

The reaction cell consisted of an Inconel crucible of 17 mm i.d. and 18 mm o.d. The crucible was made from a 22 mm o.d. and 16 mm i.d. Inconel tube. The bottom of the crucible was made from a 3 mm thick Inconel plate. The tube was first machined to exact inner dimensions and the outside was chamfered to give a thickness of 0.1 mm at

the tip where the bottom plate was force-fitted. The joint was sealed by argon arc welding. The outside of the crucible was then machined to exact dimensions.

The lid of the crucible was made by joining together two 3 mm thick Inconel plates by rivets. A 3 mm hole was drilled at the centre of the lid for inserting alumina tube into the cell. Threads were provided on the lid as well as the interior of the crucible in order to close the crucible tightly and to ensure that no gases leaked through it. Two hooks were rivetted onto the lid for introducing the cell into the reaction chamber.

An alumina crucible, 15 mm i.d. and 17 mm o.d. and 2.6 cm long was placed inside the cell for containing the graphite powder. The pellet was kept on top of the alumina crucible. The distance of separation between the pellet and graphite was varied by using varying amounts of Al_2O_3 powder at the bottom of the crucible. Fe_2O_3 pellet had a hole of 3 mm dia at the centre. An alumina tube of 3 mm o.d. was introduced through the central hole of the lid of the Inconel cell and through central hole of the Fe_2O_3 pellet into the alumina crucible. Another alumina tube of 1.5 mm o.d. was inserted through the 3 mm o.d. alumina tube. The latter tube served as the outlet for gases (CO, CO_2) to escape. Because of the small cross-section of the outlet tube the

flow of reaction gases from the cell to the surrounding was expected to be restricted so that an almost ideal closed cell could be realised.

2-1.4 Solid Electrolyte Tube

Fig. 2.2 shows the detailed arrangement. A solid oxide electrolyte tube was employed for measuring CO/CO_2 ratio in the gas comming out of the reaction cell. The principle and salient features of the solid electrolyte technique has been briefly reviewed in Chapter 1. Fig. 2.2 shows the arrangement of the solid electrolyte tube inside the reaction chamber. The reference electrode was air. The solid electrolyte was a 12.5 mm o.d. calcia stabilized-zirconia (CSZ) tube.

Contact between the electrolyte and electrodes were established by coating the inner and outer surfaces of the bottom of the tube with platinum paste (Engelhard No. 6926). The inner cylindrical wall of the tube was covered by a long roll of paper and paste was applied at the bottom with a long brush. The tube was slowly heated to a temperature of about 900°C for sintering the paste and to obtain a coating of platinum on the surface of the tube. Three layers of paste were applied and the heating and cooling were repeated. A surface resistance of about 0.5 ohms could be obtained. Electrical continuity of the platinum coating was checked.

Electrical contact between the platinised surfaces and the measuring instrument were made by employing platinum wires as lead.

A good contact was ensured by making large beads at the tips of the lead wires. The beads were then hammered so as to obtain a flat surface. After cleaning the surfaces by boiling in concentrated hydrochloric acid for about 2 hours, these were annealed and made to press against the platinised surfaces of the CSZ tube. The platinum wire used for the interior of the solid electrolyte tube was introduced through a thick alumina sheath. The bottom of the sheath rested on the platinum bead. A 0.5 Kg weight was fixed on to the alumina sheath with the help of a screw. The weight helped to make a good contact between the flat bottom of the platinum wire and the platinum coated surface of the CSZ tube by applying sufficient pressure on the contact surfaces. The CSZ tube was introduced into the reaction chamber through a tubing coupling joint. It rested on a 10 mm o.d. and 5 mm long alumina tube, which again was placed on the lid of the reaction cell and surrounded the 3 mm alumina gas outlet tube of the reaction cell. Contact between the flat portion of the platinum wire and the platinum coated outside bottom surface of the solid electrolyte tube was ensured because it was resting on the alumina tube. This arrangement helped in exposing the electrolyte to the gases as soon as

the latter came out of the reaction cell. This arrangement, therefore, allowed reliable monitoring of the instantaneous composition of the gases coming out of the reaction cell.

2-2 GAS PURIFICATION TRAIN

Purified nitrogen gas freed from oxygen and moisture was employed for maintaining an inert atmosphere in the reaction chamber while the furnace was being slowly heated to the reaction temperature. Nitrogen was also used for flushing the annular space between the Inconel reaction chamber and the surrounding fused silica tube.

2-2.1 Nitrogen Purification Train

Fig. 2.1 shows the arrangement. Nitrogen was passed through a bubbler and a capillary flow meter where the volumetric flow rate of the gas was registered. The outlet of the flow meter was connected to a nichrome wound copper gauze furnace kept at 500°C, where the bulk of the oxygen present in the gas reacted with copper turnings. The gas subsequently entered a tower filled with anhydrous $CaCl_2$ for removal of moisture and was then passed through a furnace at 200°C containing BTS reduced catalyst (BASF, Germany) for the removal of any trace of oxygen remaining. This catalyst contains finely divided copper on a suitable porous base. Because of the high specific surface area it can

efficiently absorb oxygen at a much lower temperature range, viz., 150°C to 200°C. The nitrogen coming out of the BTS catalyst furnace entered another tower filled with anhydrous $CaCl_2$. In connection with measurement of graphite reactivity this gas was again passed through another BTS reduced catalyst furnace and then through a U-tube containing anhydrous magnesium perchlorate for the removal of any further trace of oxygen and moisture. The outlet of the U-tube was connected to a three-way stopcock. The gas to the reaction chamber was taken straight from the three-way stopcock through rubber tube connection to the stainless steel inlet tube. Nitrogen for purging the annular space outside the reaction chamber was taken from the three-way stopcock through a bubbler. This arrangement was alright because nitrogen flow was maintained in the reaction chamber while heating only and used for maintainance of inert atmosphere in the annular space at the reaction temperature.

The set up is shown in fig. 2.1.

2-2.2 Carbon Dioxide Purification Train

Carbon dioxide obtained comercially in cylinders contained some oxygen. Purification of carbon dioxide was made by passing it through copper turnings kept in a 3 cm i.d. mullite reaction tube held at 500°C.

Carbon dioxide from the cylinder was first passed through a flow meter for measuring the flow rate. The out let from the flow meter was connected to an anhydrous $CaCl_2$ tower. The exit end of the $CaCl_2$ tower was connected to the mullite tube containing copper turnings. After removal of oxygen and moisture the gas was passed through a U-tube containing anhydrous magnesium perchlorate for removal of any moisture that might have been left.

2-3 APPARATUS FOR STUDY OF REACTION WITH MIXTURE OF FERRIC OXIDE AND GRAPHITE POWDER

Fig. 2.3 illustrates the set up.

The gas train described in Section 2-2.1 was employed in order to purify nitrogen used for flushing the reaction tube as well as the solid-electrolyte cell.

Unlike the set up for study of pellet-graphite reaction (Section 2-1), here the reaction assembly and the solid electrolyte tube were in separate furnaces. The solid electrolyte set up was the same as described in Section 2-1.4. Therefore only the reaction assembly shall be described here.

The reaction chamber was a 28 mm i.d. impervious mullite (McDanel Co., U.S.A.) Combustian tube 40 cm long with another 20 cm long narrow tube of 5 mm i.d. at one end. A water-cooled brass flange was fixed on to the wide end

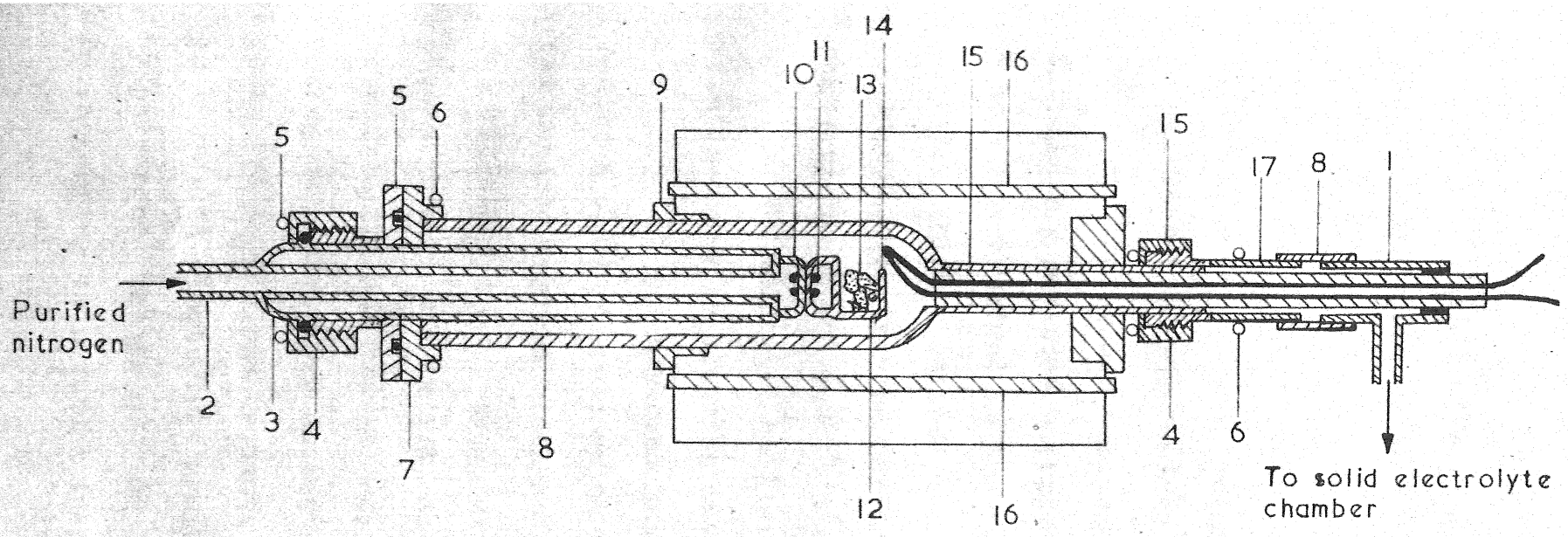

1 T-Tube
2 7mm quartz tube
3 24mm quartz tube
4 Tubing coupling
5 'O' ring
6 Water cooling coil
7 Brass flange
8 Mullite reaction tube
9 Refractory brick sleeve
10 Hook for holding
11 Nichrome wire knot
12 Silica crucible
13 Oxide / graphite pallet
14 Thermocouple bead
15 Alumina sheath
16 Globar
17 Copper tube extension
18 Polythene tube

FIG. 2·3 REACTION TUBE ARRANGEMENTS FOR POWDER MIXTURE STUDY

of the tube with the help of silicone sealant. The chamber was made gas tight by an 'O' ring kept between the inner and outer flanges. A coupling tube of 22 mm i.d. was brazed on to the outside flange through which a 22 mm o.d. quartz pusher tube could be introduced. The quartz pusher tube was joined to a 6 mm i.d. quartz tube, running throughout the length of the pusher tube and sealed at the exit end, for introducing purified nitrogen in to the reaction chamber. A hook was provided at the pushing end for holding the crucible which contained the powder mixture. By using the 22 mm o.d. quartz tube for introducing the specimen the empty space in the reaction chamber could be reduced subatantially. As indicated earlier, this is an essential precaution in order to minimize measurement lag.

It was expected that the gases comming out of the reaction chamber would be at a high temperature (perhaps a few hundred degrees centigrade). As polyethene tubing will not withstand this temperature the outlet gas was first passed through a 6 mm i.d. water-cooled copper tubing. The copper tubing was brazed onto the 10 mm water-cooled brass tubing coupling. The outlet of the copper tubing was connected to a glass T-joint. One end of the T was taken to the solid electrolyte chamber through a two-way stopcock by polythene tubing of 5 mm i.d. The thermocouple used for measuring temperature inside the reaction tube was

taken out through the other end of the T-joint. Silicone sealant was employed for sealing this end of the joint.

The reaction tube was heated in a horizontal 'Globar' rod furnace of 40 cm long. The reaction tube, pusher tube etc. were properly supported.

2-4 SET UP FOR GRAPHITE REACTIVITY STUDY

Graphite reactivity was studied by passing purified carbon dioxide over a thin bed of graphite powder loosely pressed inside an alumina crucible. Investigations were first carried out using the set up described in Section 2-1. This was to simulate the conditions of the reduction experiments. Reactivity studies were subsequently carried out employing apparatus described in Section 2-3. A few experiments were also done to determine the reactivity of graphite in a CO/CO_2 mixture.

2.4.1 Graphite Reactivity Study Using the Apparatus Described in Section 2-1

Fig. 2.4(a) shows the details of the apparatus. A 26 cm long Inconel tube constituted the reaction chamber for carrying out the reaction between graphite and purified carbon dioxide. A 12 mm o.d. transparent quartz tube introduced through the tubing coupling joint served as the inlet of carbon dioxide for the reaction chamber. The gas was passed at a rate of 2.5 litres per minute. The

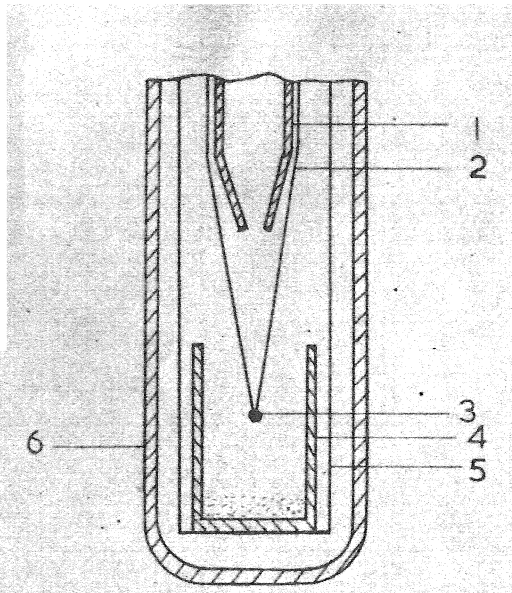

(a)

1 Silica tube 12mm
2 Thermocouple lead wire
3 Hot junction
4 Alumina crucible
5 Inconel reaction chamber
6 Silica outer tube
7 Graphite powder

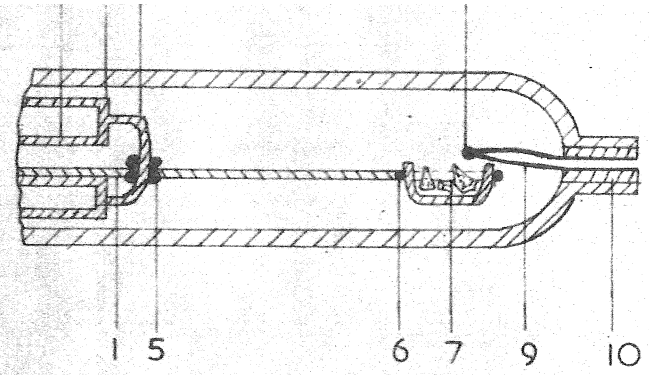

(b)

1 Nichrome wire
2 Gas inlet tube
3 Silica pushing tube
4 Hook
5 Nichrome wire knot
6 Nichrome wire ring
7 Silica crucible
8 Thermocouple hot junction
9 Thermocouple lead wires
10 Alumina sheath

FIG. 2.4 SET UPS FOR GRAPHITE REACTIVITY STUDY
(a) Vertical furnace (sec 2-1)
(b) Horizontal Globar furnace (sec 2-2)

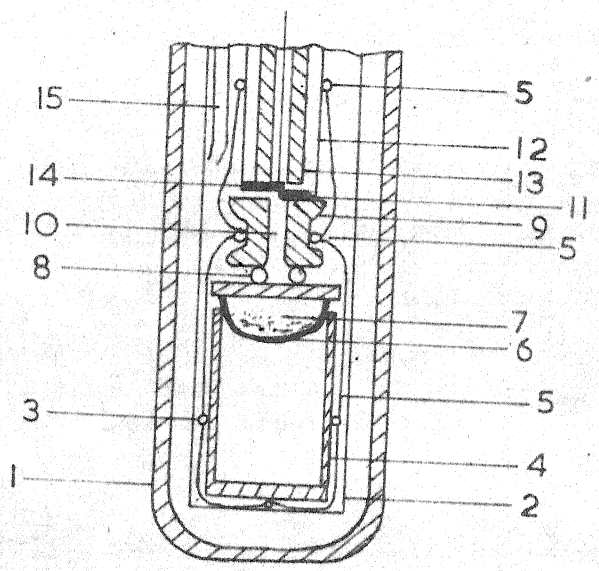

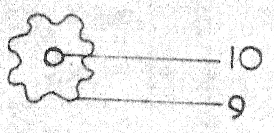

1 Silica tube
2 Inconel chamber
3 Nichrome wire knot
4 Alumina crucible
5 Nichrome wire support
6 Silica crucible
7 Graphite powder
8 Silica rod
9 Alumina supporting tube
10 Central hole in the alumina tube
11 Thermocouple bead
12 CSZ tube
13 Alumina sheath
14 Platinum bead
15 Stainless gas inlet tube

(c) Graphite reactivity study in CO / CO_2 mixture

positioning of the inlet quartz tube was adjusted so as to allow heating of carbon dioxide to the reaction temperature by the time the gas reaches graphite surfaces. A Pt/Pt - 10 Pct Rh thermocouple was introduced through the holes provided on the top flange in order to measure the temperature inside the crucible containing graphite during the course of the reaction. The hot junction of the thermocouple was about 1 cm inside the crucible.

2-4.2 Graphite Reactivity Study Using The Apparatus Described in Section 2-3

Experiments were made using this set up at various reaction temperatures. The major change in the set up was that the quartz crucible holding the graphite pellets were kept at a distance of about 10 cm from the tip of the inner tube of the pushing rod. This prevented chances of the graphite being blown off when carbon dioxide for reaction was sent in through the inner tube at a high velocity. A 10 mm dia. nickel wire was tied on to the hook of the pushing rod. The silica crucible was held on a ring made at the end of the wire. A shallow fused quartz crucible, 6 mm deep, was employed for holding the graphite. The shallow crucible was meant to prevent any lag in the diffusion of carbon dioxide to the graphite surface.

Fig. 2.4(b) shows the modification made in the set up.

2-4.3 Graphite Reactivity Study Using CO/CO_2 Mixture

The apparatus described in Section 2-1 was used for this study. The CO/CO_2 mixture was generated by passing carbon dioxide at a low velocity on to the surface of the graphite powder. Some modifications were made for ensuring the quick supply of carbon dioxide to the graphite surface. These are shown in Fig. 2.4c.

The composition of the CO/CO_2 mixture was determined using the solid oxide electrolyte described in Section 2-1.4. A 1 cm thick 14 mm o.d. and 2 mm i.d. alumina tube with a constriction at the centre was used to support the CSZ tube. The constriction at the centre was utilized for tying nichrome wire around it for hanging the crucible containing graphite powder on to the solid electrolyte tube. The graphite powder was taken in a 10 mm high, 15 mm o.d. round bottomed silica crucible blown from tube. The alumina crucible described earlier was used to support the fused quartz crucible.

Four pieces of silica rod cut to 19 mm length were tied together and kept on the silica crucible. The alumina tube supporting the CSZ tube rested on top of this. It was expected that the gas mixture generated as a result of reaction of carbon dioxide with the graphite would primarily escape through the central hole of the alumina

supporting tube. As the thermocouple bead used for contact with the gaseous electrode and electrolyte for emf measurement was kept on the top side of this hole the gas composition was supposed to be the same as that at the graphite surface.

Supply of carbon dioxide to the graphite surface rather than to the electrolyte tube surface was ensured because of the slight bend towards the Inconel tube wall given to the tip of the stainless gas inlet tube. About 8-10 grooves were made along the thickness of the alumina supporting tube for further ensuring the supply of carbon dioxide to the graphite surface.

2-5 SET UP FOR MEASUREMENTS

The following measurements were made during the reduction experiments.

(a) Emf of the solid electrolyte cell

(b) Temperature of the reaction cell

(c) Flow rates of CO and CO_2 generated as a result of reaction.

The set up used for measurement of emf has been explained in Section 2-1.4.

2-5.1 Temperature Measurement

Figs. 2.3 and 2.5 illustrate the arrangement of the thermocouples in the two reaction set ups used.

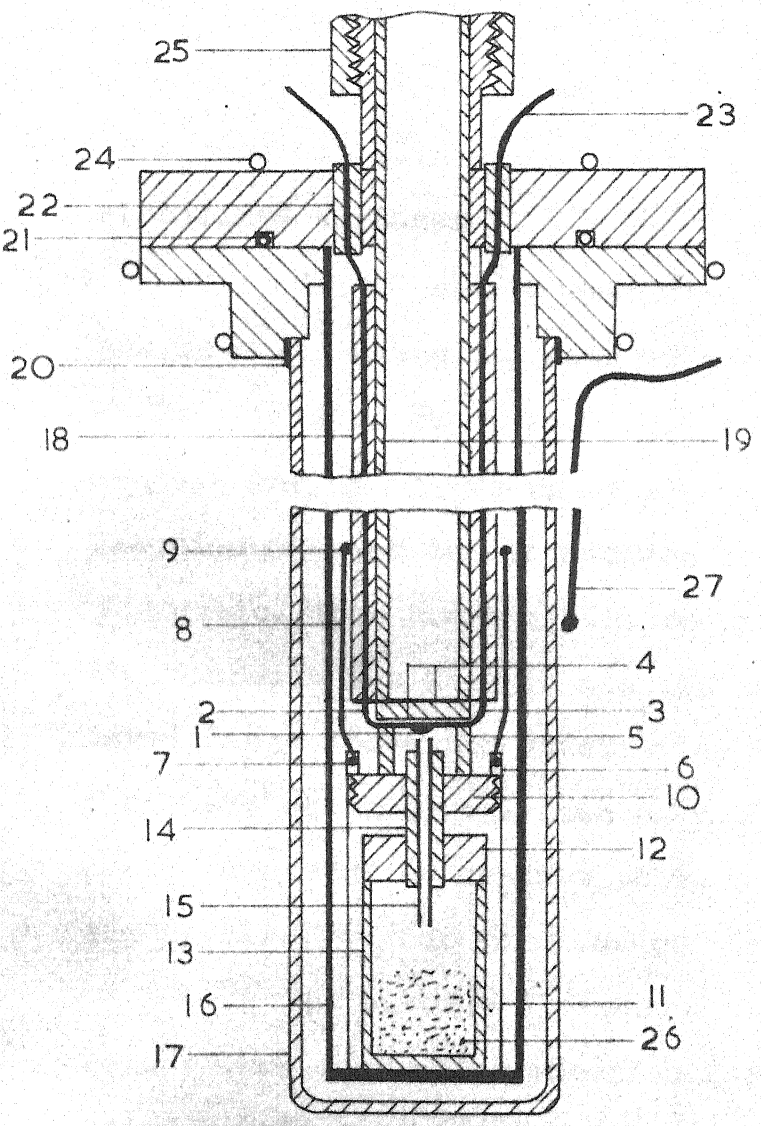

1 Thermocouple bead
2 Pt–wire
3 Pt–10 % Rh wire
4 Pt–coating
5 Alumina support
6 Hook with hole
7 Nichrome wire knot
8 Nichrome wire
9 Nichrome wire ring
10 Inconel lid
11 Inconel cell
12 Pellet
13 Alumina crucible
14 Alumina tube
15 Alumina tube
16 Inconel chamber
17 Silica tube
18 Alumina sheath
19 CSZ tube
20 Silicone sealant
21 'O' ring
22 Taffion tube
23 Thermocouple
24 Cooling coil
25 Tubbing coupling
26 Graphite powder
27 Control thermocouple

. 2·5 DETAILS OF THERMOCOUPLE ARRANGEMENT
(Pellet - Graphite system)

Temperature measurement in the reaction tube shown in fig. 2.3 was made by using a Pt/Pt-10 Pct Rh thermocouple. The hot junction of this thermocouple was placed above the crucible carrying the reactants. The furnace temperature in this case was maintained constant by supplying a constant stabilized voltage.

In the set up described in Section 2-1, temperature was measured using two sets of thermocouples both made from Pt/Pt - 10 Pct. Rh wires. Fig. 2.5 illustrates the arrangements. One of the thermocouples was kept outside the reaction chamber and in between the mullite furnace tube and the silica tube covering the reaction chamber. The other thermocouple was kept inside the reaction chamber and immediately above the reaction cell. The latter had a large flat bead which served both as hot junction for temperature measurement and as contact between the gaseous electrode and the electrolyte for emf measurement.

The outside thermocouple was connected to the temperature controller (Section 2-1.1) whereas the inside thermocouple was used for measuring instantaneous temperature during the course of the reaction.

2-5.2 Set Up for Measurement of Flow Rates of Gases Generated During Reduction Reaction

Capillary flow meters were designed and fabricated to measure flow rates of the product gases of

reaction. Reaction rates in the experiments with graphite and Fe_2O_3 pellet kept in separation were much less compared to those with the powder mixtures of Fe_2O_3 and graphite. The flow meter designed for these experiments could measure flow rates of about 1 cc per minute very accurately.

A 2.5 meters long and 1 mm bore capillary tube was coiled by glass blowing. A 22 gauge nichrome wire was introduced through the capillary so as to reduce the cross-section of the latter. This helped to make the flow meter more sensitive. The capillary coil was kept immersed in a thermos flask containing water. This was done in order to minimize irreproducibility in measurements resulting from thermal convection in the capillary at such low flow rates. Temperature of the water bath was measured with a thermometer.

The capillary was connected to a manometer with dibutyl phthalate as the liquid by polythene tubing. The flow meter was calibrated with nitrogen. Viscosity correction for CO/CO_2 gas mixture were made while computing flow rates.

The second capillary used for measuring the flow rates in reaction studies on powder mixtures was made in a similar manner as described above, the only difference being that the latter was designed to measure higher flow rates (80 cc per minute maximum).

The outlet gases from the solid electrolyte chamber was taken to the flow meter through a bubbler.

The bubbler was used to prevent air from the atmosphere to enter into the reaction chamber.

2-6 SOLID ELECTROLYTE CALIBRATION SET UP

The solid electrolyte tube used for monitoring the instantaneous gas composition was calibrated using a hydrogen-water vapour mixture. The set up was similar to the one used by Basu[50] for gas equilibration experiments.

A mixture of hydrated and anhydrous oxalic acid was chosen for generating controlled hydrogen-water vapour mixture. The hydrated acid decomposes as shown in equation (2-1).

$$(COOH)_2 \cdot 2H_2O = (COOH)_2 + 2H_2O \qquad (2\text{-}1)$$

The equilibrium partial pressure of water vapour (p_{H_2O}), which the ambient gas in contact with the mixture develops, was determined by Baxter and Lansing[51] as a function of temperature as:

$$\log p_{H_2O}\ (mm) = 18.053 - \frac{9661}{T + 250}\ ,$$

$$273.2 \quad T \quad 323.2°K \qquad (2\text{-}2)$$

A.R. Grade oxalic acid dihydrate was mixed with 10 Pct. anhydrous oxalic acid in a porcelain mortar. The mixture was ground to a fine powder and filled inside a series of glass U-tubes compactly blown together into one

assembly. This assembly was subsequently placed inside a constant temperature water bath. The temperature of the water bath could be controlled to $\pm 0.1^{\circ}C$ using a mercury expansion relay. Inside the water bath the temperature remained uniform throughout because of mechanical stirring. Oxygen and moisture free hydrogen gas was passed through this U-tube and the resulting H_2O/H_2 mixture was introduced into the solid electrolyte chamber via a three-way stop cock. Depending on the temperature of the water bath, the hydrogen gas flowing through the moisture generator develops a definite water vapour partial pressure.

CHAPTER 3

MATERIALS AND EXPERIMENTAL PROCEDURE

Preparation of materials used for the reduction experiments as well as for graphite reactivity and the procedure involved in the experiments are discussed under two main headings.

3-1 MATERIALS PREPARATION

3-1.1 Starting Materials

The following basic raw materials were used in the experiments.

Ferric Oxide (Fe_2O_3)	:	Fisher certified reagent grade, Fisher Scientific Co., U.S.A.
Graphite	:	Low ash, graphite electrode (imported)
Oxalic Acid Dihydrate ($(COOH)_2 \cdot 2H_2O$)	:	Analytical reagent grade, British Drug House, Bombay, India

3-1.2 Preparation of Ferric Oxide Powders and Pellets

Ferric Oxide powder was first dried in an oven at 150°C for 48 hours and screened to -325 mesh size using a sieve shaker. As it was found that the fine particles of Ferric Oxide stick to the surface of the screen, the

procedure followed was to put ceramic balls of about 6 mm size into the screen along with iron oxide powder during screening. The balls subjected the screen to impact and vibration. The ceramic balls were first cleaned in water and then in acetone. They were then heated to 250°C for 48 hours. The screen used was cleaned in water using Fisher Ultrasonic Cleaner, U.S.A., then dried in the oven for 24 hours and finally cleaned with acetone.

A steel die and punch assembly was fabricated to prepare ferric oxide pellets. The ferric oxide powder of -325 mesh size was mixed thoroughly using an agate mortar and pestle. Samples weighing 2.5 grams each were packed in paper. Each paper packet was kept in the moisture oven for 8 hours. Pellets were then made from each sample. This modified procedure was followed as it had been found in the initial trials very difficult to remove the pellet from the die after it was pressed. The presence of moisture in the fine ferric oxide powder made it stick to the surface of the die.

The die had an internal bore of 18.5 mm. The die size had to be exact as the fired pellet had to be bigger than 15.3 mm and smaller than 17 mm. This restriction on the size of the pellets was necessary in order to make them sit properly on the top of the alumina crucible containing graphite powder placed inside the inconel reaction cell.

A few pellets were made in the beginning without a hole at the centre. As it was difficult to collect gas samples from the inner space between the oxide pellet and graphite powder, it was decided to make pellets with holes at the centre. Thus the die design was modified accordingly. A 2 mm dia. 6 mm thick elevated portion was machined at the centre of the bottom plunger. The top plunger had a central hole of 2.5 mm dia drilled through and through.

A hydraulic press operated by hand was used for pressing the pellets. The pressure applied was 3000 psi. The plunger was taken out slowly by applying gentle pressure so as to avoid breakage. Pellets were removed from the die plunger using a sheet of paper and transferred on to a 10 cm x 10 cm zirconia plate. About 12 pellets were made at a time and fired in a Globar muffle furnace. The furnace was heated slowly to the firing temperature and held there for 2 hours and then slowly cooled. Firing temperatures of 925°C and 1100°C were chosen for making porous and dense pellets respectively. Rate of heating and cooling of the furnace was 60°C to 70°C per hour.

A 3 mm drill bit was used for imparting the final size to the central hole. Then the pellet surface was cleaned with acetone. It was not possible to make holes on the dense pellets using a drill bit as the pellet

was very hard and brittle. A round diamond file was employed for this purpose. The pellets were stored in a desiccator.

3-1.3 Preparation of Small Spherical Pellets of Ferric Oxide

Small amounts of -325 mesh particles of ferric oxide were taken in a watch glass and mixed with distilled water using a stainless steel spatula. Portions of the moist ferric oxide was picked up at the tip of the knife. Small amounts were taken from this and pellets were made by hand. An alumina boat containing the pellets was kept at the low temperature zone of a horizontal tube furnace for a few hours and then slowly introduced into the hot zone kept at 925°C. After firing the pellets for two hours the alumina boat was slowly withdrawn to a lower temperature zone and cooled to room temperature.

3-1.4 Preparation of Graphite Powder

A 5 cm dia. graphite rod was machined on a lathe for making coarse graphite powder. Precautions were taken to avoid contamination from the machine. This was then ground to finer sizes using a porcelain mortar and pestle. The fine graphite powder was next screened to - 200 + 230 mesh size using USS screens, and stored carefully. Magnets did not reveal inclusion of iron particles.

3-1.5 Preparation of Graphite Pellets

Graphite reactivity studies were made using graphite powder as well as graphite pellets.

-200, +230 mesh graphite powder described in Section 3-1.4 was used for making pellets. Pellets weighing about .5 grams each were made in a 20 mm die at a pressure of about 50 psi. These pellets were kept in the oven for drying till constant weights were obtained. Each pellet was broken to three or four pieces and these pieces were used for reactivity study.

3-1.6 Preparation of Powder Mixture of Ferric Oxide and Graphite

Twentyfive grams of ferric oxide and 10 grams of -200, +230 mesh particles of graphite were mixed thoroughly in a glass dish, and then mixed further in an agate mortar and pestle. This mixture was then carefully transferred into a glass bowl so as to avoid any segregation of graphite and ferric oxide and then stored in a desiccator. Small samples were taken from the powder mixture and pellets were made at approximately 50 psi pressure. The pellets were then broken into smaller pieces and used for studies.

3-2 EXPERIMENTAL PROCEDURE

There were three main sets of experiments concerning the following.

(i) Reaction between ferric oxide pellet and graphite powder with known distances of separation between them.

(ii) Reaction of powder mixtures of ferric oxide and graphite, and

(iii) Reactivity of graphite powder.

These are discussed below separately.

Calibration of the solid electrolyte tube is discussed in another separate heading. Some experiments were also performed on the identification of phases in the reduced sample. A discussion on this also has been included.

3-2.1 Experiments with Separated Ferric Oxide Pellet and Graphite Powder

The set up is illustrated in figs. 2.1, 2.2 and 2.5.

Porous pellets of iron oxide with a 3 mm central hole were prepared and stored in a desiccator as described earlier. One pellet was taken out from the lot and the diameter and thickness were measured at different locations using a Vernier callipers. Average of these values were taken as the real dimensions. The pellet was then kept in

an oven for 8 hours in order to remove any moisture that might have been picked up by it while handling. It was cooled in a desiccator and weighed in a single pan semi-micro balance.

The 3 mm o.d. alumina tube containing the 1.5 mm o.d. alumina gas outlet tube was introduced through the central hole of the pellet. Length of the alumina tubes were determined according to the distance of separation between the graphite surface and the pellet so as to give a clearance of about 1 to 2 mm between the top surface of graphite and the tip of the alumina tube. The other end of the alumina tube projected out through the central hole provided in the Inconel lid of the reaction cell. The tube was held tightly by the lid by making clearance between the tube and the hole in the lid of the reaction cell as small as possible. Weight was determined again with the lid, alumina tube and the iron oxide pellet in position.

Graphite powder kept in the bottle was mixed well and about 10 grams were taken on a clean watch glass, and kept in an oven for 24 hours for removal of moisture. The watch glass along with the graphite was then cooled in a desiccator.

A recrystallised alumina crucible (15.3 mm i.d.) was cleaned and heated in the oven to remove moisture adhering onto the surface. After cooling it inside a

desiccator the weight was determined in semi-micro balance.

The moisture free graphite was taken out of the desiccator and mixed well. About 1.5 grams of this was taken out, weighed and then transferred into the weighed alumina crucible carefully so as to avoid any segregation of the particles as well as adherence of graphite onto the walls of the crucible. The graphite in the crucible was mixed well using the stainless steel knife so as to ensure uniform distribution of the graphite particles throughout.

A brass rod machined to give a good fit inside the crucible was employed in order to press the graphite powder in the crucible uniformly. Any loose particles of graphite remaining in the crucible was removed by tilting the same. Graphite particles adhering to the surface of the crucible was removed by using a piece of cotton wet in acetone.

The brass rod used for pressing the graphite had a piece of graph paper pasted along its length and covered by cellophane tape. This helped in finding out the level of graphite surface inside the crucible accurately.

The alumina crucible with the graphite was kept in an oven for a few hours again and after cooling in a desiccator the weight of the crucible and graphite was determined by semi-micro balance. The alumina crucible was then placed inside the moisture free Inconel crucible of the reaction cell. This assembly was then weighed accurately.

The lid of the Inconel crucible holding the 3 mm alumina tube and iron oxide pellet was screwed into the Inconel crucible containing the alumina crucible with graphite. Vertical positioning of the pellet on the alumina tube was such that the pellet rested on the alumina crucible when the lid was tightened.

Two pieces of 22 gauge nichrome wires were tied on to the two hooks provided on the lid of the Inconel reaction cell. The wires were insulated from electrical contact with the platinised surface of the solid electrolyte tube with 1.5 mm o.d. alumina sheath. A 6 mm long and 9 mm dia alumina tube was placed on the lid surrounding the gas outlet tube as support for the CSZ tube.

The solid electrolyte tube (platinised and tested for electrical continuity as described in Section 2-1) was inserted through the tubing coupling. Next the tubing coupling was tightened so as to tightly hold the solid electrolyte tube in position. The top flange with the solid electrolyte tube was then held firmly by the holder above the furnace described in Section 2-1. Assembling of the cell etc. were done in this position and is described below.

A Pt/Pt - 10 Pct Rh thermocouple with a large bead at one end served as thermocouple as well as the lead for emf measurement. The thermocouple was annealed and standardised against a standard Pt/Pt - 10 Pct Rh

thermocouple supplied by Engelhardt Inc., U.S.A. Thermocouple wires were insulated by 1.5 mm o.d. alumina sheaths which were taken out of the reaction chamber through holes in the top flange. 1.5 mm o.d. teflon tubes were used as insulation against electrical contact between the thermocouple wires and the brass flange. The alumina sheaths covering the thermocouple wires were tied firmly on to the solid electrolyte tube with 22 gauge nichrome wire.

Reaction cell with all the fixtures was hung from the solid electrolyte tube and tied firmly to it using a 32 gauge nichrome wire. The reaction chamber was cleaned well by acetone before each experiment. Solid electrolyte assembly was then introduced in to the reaction chamber and the two flanges were screwed tightly. The holes on the flange with teflon tube insulation and thermocouple wires were sealed using silicone sealant. The reaction chamber with the reaction cell and the solid electrolyte set up was then flushed with purified nitrogen at the rate of about 10 cc per minute. Heating rate of the furnace was controlled by controlling the voltage input to the furnace. Great care was exercised in heating the furnace as the solid electrolyte tube was liable to crack at high heating rates. The rate was kept within 50°C per hour for this reason.

A capillary manometer was connected to the gas outlet tube and temperature of the capillary thermostat was

recorded. Nitrogen flushing of the reaction chamber was continued till the furnace reached a temperature of about 800°C. After that the flow was diverted to the annular space outside the Inconel tube only.

Thermocouple wires coming out of the reaction chamber were taken to the cold junction thermostatic bath using compensating lead wires, and emfs were measured by millivolt potentiometer (model 8686 Leeds and Northrup).

The temperature, the emf of the solid electrolyte cell as well as the flow rate of product gases from the reaction chamber were monitored at intervals of five minutes or 15 minutes. In the beginning when the reaction rate as well as the gas composition changed rapidly measurements were made at intervals of 5 minutes. Later on when the reaction rate as well as the gas composition became steady the time interval for measurements were 15 minutes.

After the reactions were over which was indicated by the virtual cessation of flow of the CO/CO_2 gases, cooling was started under flowing nitrogen at a rate of 50°C to 70°C per hour.

After the chamber had cooled to room temperature the solid electrolyte assembly was taken out and hung from the holder, fixed above the furnace, as mentioned earlier. Reaction cell was detached from the solid electrolyte tube and the Inconel lid was removed slowly by unscrewing. The

pellet was detached from the alumina tube and weighed. In cases where the pellet was sticking it was weighed with alumina tube and the latter was then weighed separately.

Inconel crucible with alumina crucible and graphite was weighed. Then the alumina crucible along with graphite was taken out of the Inconel crucible and weighed again. Graphite was pressed using the brass rod and the level was determined.

The dimensions of the iron oxide pellet after reaction were measured using a Vernier callipers.

Carbon deposition is a problem in studies of this kind. Here it was not expected much due to presence of appreciable concentration of CO_2 in CO. This was verified by visual inspection as well as weighing of Inconel crucible and reaction chamber and was found to be negligible.

3-2.2 Studies on Powder Mixtures of Ferric Oxide and Graphite

The experimental arrangement is shown in fig. 2.3.

About 2 to 3 grams of the mixture explained in Section 3-1.5 was taken on a clean watch glass and mixed thoroughly using a stainless steel knife. This was then carefully transferred to a 15.3 mm i.d. moisture free and weighed alumina crucible so as to avoid any segregation of iron oxide and graphite. After mixing the mixture thoroughly once again inside the crucible it was pressed by hand using

a brass rod which fitted tightly inside the crucible and kept in an oven for a few hours. The crucible with the powder mixture was removed from the oven and cooled in a desiccator. Weight of the powder mixture along with the alumina crucible was then determined using a semi-micro balance.

Globar furnace was heated to a constant temperature by a constant supply of stabilized voltage. The quartz pushing tube discussed in Section 2 was held in position using a stand support for introduction into the mullite reaction tube. Alumina crucible with the powder mixture was tied on to the hook of the pusher tube. The pusher tube alongwith the crucible was then introduced into the reaction tube through the tubing coupling. The crucible was kept in the low temperature zone of the tube and the tubing coupling was tightened. Purified nitrogen was passed through reaction tube at about 20 cc per minute. The nitrogen came out of the tube at the other end which was connected to the solid electrolyte chamber. Gas from the solid electrolyte entered into the capillary and then escaped to the atmosphere.

After passing nitrogen for about 10 minutes the tubing coupling was loosened and the pusher tube with the alumina crucible was slowly pushed to the end of the reaction chamber. Temperature of the reaction tube, and solid electrolyte chamber were measured. The emfs and flow

rates were monitored. The measurements were continued at an interval of either 2 minutes, or one minute. At low temperatures the reaction rates were slow and thus the measurements were taken at 2 minutes intervals. At high temperatures the measurements were done at one minute interval as the rate of reaction was fast.

End of the reaction was judged by the cessation of gas evolution as indicated by the flow meter. The pusher tube along with the reaction crucible was then withdrawn to the colder region of the reaction tube and held for about half an hour. Nitrogen flow was started and inert atmosphere maintained during cooling. The reaction tube was opened and the crucible with contents were weighed accurately. Total weight loss of the reactants were obtained from the difference of the initial and final weights.

3-2.3 Graphite Reactivity Studies

Graphite reactivity was determined with three sets of experiments.

Set I : With graphite powder in pure carbon dioxide using the vertical furnace and set up described in Section 2-4 and fig. 2.4(a). This was done so as to simulate the experimental arrangement for pellet/graphite reaction studies.

Set II : With thin pellets of graphite in pure carbon dioxide in the horizontal Globar furnace described in Section 2-4 and fig. 2.4(b). These studies were taken up due to the irreproducibility of results of experiments in Set I.

Set III: With graphite powder in CO/CO_2 mixture using the set up shown in fig. 2.4c.

3-2.3.1 Reactivity Study Using Pure Carbon Dioxide - Set I

Room temperature studies were conducted with a CO_2 flow rate about five to six times larger than that of the actual flow rate in order to check whether there was any ejection of graphite due to the high velocity of CO_2. The distance between CO_2 outlet and graphite surface was kept the same as that in actual experiment. The distance of separation was 10 cm. Weight of graphite before and after passing carbon dioxide was determined using the Aisenworth semi-micro balance. The weight remained the same at room temperature even when the gas flow was continued for 20 minutes. This ensured that the graphite was not being blown off during reaction by the high velocity CO_2.

About 10 grams of -200, +230 mesh graphite powder was taken in a glass dish and kept in the oven till constant weight was obtained. 0.2 to 0.3 gram samples of

this were taken in an alumina crucible, of 15.3 mm i.d., previously heated for constant weight. The graphite was pressed inside by hand with a brass rod. The crucible carrying graphite was supported by a nichrome wire basket and was tied to the silica tube used as CO_2 inlet. The reaction chamber was heated under purified nitrogen and temperature measurements were made using a Pt/Pt - 10 Pct Rh thermocouple placed at a distance of about 1 cm from the graphite surface.

Pure CO_2 was introduced into the reaction chamber through the 12 mm silica tube whose tip was kept 5 cm above the graphite surface. The rate of CO_2 measured at room temperature was about 2.5 litres per minute. Carbon dioxide was passed for about 5 to 10 minutes. After stopping the flow of CO_2, nitrogen was passed at a rate of about 1.5 litres per minute for a few minutes so as to flush out all the residual CO_2 present inside the reaction chamber. Cooling of the furnace was also started side by side. A nitrogen flow of about 200 cc per minute was continued till the furnace was cooled to room temperature. The crucible was taken out and the weight determined using a semimicro balance. The difference between the weights before and after the reaction was divided by the reaction time to determine the rate.

3-2.3.2 Reactivity Study Using Pure Carbon Dioxide - Set II

Due to the irreproducibility of the results in set I, it was decided to conduct the experiments in flowing carbon dioxide in a horizontal furnace. The main drawback of the experiments in set I was that the CO_2 gas was not flowing across the sample. Also the presence of the inconel chamber could adversely affect the reaction.

Figs. 2.3 and 2.4b show the experimental set up. A shallow silica crucible about 1 cm in depth and about 20 mm dia. held the graphite pellets. The pellets were prepared under very low pressures as discussed in Sec. 3-1.5. The pellets were broken and a few pieces were taken for each experiment. The broken pellets along with the silica crucible were heated in the moisture oven till constant weight was obtained. A 16 gauge Nickel wire with a ring at the end for holding the silica crucible was tied on to the book of the pusher tube. About 5 cm length of the wire was extending out from the tip of the pusher tube. This arrangement was necessary for preventing the blowing off of the graphite pellet by the high flow rate of CO_2. As the reaction tube was much bigger in dia. (35 mm) as compared to the passage of the pusher tube, the velocity was not sufficient to blow off the graphite particles kept at about 5 cms from the exit of the control tube.

The crucible along with the graphite was kept at a low temperature zone of the furnace first and purified nitrogen was passed to flush out the entrapped air. The crucible was then pushed to the constant temperature zone of the reaction furnace. The reaction chamber was then connected to the gas train by means of the three way stop cock. The flow rate of carbon dioxide was maintained at about 2 litres per minute. At the end of the period of reaction the chamber was flushed with nitrogen. The crucible was pulled out to the cooled zone of the furnace and kept in the nitrogen atmosphere till the sample was sufficiently cool. The reaction chamber was then opened and the crucible was taken out, kept in a desiccator and weighed afterwards.

Experiments were carried out at three temperatures mainly. Four experiments were done at each temperature.

3-2.3.3 Graphite Reactivity in CO/CO_2 Mixture - Set III

A few experiments were conducted in CO/CO_2 mixture. They were done in the set up described in Sec. 2-1 with the modifications shown in Fig. 2.4c.

Shallow silica crucibles of about 1 cm height and 12.5 mm dia. were made. Four silica rods 3 mm dia. and 12.5 mm long were fastened to the top of the crucible.

The crucible along with the graphite pellets weighed accurately was then fastened to the alumina crucible described earlier (Sec. 2-1.4). This was then tied on to the CSZ tube as explained earlier (Secs. 2-1.4 and 3-2.1).

The furnace along with the CSZ tube and the crucible containing graphite was heated slowly to the reaction temperature under purified nitrogen atmosphere. Purified CO_2 was introduced after the reaction temperature had been attained.

CO/CO_2 ratio was monitored by a solid oxide electrolyte cell. The ratio was kept constant by controlling the flow rate of CO_2. The reaction was continued for about 10 to 20 minutes. After that CO_2 flow was stopped and N_2 was introduced into the chamber. The furnace was cooled under nitrogen atmosphere. The crucible with graphite was taken out and weighed for determining the reaction rate.

3-2.4 Calibration of Solid Oxide Electrolyte Tube

Calibration of solid oxide electrolyte tube was done by using a gas mixture of known oxygen potential.

Hydrogen-water vapour mixture was used for this purpose. The set up has been described in Sec. 2-6. When hydrogen is passed over a mixture of hydrated and anhydrous oxalic acid, the ambient gas picks up water vapour and

under certain conditions the process attains equilibrium. The equilibrium relationship given by Baxter and Lansing.[51]

$$\log p_{H_2O}\ (mm) = 18.053 - \frac{9661}{T + 250},$$

$$273.2 \leq T \leq 323.2°K.$$

Therefore depending upon the temperature of the water bath, the hydrogen gas flowing through the moisture generator would develop a definite water vapour partial pressure. The H_2O/H_2 mixture thus generated was then passed through the inconel chamber containing the solid oxide electrolyte tube. Both the temperature and the EMF at the point of contact between the platinum lead wire and the solid oxide electrolyte surface, coated with platinum paste was recorded. The reference electrode was air.

Two different oxygen potentials were maintained by using two bath temperatures. At each bath temperature the temperature of the CSZ cell was varied and EMF recorded at several cell temperatures.

3-2.5 Identification of Phases

Attempts were made to examine the phases present in the partially reduced oxide pellets. As the pellets were very fragile it was found difficult to do micro-structural analysis.

Layers of the pellet from the bottom, middle, perifery and top portions were taken out with the help of a diamond file and oxidised at about 850°C till constant weights were obtained. The difference in the weights of each layer before and after oxidation was taken as an indication of the extent of reduction and the nature of the oxide phase.

CHAPTER 4

RESULTS ON OXIDE PELLET-GRAPHITE POWDER REACTION

Extensive calibration of the measuring equipments had been undertaken. The results of these calibration shall be presented first. Amongst all the experiments carried out the principal series dealt with the situation where iron oxide was in tablet form and some distance of separation was maintained between the oxide tablets and graphite powder.

In addition several auxilliary investigations were also carried out in order to have a better understanding of the reaction. In this chapter only the results of the principal series of investigation shall be presented. Those pertaining to the auxilliary experiments shall be presented in the next chapter.

4-1 CALIBRATION

The microvoltmeter used for measuring the EMF of the solid solid electrolyte cell, the capillary flowmeters employed for measurement of the flow rates of the product gases and the CSZ cell used for determination of composition of the evolved gases were calibrated. The results are presented here under separate headings.

4-1.1 Microvoltmeter

The microvoltmeter employed for measuring the EMF of the solid oxide electrolyte cell was calibrated against potentiometer, ~~as discussed in Section 3-3.2.~~ Calibration was done a number of times mainly for the range of EMF which was encountered in the present investigation.

Linear least square data fitting technique was adopted to obtain the correlation between the voltage indicated by the microvoltmeter (V_i) and the correct voltage as indicated by the potentiometer (V). The correlation is as follows.

$$V = 1.129\ V_i - 0.0594 \qquad (4\text{-}1)$$

where the values are in volts.

Figure 4.1 shows the calibration curve.

4-1.2 Capillary Flowmeter

The capillary flowmeters discussed in Section 2-5.2 were used for measuring the flow rates of gases evolved during the reduction experiments. They were calibrated against nitrogen using a soap bubble meter.

Linear least square lines were obtained correlating the flow rate of nitrogen (Q, cc (NTP)/sec.) and the height of rise of the fluid in the open end of the manometer tube (h, cm.). The equations of the lines were:

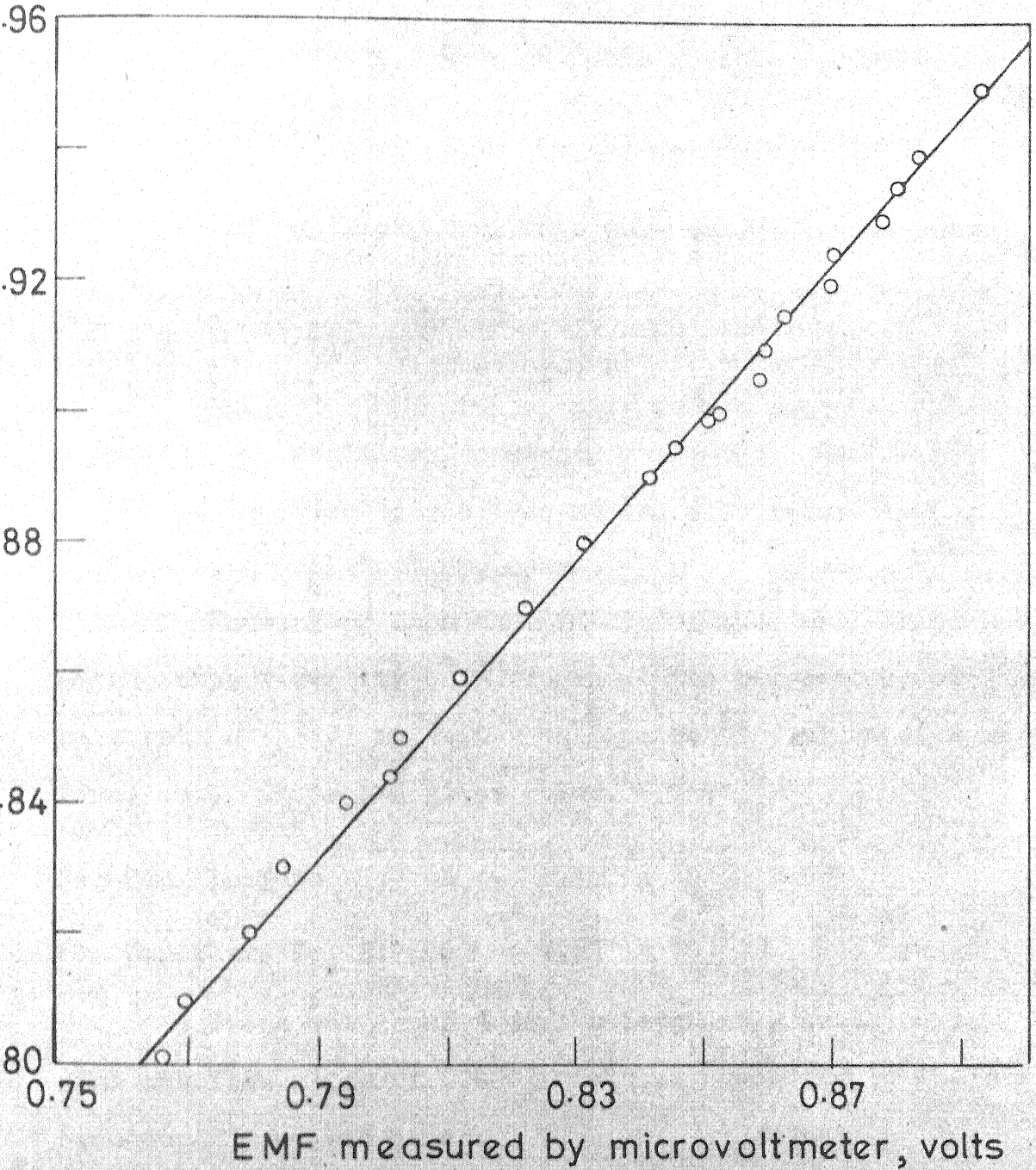

FIG. 4·1 CALIBRATION CURVE FOR MICROVOLTMETER

for capillary No. 1: $Q = 0.00535 \times \Delta h - 0.000974$

for capillary No. 2: $Q = 0.04976 \times \Delta h - 0.01061$ (4-2)

The capillary constants were calculated as shown below:

$$A = \frac{Q}{\Delta h} \cdot \mu \qquad (4\text{-}3)$$

where, A = capillary constant

and μ = viscosity of gas at the temperature of calibration, poise.

Knowing $\frac{Q}{\Delta h}$ from eqn. (4-2) for the capillaries and noting that viscosity of nitrogen at the temperature of calibration (33°C) is 1.80×10^{-6} poise[52] values of A were found out. These are given below.

For Capillary No. 1: $A = 8.550 \times 10^{-7}$

For Capillary No. 2: $A = 7.51 \times 10^{-6}$

These values of A were subsequently employed to find the flow rates of CO-CO_2 mixtures according to the procedure described later.

4-1.3 Solid Oxide Electrolyte Cell

The performance of the CSZ cell was checked against a known oxygen potential, which was generated by passing

hydrogen over a mixture of anhydrous oxalic acid and oxalic acid dihydrate (Section 2-6 and 3-3.1).

Two different oxygen potentials were generated by keeping the oxalic acid mixture at two different water bath temperatures. P_{H_2O}/P_{H_2} ratio corresponding to each bath temperature was calculated using the following empirical formula given by Baxter and Lansing.(51)

$$\log p_{H_2O}\ (\text{mm. Hg}) = 18.053 - \frac{9661}{T + 250}\ ,$$

$$273.2 \leq T \leq 323.2°K \qquad (4\text{-}4)$$

Since, $p_{H_2O} + p_{H_2} = 760$ mm. Hg

$$p_{H_2O}/p_{H_2} = p_{H_2O}/(760 - p_{H_2O}) \qquad (4\text{-}5)$$

p_{H_2O}/p_{H_2} ratios obtained from eqns. (4-4) and (4-5) were compared with those calculated from the EMF of the CSZ cell. The calculation procedure was as follows.

$$2H_2(g) + O_2(g) \rightleftharpoons 2H_2O(g), \qquad \Delta G^\circ_H \qquad (4\text{-}6)$$

$$\Delta G^\circ_H = - RT \ln K_e$$

$$= - 2.303\ RT \log \frac{p^2_{H_2O}}{p^2_{H_2} \cdot p_{O_2}} \qquad (4\text{-}7)$$

$$\text{or,} \quad \frac{1}{2}\log p_{O_2} = \frac{\Delta G_H^\circ}{2 \times 2.303\ RT} + \log \frac{p_{H_2O}}{p_{H_2}} \qquad (4\text{-}8)$$

$$\text{Again,} \quad 2.303\ RT \log \frac{p_{O_2}}{p^r_{O_2}} = -ZFE \qquad (4\text{-}9)$$

where $p^r_{O_2}$ = p_{O_2} of the reference electrode

= 0.21 atm. for air

Z = Number of electrons taking part in the cell reaction

= 4

F = Faraday's constant

= 23,060 cals/volt. gm. equiv.

E = EMF of the cell in volts

$$\text{or,} \quad \log p_{O_2} = -20.159\ \frac{E}{T} - 0.678 \qquad (4\text{-}10)$$

The values of E and T of the CSZ cell for these experiments are presented in table 4.1. From E and T, p_{O_2} were calculated with the help of the eqn. (4-10). Putting these values of p_{O_2} in eqn. (4-8), p_{H_2O}/p_{H_2} were calculated.

ΔG_H° values were interpolated from the data given by Elliott and Gleiser[53] (table 4.2).

Results of p_{H_2O}/p_{H_2} ratios (eqns. (4-4) and (4-5)) obtained from the empirical formula as well as from

Table 4.1 Performance of Solid Oxide Electrolyte Cell

Reference electrode : air

Flow rate of Hydrogen = 25 to 30 cc per minute

Serial No.	Temp. of water bath, °K	p_{H_2O}/p_{H_2} from formulae$^{\oplus}$	Temp. of CSZ cell °K	EMF of CSZ cell volts* (corrected)	p_{H_2O}/p_{H_2} from EMF
1	318.8	0.0156	1193	1.114	0.0144
2	318.8	0.0156	1193	1.114	0.0144
3	318.8	0.0156	1242	1.108	0.0146
4	318.8	0.0156	1246	1.108	0.0146
5	318.8	0.0156	1246	1.108	0.0146
6	318.8	0.0156	1270	1.103	0.0153
7	318.8	0.0156	1271	1.103	0.0153
8	318.8	0.0156	1272	1.103	0.0155
9	322.8	0.0207	1265	1.087	0.0207
10	322.8	0.0207	1263	1.089	0.0200
11	322.8	0.0207	1208	1.095	0.0199
12	322.8	0.0207	1206	1.095	0.0199

$\oplus$ $\frac{p_{H_2O}}{p_{H_2}}$ calculated from $(COOH)_2.2H_2O$–$(COOH)_2$ equilibrium.

* EMF values were read in microvoltmeter. These readings were corrected by considering calibration of microvoltmeter against potentiometer.

Table 4.2 ΔG_H^o Values for Formation of H_2O from H_2 and O_2 at Various Temperatures[53]

Temperature °K	ΔG_H^o cals/mole of H_2O
800	-48,640
900	-47,350
1000	-46,030
1100	-44,700
1200	-43,360
1300	-43,360
1400	-40,640

calculations using the EMF values of the CSZ cell are given in table 4.1.

4-2 REACTION OF OXIDE PELLET WITH GRAPHITE POWDER IN SEPARATION

The set up used for this investigation and the procedure adopted have been discussed earlier in Sections 2-1 and 3-2.1.

Rate of evolution of product gases of reaction was obtained from the difference in the manometer fluid levels of the capillary flowmeter (Δh) taken at intervals of 5 or 15 minutes. Five minutes interval was chosen for the early stages of reaction when the change in rate was very rapid. As the reaction approached the steady state the change in gas evolution rate was sluggish. Then the readings were taken only at 15 minutes interval.

Temperature (T) and EMF (E) of the CSZ cell were also noted almost simultaneously when the manometer readings were taken. These constituted the three basic data from which the gas composition, instantaneous reaction rates and cumulative weight losses were calculated.

A number of experiments were carried out using porous as well as dense iron oxide pellets and graphite powder. The experimental conditions are given in table 4.3.

Table 4.3 Experimental Conditions for Ferric Oxide Pellet-Graphite Powder Reactions

Oxide Particle Size = -325 mesh, Theoretical Density = 5.25 g/cc
Graphite Particle Size: 0.0062-0.0074 cm, (-200, +230 mesh)
Theoretical Density of Graphite = 2.25 g/cc

Expt. No.	Distance of separation, cm.	Weight of graphite, gms.	Temp., °C	pct. CO at steady state (region III)	Oxide Pellet				
					Weight, gms.	Dia, cm.	Thickness, cm.	Density, gms/cc	Porosity
7	1.67	1.0273	1001	82.6	3.9198	1.72	0.63	2.68	0.49
9	1.65	1.0454	1007	85.0	3.7332	1.72	0.60	2.68	0.49
14	0.80	1.5388	1018	87.2	1.7795	1.73	0.28	2.67	0.49
17	1.60	1.5472	956	84.0	1.9162	1.67	0.29	2.99	0.43
18	1.60	1.5545	1017	85.2	4.1020	1.62	0.66	3.02	0.42
19	1.60	1.5449	883	82.6	1.8671	1.68	0.29	2.99	0.43
20	1.60	1.5440	926	88.1	1.8423	1.65	0.30	2.87	0.45
21	1.60	1.5434	951	87.7	1.8411	1.64	0.30	2.91	0.45
22	1.60	1.5422	956	87.9	1.8147	1.64	0.30	2.87	0.45
23	0.00	1.5420	958	87.6	1.8372	1.65	0.30	2.88	0.45
24	0.25	1.5404	957	84.6	1.8156	1.64	0.30	2.88	0.45
25	0.75	1.5440	986	87.4	1.8802	1.65	0.30	2.93	0.44
26	0.00	1.5438	975	81.8	3.2205	1.52	0.40	4.42	0.16
27	1.25	1.5551	972	83.0	3.7296	1.52	0.47	4.40	0.16
28	0.00	1.5511	974	90.9	3.7516	1.52	0.47	4.42	0.16

Capillary 1 was used for flow measurements.

The principal variables were temperature and the distance of separation between the oxide tablet and graphite powder. Values of E, T and Δh are reported in the Appendix AI as function of time (t). t was arbitrarily set at zero as soon as the rate was appreciable enough to be recorded. As will be seen later this choice does not affect interpretation of results significantly. Absolute value of t is not important.

The raw results as such are not of much use. The nature of change of E, T and Δh with time are shown for one of the experiments in fig. 4.2 just for illustration purposes.

4-2.1 Calculation of CO/CO_2 Ratio in the Product Gas

The EMF of the solid oxide electrolyte cell (E) and temperature (T) were the data used for calculating the gas composition. Free energy of formation of CO_2 from CO (ΔG°_c) at various temperatures were interpolated from the data given by Elliott and Gleiser[53]. Original data are reproduced in table 4.4.

The interpolation formula was:

$$\Delta G^\circ_c = -85{,}020 + 41.4(T - 1200) \text{ cals/mole} \qquad (4\text{-}11)$$

Procedure for calculation of CO/CO_2 ratio in the product gas is given below. It is based on the assumption of equilibrium of reaction (4-12) in the gas mixture.

Table 4.4 Free Energy of Formation of CO_2, CO and Oxides of Iron at Various Temperatures[53]

Temperature °K	ΔG^{o}_{CO} cals/mole	$\Delta G^{o}_{CO_2}$ cals/mole	$G^{o}_{Fe_{0.947}O}$ cals/mole	$\Delta G^{o}_{Fe_3O_4}$ cals/mole	$\Delta G^{o}_{Fe_2O_3}$ cals/mole
800	-43,680	-94,540	-34,800	-124,800	-81,400
900	-45,820	-94,580	-33,600	-118,900	-75,300
1000	-47,940	-94,610	-32,400	-112,900	-57,100
1100	-50,050	-94,640	-31,200	-107,000	-51,000
1200	-52,150	-94,640	-27,650	-89,000	-32,900
1300	-54,240	-94,680	-26,500	-83,000	-26,900
1400	-56,310	-92,690	-25,300	-77,000	-20,900

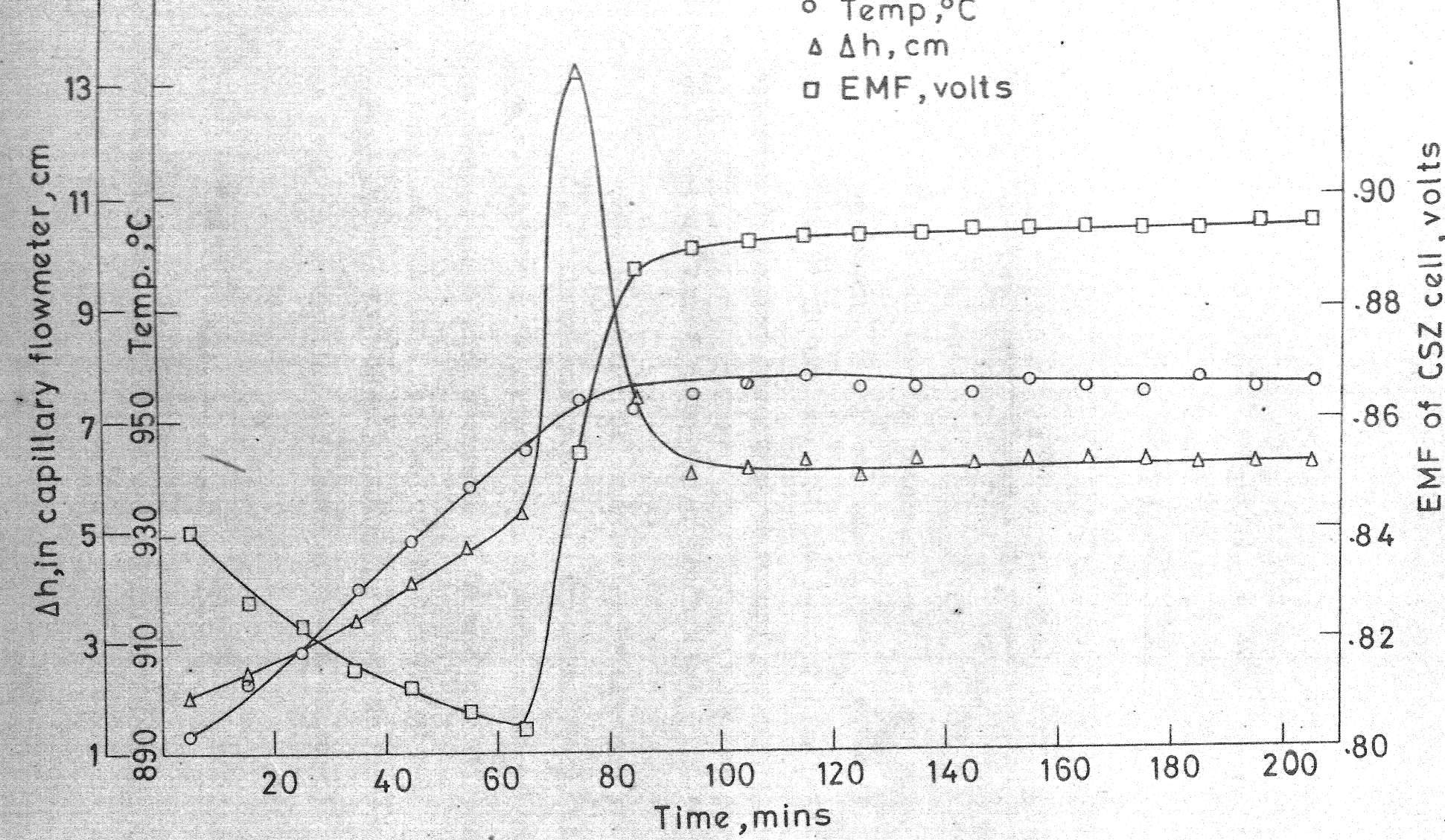

FIG. 4.2 Δh, EMF AND TEMPERATURE AS A FUNCTION OF TIME FOR EXPERIMENT 17

$$2CO(g) + O_2(g) \rightleftharpoons 2CO_2(g) \; ; \qquad \Delta G_c^\circ \tag{4-12}$$

$$\Delta G_c^\circ = -2.303\, RT \log \frac{p_{CO_2}^2}{p_{CO}^2 \cdot p_{O_2}} \tag{4-13}$$

or,
$$\log p_{O_2} = \frac{\Delta G_c^\circ}{2.303\, RT} + 2\log \frac{p_{CO_2}}{p_{CO}} \tag{4-14}$$

Since air was the reference gas, $\log p_{O_2}$ were computed using eqn. (4-10) and then p_{CO}/p_{CO_2} ratio (i.e. the gas composition) determined with the help of eqn. (4-14). (Appendix AI present the gas composition).

4-2.2 Estimation of Viscosity of Product Gas

The calibration of capillaries by nitrogen yielded values of capillary constants (A). From eqn. (4-3), it may be noted that the determination of Q needs values of viscosity. The product gases were a mixture of CO and CO_2. Viscosity of a gas mixture is a function of the individual mole fractions. The following relationship given by Bird et al[54] was used for estimating viscosity of CO-CO_2 mixture.

$$\mu_{mix} = \sum_{i=1}^{2} \frac{X_i\, \mu_i}{\sum_{j=1}^{i} X_i\, \phi_{ij}} \tag{4-15}$$

where, $$\phi_{ij} = \frac{1}{\sqrt{8}} \left(1 + \frac{\mu_i}{\mu_j}\right)^{-\frac{1}{2}} \left[1 + \left(\frac{\mu_i}{\mu_j}\right)^{\frac{1}{2}} \left(\frac{M_i}{M_j}\right)^{\frac{1}{4}}\right]^2 \qquad (4\text{-}16)$$

X_i = Mole fraction of species i in the mixture

M_i = Molecular weight of species i

μ_i = Viscosity of pure species i

Here the gas mixture is a binary one consisting of CO and CO_2. $M_{CO} = 28$ and $M_{CO_2} = 44$. X_{CO} and X_{CO_2} corresponding to flowmeter readings have already been calculated by the procedure described in Section (4-2.1).

Viscosities of pure CO and pure CO_2 were estimated by the procedure given by Bird et al[55]. Hence eqn. (4-15) may be written in a simplified form as:

$$\mu_{mix} \text{ (in poise)} = Y_1 + Y_2 \qquad (4\text{-}17)$$

where, $$Y_1 = \frac{1.802 \times 10^{-4}\, p_{CO}}{p_{CO} + 1.360\, p_{CO_2}} \text{ poise} \qquad (4\text{-}18)$$

$$Y_2 = \frac{1.520 \times 10^{-4}\, p_{CO_2}}{p_{CO_2} + 0.730\, p_{CO}} \text{ poise} \qquad (4\text{-}19)$$

p_{CO} and p_{CO_2} are in atmospheres.

4-2.3 Instantaneous Rates of Gas Evolution

By using the values of μ_{mix} obtained from eqn. (4-17) to (4-19) the flow rates of the product gas can be obtained using the following relation (see eqn. (4-3))

$$Q = A \times \frac{\Delta h}{\mu_{mix}} \text{ cc (NTP)/sec.} \qquad (4\text{-}20)$$

Also $$Q_{CO} = Q \cdot X_{CO} \text{ cc (NTP)/sec.} \qquad (4\text{-}21)$$

$$Q_{CO_2} = Q \cdot X_{CO_2}$$

$$= Q \cdot (1 - X_{CO}) \text{ cc (NTP)/sec.} \qquad (4\text{-}22)$$

where Q_{CO} and Q_{CO_2} refer to volumetric flow rates of CO and CO_2 respectively.

4-2.4 Calculation of Instantaneous Rates of Loss of Carbon and Oxygen

As one mole of CO has one mole of carbon and oxygen each, and one mole of CO_2 has one mole of carbon and two moles of oxygen, the rates of weight loss of carbon and oxygen can be obtained from the flow rates as follows.

$\dot{W}_c$ = Instantaneous rate of weight loss of carbon

$$= \frac{(Q_{CO} + Q_{CO_2}) \times 12}{22{,}400 \times 60} \text{ gms./sec.} \qquad (4\text{-}23)$$

and $\dot{W}_o$ = Instantaneous rate of weight loss of oxygen

$$= \frac{(Q_{CO} + 2Q_{CO_2}) \times 16}{22{,}400 \times 60} \text{ gms./sec.} \qquad (4\text{-}24)$$

4-2.5 Cumulative Weight Loss of Carbon and Oxygen and Percentage Reduction of the Iron Oxide

The total weight of oxygen fed into the reaction chamber can be found out from the weight of the Fe_2O_3 pellet by multiplying it by 0.3. Percentage weight loss of oxygen at any instant can be obtained by dividing the cumulative weight loss at that instant by the total oxygen initially present in the pellet (W_o^o).

$$\text{Pct. Reduction} = \frac{100 \times \int_o^t \dot{W}_o \, dt}{W_o^o} \qquad (4\text{-}25)$$

Simpson's rule was employed for numerical integration of $\dot{W}_c$ and $\dot{W}_o$ with respect to time. This gave the cumulative weight loss of carbon (ΔW_c) and of oxygen (ΔW_o) at any time (t).

$$\Delta W_c = \int_o^t \dot{W}_c \, dt \qquad (4\text{-}26)$$

$$\Delta W_o = \int_o^t \dot{W}_o \, dt \qquad (4\text{-}27)$$

Both ΔW_c and ΔW_o were calculated by Simpson's integration. Since there were about 50 to 75 data points in each experiment, the integration errors were not significant. Values of pct. reduction with respect to time are given in Appendix AI.

The cumulative weight losses of oxygen and carbon were also found out by weighing the oxide pellet and graphite powder separately before and after each experiment. These are denoted as ΔW_o(expt.) and ΔW_c(expt.) respectively. In contrast ΔW_o and ΔW_c calculated with the help of Simpson's integration are designated as ΔW_o(calcd.) and ΔW_c(calcd.). Table 4.5 present these values for all the experiments.

4-2.6 Correction of Gas Composition and Instantaneous Rates

Assuming the experimental weight losses (i.e. ΔW_o(expt.) and ΔW_c(expt.)) to be more accurate, gas compos tions, flow rates etc. were corrected as shown below.

$$Q_{(corr.)} = Q_{(original)} \times \frac{\Delta W_c(expt.)}{\Delta W_c(calcd.)}$$

$$\dot{W}_{c(corr.)} = Q_{(corr.)} \times \frac{12}{22,400}$$

$$\dot{W}_{o(corr.)} = \dot{W}_{o(original)} \times \frac{\Delta W_o(expt.)}{\Delta W_o(calcd.)}$$

Table 4.5 Cumulative Weight Losses Calculated Using Computer and Measured Experimentally

Expt. No.	ΔW_c Calculated, gms.	ΔW_c Experimental, gms.	ΔW_o Calculated, gms.	ΔW_o Experimental, gms.
7	0.7183	0.6346	1.187	1.170
9	0.3639	0.4129	0.6259	0.6650
14	0.3408	0.3563	0.5634	0.5100
17	0.3458	0.3318	0.5617	0.5731
18	0.2958	0.3126	0.5638	0.5694
19	0.1022	0.1198	0.2265	0.1724
20	0.1289	0.3469	0.2250	0.5387
21	0.3574	0.3393	0.5668	0.5091
22	0.2527	0.2754	0.4097	0.4158
23	0.3307	0.3275	0.5304	0.5395
24	0.3299	0.3405	0.5329	0.5541
25	0.3606	0.3338	0.5910	0.5359
26	0.3364	0.3931	0.5392	0.7953
27	0.2683	0.2471	0.5478	0.4327
28	0.3177	0.3182	0.5415	0.5451

$$Q_{CO_2(corr.)} = \dot{W}_{o(corr.)} \times \frac{22,400}{16} \qquad (4-31)$$

$$Q_{CO(corr.)} = Q_{(corr.)} - Q_{CO_2(corr.)} \qquad (4-32)$$

$$X_{CO(corr.)} = \frac{Q_{CO(corr.)}}{Q_{(corr.)}} \qquad (4-33)$$

However it was not found advisable to use these corrected values and for all purposes the values obtained by procedure described in Sections 4-2.1 to 4-2.3 were accepted.

4-2.7 Computer Programme

On the basis of the equations and procedures as outlined in Sections 4-2.1 to 4-2.6, a master computer programme was worked out and employed to make all calculations. An IBM 7044 computer was used. The computer flow diagram is shown in fig. 4.3. The computer programme is given in the Appendix AII.

4-2.8 Computed Results

Tables in the Appendix AI present the computed results of the experiments. There were 50 to 75 data points in each experiment. However only some of them have been presented for the sake of conciseness, since these should suffice for any future use of the data of this investigation.

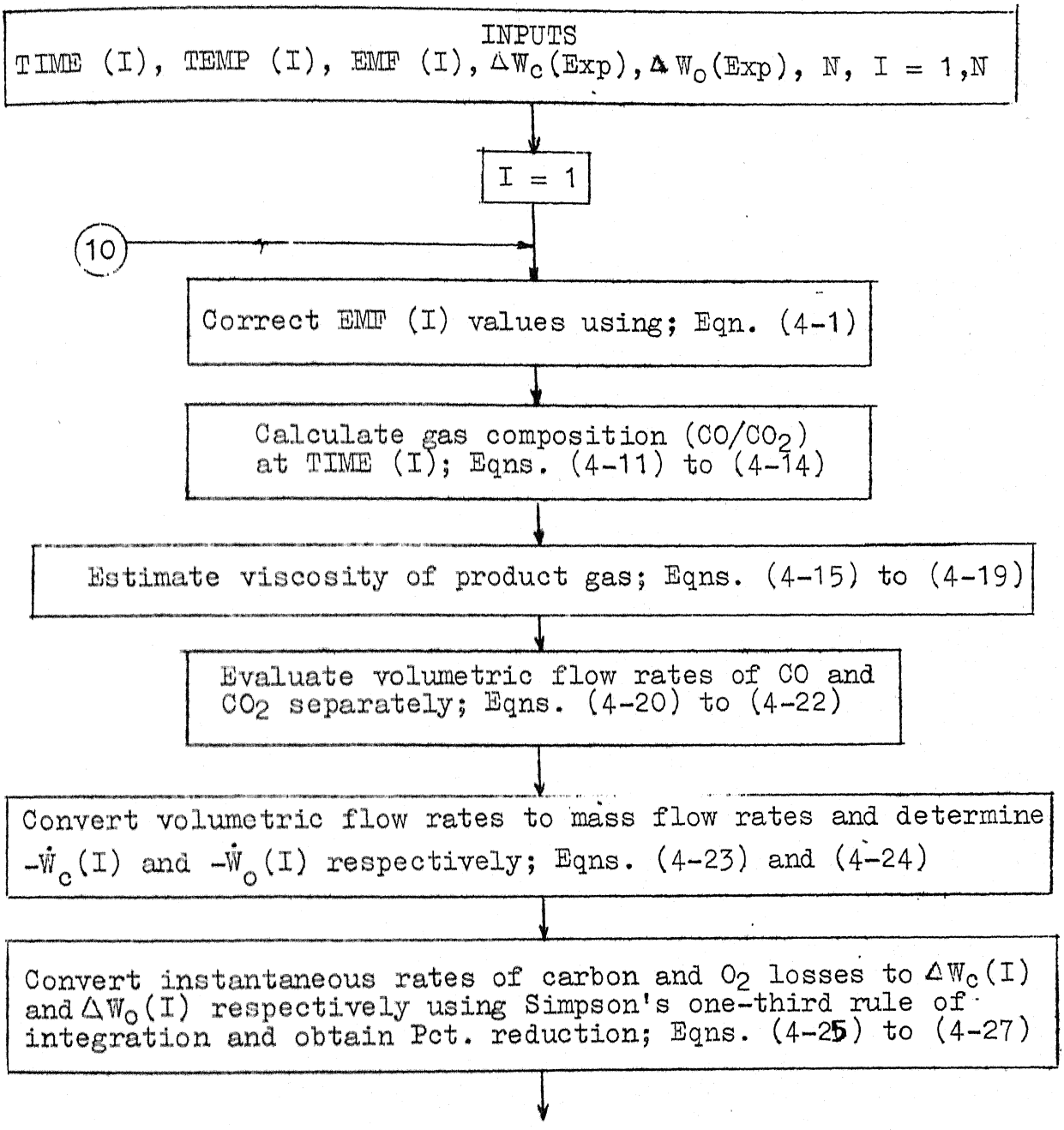
INPUTS
TIME (I), TEMP (I), EMF (I), ΔWc(Exp), ΔWo(Exp), N, I = 1,N
I = 1
10
Correct EMF (I) values using; Eqn. (4-1)
Calculate gas composition (CO/CO2) at TIME (I); Eqns. (4-11) to (4-14)
Estimate viscosity of product gas; Eqns. (4-15) to (4-19)
Evaluate volumetric flow rates of CO and CO2 separately; Eqns. (4-20) to (4-22)
Convert volumetric flow rates to mass flow rates and determine -Ẇc(I) and -Ẇo(I) respectively; Eqns. (4-23) and (4-24)
Convert instantaneous rates of carbon and O2 losses to ΔWc(I) and ΔWo(I) respectively using Simpson's one-third rule of integration and obtain Pct. reduction; Eqns. (4-25) to (4-27)

Continued...

Continued

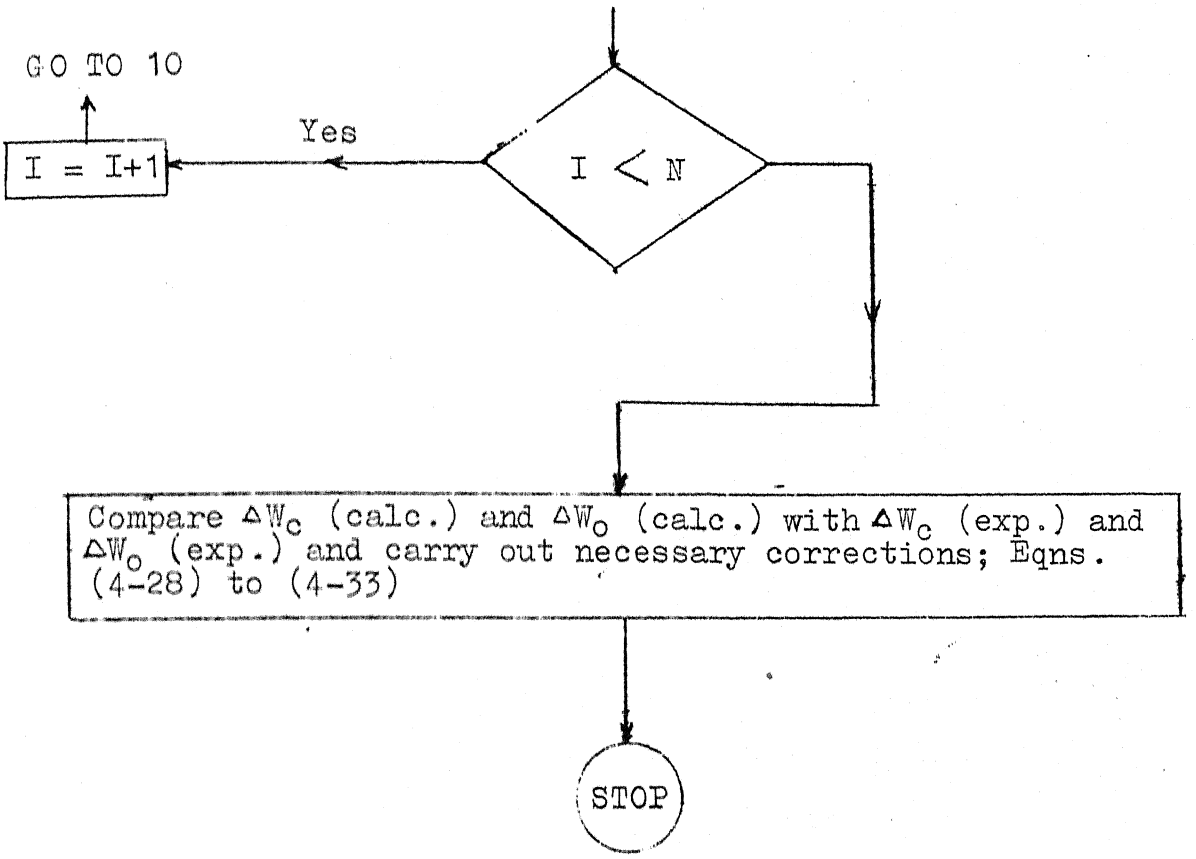

Fig. 4.3 COMPUTER FLOW DIAGRAM

4-3 EXAMINATION OF REDUCED PELLETS

Visual examination of the reduced pellets were made. It was found that the pellets were cracking as well as increasing in volume due to reduction.

As the reduced pellets were extremely fragile, no microstructural examination could be made.

When the pellet diameter was bigger than the crucible diameter it was found that the portion not exposed to the inner surface of the crucible was less reduced. This was revealed during oxidation test described below.

Portions of the partially reduced pellets were taken out from the top, middle and bottom of the pellet by using a diamond file and subjected to oxidation test. The layers were weighed separately in a semi-micro balance and oxidized at 900°C till constant weight was obtained. The difference in weight of each layer before and after oxidation was expressed as percentage of the initial weight. The results are shown in table 4.6.

4-4 REDUCTION BY QUICK HEATING AND COOLING

Two experiments were conducted at 967°C by introducing the crucible with graphite and pellet, kept in separation, suddenly into the reaction chamber. As the CSZ tube was not introduced EMF could not be observed.

Table 4.6 Results of Layer Analysis by Oxidation Test of Reduced Pellets

Expt. No.	Position in the pellet	Increase in wt., pct. in terms of initial wt. of the layer	pct. reduction of the pellet
I	Bottom	3.289	18
	Middle	4.463	
	Top	1.286	
	Periphery	1.507	
II	Bottom	8.874	25
	Middle	8.180	
	Top	2.462	
	Periphery	2.732	

The assembly was taken out by opening the top of the furnace and air cooled from the reaction temperature to the room temperature. Weighing before and after the experiment gave values of ΔW_o and ΔW_c. $\dot{W}_o$ and $\dot{W}_c$ were calculated as follows.

$$\dot{W}_o = \frac{\Delta W_o}{t \times 60} \quad \text{gms/sec.} \qquad (4\text{-}34)$$

$$\dot{W}_c = \frac{\Delta W_c}{t \times 60} \quad \text{gms/sec.} \qquad (4\text{-}35)$$

where t = Duration of the assembly in the furnace in minutes.

The results are presented in table 4.7.

Table 4.7 Results of Reduction of Oxide Pellet by Quick Heating and Cooling

Expt. No.	Wt. of oxide pellet gms.	Wt. of graphite powder, gms.	Porosity of oxide pellet	Temp., °C	pct. reduction	$-\dot{W}_o \times 10^5$ g/sec.	$\dot{F}_c$, sec^{-1}
1	1.8134	1.4738	0.45	967	32.0	1.93	0.760
2	1.7846	1.4799	0.45	967	27.2	1.87	0.812

CHAPTER 5

RESULTS OF AUXILLIARY EXPERIMENTS

Reaction between powder mixtures of iron oxide (-325 mesh) and graphite (-200, +230 mesh) and mixtures of micro-pellets (~2 mm dia.) of oxide and graphite powder were investigated as described in Section 3-2.2. Reactivity studies of graphite powder (-200 + 230 mesh) in pure CO_2 and in CO-CO_2 mixture were also undertaken as outlined in Section 3-2.3. The results of these investigations shall be presented here under separate headings.

5-1 POWDER MIXTURES OF FERRIC OXIDE AND GRAPHITE

Standardisation of the equipments used for the investigation was carried out first. The results have already been presented in Section 4-1. The details of the CSZ cell used for determination of gas composition as well as the microvoltmeter employed for measuring the voltage of the cell have been given in Section 4-1.

Capillary No. 2 was used for measuring the flow rates of product gases of reaction. Capillary constant was calculated to be:

$$A = 7.51 \times 10^{-6} \qquad \text{(Section 4-1)}$$

The experimental data consisted of Δh (cm.) of the flowmeter, EMF (E, volts) of the CSZ cell and temperatures (°C) of the reaction furnace and of the CSZ cell. These were the basic data from which the gas compositions, instantaneous reaction rates and cumulative weight losses were calculated.

The time interval for collecting the data was 1 minute or 2 minutes depending on the change in rate of evolution of gases. One minute was chosen when the change in rate of gas evolution was rapid. Otherwise the interval was kept at 2 minutes. Collection of data was started immediately after introducing the sample. This was noted as zero time.

A number of experiments were carried out with temperature as the variable. The experimental conditions are given in table 5.1.

As in the case of oxide pellet-graphite powder system (Section 4-2), here also the raw results as such are of not much use. The nature of change of E, T and Δh with time are shown for one of the experiments in Fig. 5.1, for the sake of illustration. Tables in Appendix AIII present the values of E (volts), T (°C) and Δh (cm.) for all experiments.

Table 5.1 Experimental Conditions for Reactions of Iron Oxide Powder and Graphite Powder Mixture and Oxide Micro-Pellets and Graphite Powder Mixture

Expt. No.	Temp. of CSZ cell, °C	Reaction zone temperature, °C		Weight of oxygen in oxide, gms.	Graphite weight, gms.	Pelletising pressure psi.	Stoichiometric ratio carbon/oxygen
		Initial	Average				
M-2	770	974	992	0.522	0.786	0	2.01
M-3*	778	955	945	0.360	0.538	0	1.99
M-4	768	945	940	0.680	1.020	0	2.00
M-5	770	1046	1042	0.400	0.602	0	2.00
M-6*	793	967	962	0.329	0.519	0	2.05
M-7	793	972	963	0.296	0.443	200	2.00
M-8	791	954	945	0.265	0.418	200	2.05
M-9	784	1009	999	0.468	0.701	200	2.00

*Oxide in the form of micro-pellets (approx. 2 mm dia.).

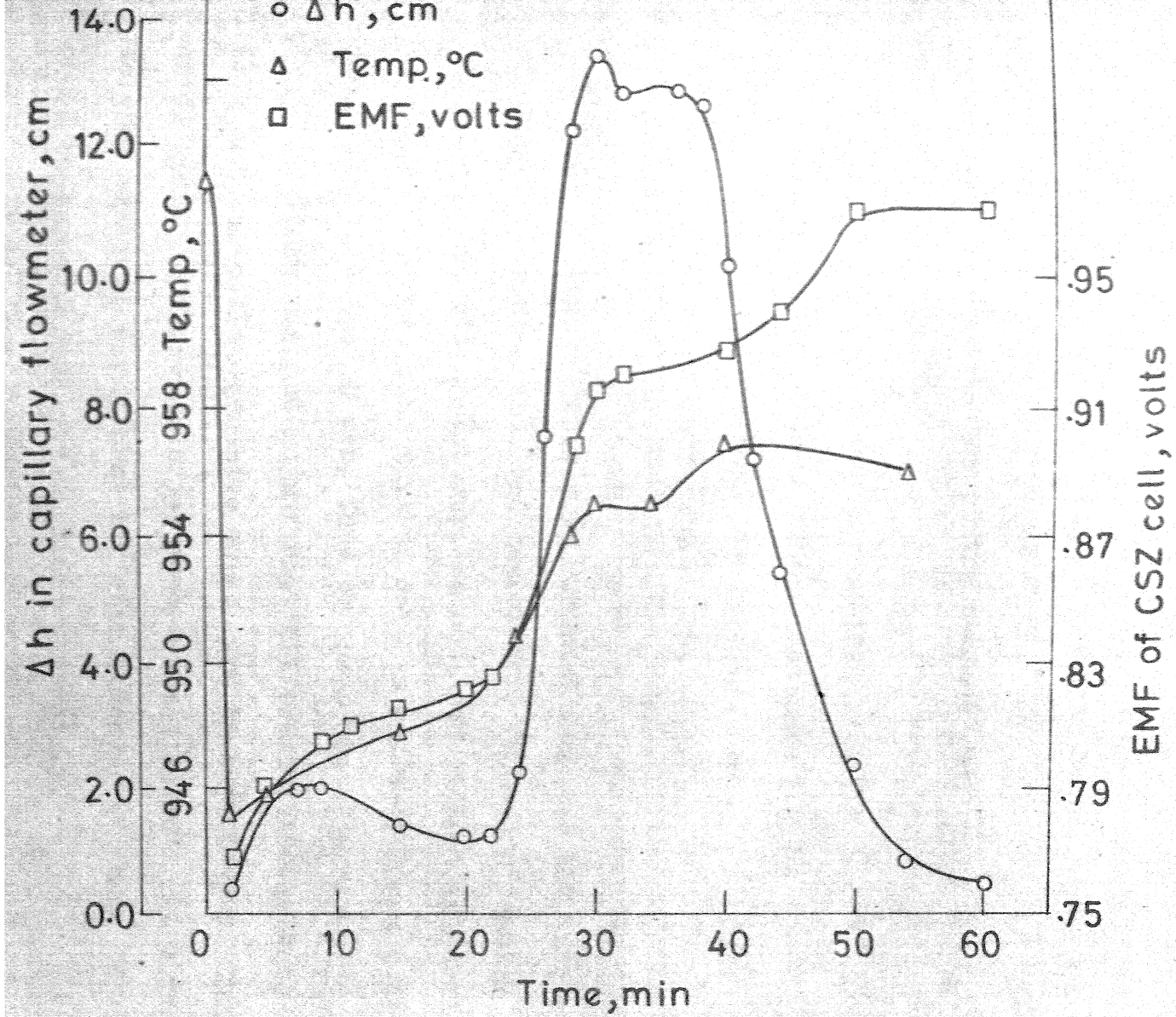

FIG. 5.1 Δh, TEMPERATURE AND EMF Vs. TIME FOR EXPERIMENT M-4

5-1.1 Calculation of Gas Compositions, Instantaneous and Cumulative Weight Losses

Tables in Appendix AIII present the values of the following for powder mixtures.

a) Compositions of the product gas, which was a mixture of CO and CO_2.

b) Instantaneous carbon loss rate ($-\dot{W}_c$)

c) Instantaneous oxygen loss rate ($-\dot{W}_o$)

d) Temperature of the reaction zone

e) Percent reduction of the oxide.

All the above informations have been presented at intervals of time. These were computed from the EMF (E), flowmeter reading (Δh), and temperature (T) using exactly the same calculation procedure as outlined in Section 4-2.1 to 4-2.5. Therefore no further details would be given here about the calculation procedure or the computer program.

There was one significant difference between this work and the pellet-graphite work. In the latter case, the oxide pellet and the graphite powder could be individually weighed after an experiment was over. Hence ΔW_o and ΔW_c could be experimentally determined separately.

In the oxide powder-graphite powder mixture, only the total weight loss, viz. $[-(\Delta W_o + \Delta W_c)]$ could be

experimentally determined. Table 5.2 compares calculated and experimental total weight loss.

5-2 MIXTURE OF FERRIC OXIDE MICRO-PELLETS AND GRAPHITE POWDER

Two experiments were made with small spherical pellets (~ 2 mm dia.) after mixing them uniformly with graphite powder (-200, +230 mesh). The pellets were prepared as described in Section 3-1.3.

The time interval for taking the readings were either 1 minute or 2 minutes. Collection of data was started immediately after introducing the sample into the reaction furnace, which was maintained at a constant temperature.

Processing of the basic data was exactly similar to that employed for processing the data on powder mixture study (Section 5-1.1). The results, raw as well as processed, are presented in Appendix AIV. Figure 5-2 shows variation of E, Δh and temperature with time. Experimental conditions are given in table 5.1.

5-3 GRAPHITE REACTIVITY STUDY

The total ash content of the graphite was determined as 0.112 pct. The ash was further analysed

Table 5.2 Cumulative Weight Loss Calculated Using a Computer and Measured Experimentally

Expt. No.	Weight loss calculated, gms.	Weight loss experimental, gms.
M-2≠	0.968	1.004
M-4≠	1.100	1.022
M-5≠	0.955	0.560
M-6*	0.348	0.302
M-7⊕	0.543	0.431
M-8⊕	0.556	0.435
M-9⊕	0.911	0.770

≠ Powder mixture of oxide and graphite, unpressed

⊕ Powder mixture of oxide and graphite, pressed

* Micro-pellets-graphite powder mixture.

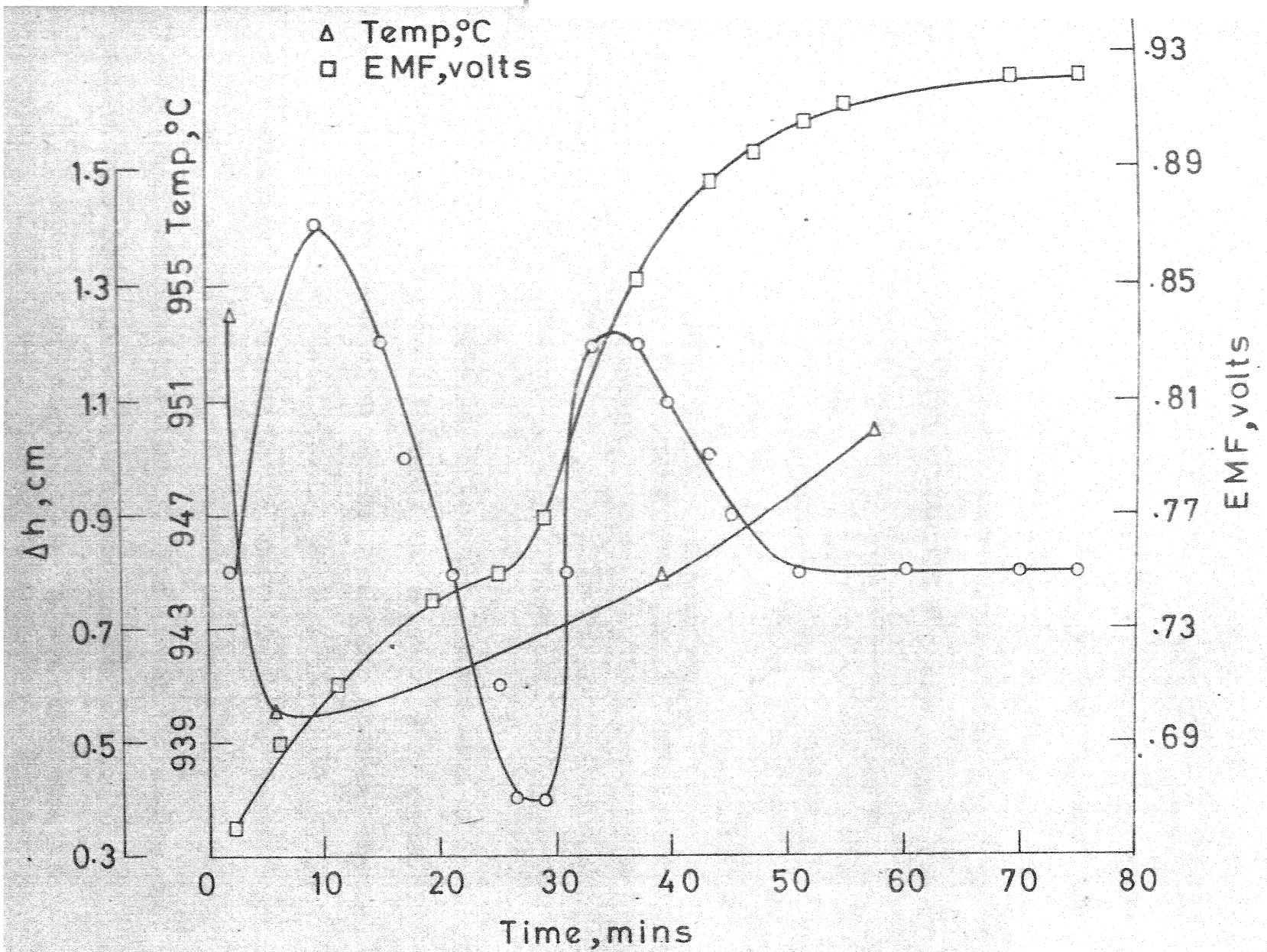

FIG. 5.2 Δh, TEMPERATURE AND EMF Vs. TIME FOR EXPERIMENT M-3

spectrographically at the BARC, Bombay. As the concentrations of the impurities in the sample were much beyond the range for which the spectrograph was standardised, substantial dilution (1:80) of the sample was necessary to adjust the impurities concentration within the workable range. The analysis was carried out on a semiquantitative basis. Results are shown below.

Chemical Analysis of the Ash

Impurities	Concentration
Cobalt	0.8 pct.
Iron	0.56 pct.
Nickel	0.88 pct.

As explained in Section 3-2.3 three sets of experiments were made to study the reactivity of graphite. The first two sets of experiments were for studying the reactivity of graphite with CO_2 whereas the third set was for studying the reactivity in CO-CO_2 mixture. Results of the first set of experiments are not presented here as they were found somewhat unreliable. Results of the second and third sets of experiments are shown in table 5.3.

Rate of reaction ($\dot{F}_c$, sec^{-1}) was calculated as follows:

Table 5.3 Graphite Reactivity Data in Pure CO_2 and CO/CO_2 Mixture

Expt. No.	Reaction Temp., °C	Weight of graphite gms.	Gas Composition	Time of expt., min.	Weight loss of graphite gms.	Reactivity $\dot{F}_c \times 10^4$ sec^{-1}	$K_i \times 10^4$ gm-mole/gm sec.
1	905	0.3823	Pure CO_2	20	0.04192	0.83	1.142
2	905	0.3324	"	22	0.03384	0.76	1.046
3	895	0.4144	"	30	0.04448	0.60	0.820
4	899	0.2660	"	31	0.03379	0.68	0.933
5	970	0.6618	"	21	0.11189	1.35	1.941
6	962	0.4601	"	20	0.06538	1.18	1.686
7	963	0.5951	"	21	0.09156	1.23	1.758
8	964	0.4355	"	29	0.09559	1.27	1.818
9	1032	0.5146	"	10	0.08270	2.68	4.008
10	1032	0.3232	"	21	0.10208	2.50	3.739
11	1030	0.2426	"	16	0.06940	2.98	4.457
12	1030	0.2850	"	10	0.05399	3.15	4.707
13	962	1.1742	43.9 pct. CO	95	0.0748	0.118	-
14	962	0.6989	33.8 pct. CO	95	0.0422	0.224	-
15	962	0.7343	29.2 pct. CO	80	0.0793	0.225	-

$$\dot{F}_c = \frac{-\Delta W_c}{W_c^o \times t \times 60}, \text{ sec}^{-1} \qquad (5\text{-}1)$$

where ΔW_c = Weight loss of carbon, gms.

W_c^o = Initial weight of graphite, gms.

t = Time, min.

The values of $\dot{F}_c$ for these experiments are presented in table 5.3.

CHAPTER 6

DISCUSSION OF RESULTS ON GRAPHITE REACTIVITY AND POWDER MIXTURE STUDIES

As will be evident later, graphite reactivity would come into picture in discussions of iron oxide-graphite reaction. Hence, although the measurements of reactivity of the graphite powder employed in this investigation constituted one of the auxilliary investigations, it is being discussed first.

Investigation on the powder mixtures of oxide and graphite was undertaken mainly with the idea of checking the agreement of these results with those of other workers. Again, interpretation of data on oxide pellet-graphite powder reactions would draw extensively from the existing knowledge of the behaviour of powder mixture of iron oxide and carbon. Hence the results of investigation on powder mixtures also shall be taken up in this chapter, although they also constitute only a set of auxilliary studies.

6-1 GRAPHITE REACTIVITY

Here an attempt will be made to compare the results of this investigation with the results on $C-CO_2$

reaction available in the literature. The results have been presented in table 5.3 already.

6-1.1 Results of Reaction of Graphite with Pure CO_2

Figure 6.1 presents $\dot{F}_c$ as a function of temperature in an Arrhenius type of plot for the present investigation as well as for the investigations done by others[36,38]. The reaction rate obtained by Rao and Jalan[38] is the same as that of the present study at about 1050°C. However, at 962°C, value reported by them is about one-half of those of the present investigation. The reactivity of metallurgical coke of Turkdogan and Vinters[36] is the same as that for the present study at about 980°C. At 1030°C, their value is almost double of that of this investigation. In contrast to this, the reactivity of coconut charcoal is 10 times higher at about 1030°C while that of electrode graphite is 10 times lower as compared to the present results at this temperature.

Results of reactivity study of many other investigators are also available in the literature. For the sake of conciseness and clarity they have not been presented here.

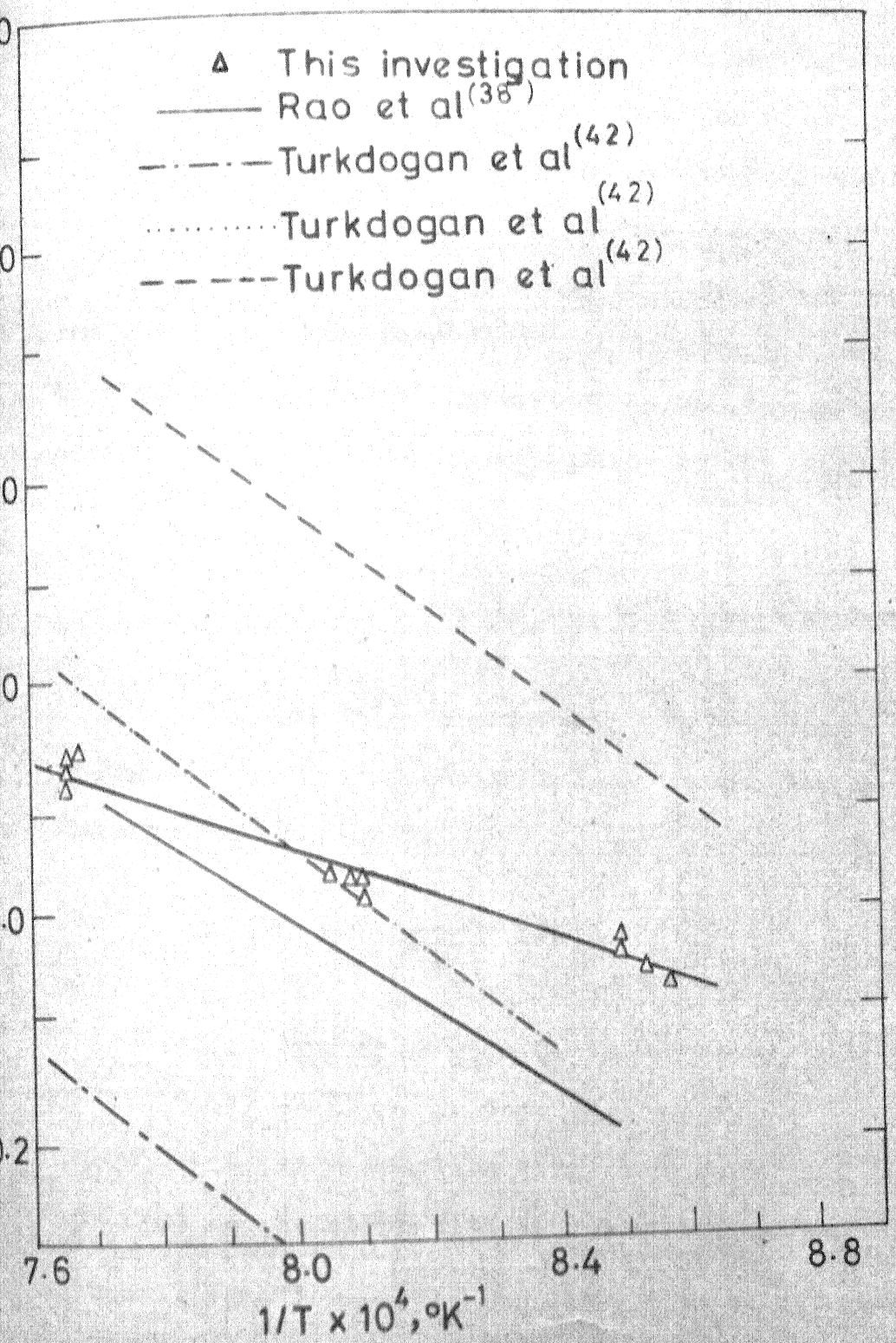

6.1 GRAPHITE REACTIVITY AS FUNCTION OF TEMPERATURE IN PURE CO_2

The other features of the plot are that the three lines corresponding to the three types of carbon (coconut charcoal, metallurgical coke, and electrode graphite) investigated by Turkdogan and Vinters are parallel to one another. The line corresponding to that of Rao and Jalan has a little lower temperature dependence and that corresponding to the present investigation has a much smaller temperature dependence in comparison to all other lines presented here.

6-1.2 Rate Equations Applicable to Reaction Between C and CO_2

Rao and Jalan based their rate expression on that of Ergun[56]. The mechanism assumed is the 2-stage one as discussed in Chapter 1.

$$CO_2(g) + C_f \underset{k_{-1}}{\overset{k_1}{\rightleftharpoons}} C(O) + CO(g) \qquad (1\text{-}13)$$

$$C(O) \underset{k_{-2}}{\overset{k_2}{\rightleftharpoons}} CO(g) + C_f \qquad (1\text{-}14)$$

C_f = Free reaction site

$C(O)$ = Reaction site with adsorbed oxygen.

As usual, reaction (1-13) was assumed to be reversible, and (1-14) as slow and irreversible. Going through the derivation steps,[56,38]

$$\dot{F}_c = \frac{12\, k_1 k_2 [\sum C]\, p_{CO_2}}{(k_1 p_{CO_2} + k_{-1} p_{CO} + k_2)} \qquad (6\text{-}1)$$

where $$\sum C = [C_f] + [C(O)] \qquad (6\text{-}2)$$

$$= \text{Total No. of reaction sites, g-mole/gm. of carbon}$$

Defining $I_1 = k_1 [\sum C]$, $I_2 = k_{-1}/k_1$ and $I_3 = k_1/k_2$,

$$\dot{F}_c = 12\, I_1\, p_{CO_2}/(1 + I_2\, p_{CO} + I_3\, p_{CO_2}) \qquad (6\text{-}3)$$

In pure CO_2, the above equation gets simplified as:

$$\dot{F}_c = 12\, I_1\, p_{CO_2}/(1 + I_3\, p_{CO_2}) \qquad (6\text{-}4)$$

Rao and Jalan have instead arrived at the equation (6-5) given below.

$$\dot{F}_c = \frac{12\, I_3\, k_i\, p_{CO_2}}{(I_3\, p_{CO_2} + 1)} \text{ gm-mole/gm-C. min.} \qquad (6\text{-}5)$$

The difference in the form of equations (6-4) and (6-5) is because in equation (6-5), a parameter k_i was defined as follows.

$$k_i = k_2 [\sum C] \text{ gm-mole/gm-C.min} \qquad (6\text{-}6)$$

$$= \text{intrinsic rate constant.}$$

For pure CO_2 at 1 atm. pressure this can be simplified further as

$$\dot{F}_c = \frac{12k_i}{(1 + \frac{1}{I_3})} \qquad (6\text{-}7)$$

k_i can be calculated from $\dot{F}_c$ if the value of I_3 is known. The values of I_3 for various temperatures have been computed from Fig. 6.2. The variation of k_i with temperature was obtained by Rao and Jalan[38] as:

$$k_i = 10^{9.51} \exp.(-79{,}600/RT) \text{ gm-mole/gm-carbon sec.} \qquad (6\text{-}8)$$

In the present investigation the following relation was obtained for k_i

$$k_i = 1.00 \times 10^2 \exp\left(\frac{-32{,}300}{RT}\right) \text{ gm. mole/gm of C sec.} \qquad (6\text{-}9)$$

Darken and Turkdogan[36] postulated the following mechanism of reaction.

$$CO_2(g) = CO_2(ads) = (CO_2)^+ \longrightarrow C(gr) + 2O(ads) \qquad (6\text{-}10)$$

and

$$C(gr) + O(ads) = (CO)^+ \longrightarrow CO(g) \qquad (6\text{-}11)$$

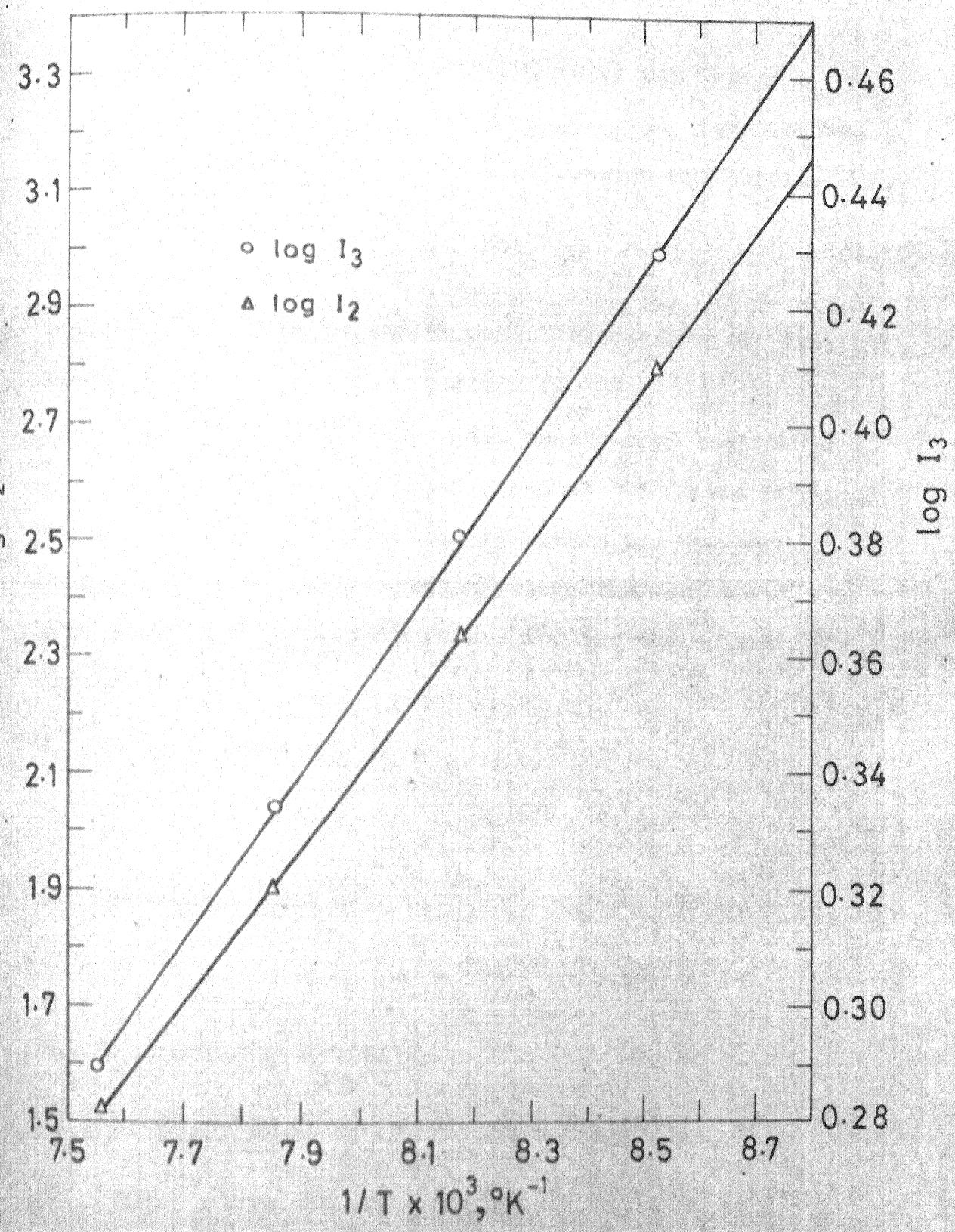

FIG. 6·2 LOG I_3 AND LOG I_2 Vs. 1/T

where $(CO_2)^+$ and $(CO)^+$ are the activated complexes.

For $p_{CO} \rightarrow 0$, the rate controlling reaction was assumed to be (6-10). The rate expression was obtained as:

$$\dot{F}_c = \phi_2 (p_{CO_2})^{\frac{1}{2}}/60, \quad sec^{-1} \qquad (6\text{-}12)$$

where ϕ_2, the rate parameter was obtained from the Absolute Reaction Rate Theory for reaction (6-10).

The value of activation energy for reaction of CO_2 with carbon for all three types of carbon was obtained as 69 k cal/gm atom of carbon by Darken and Turkdogan. Using this value of activation energy they expressed the variation of ϕ_2 with temperature for the three types of carbon as:

for coconut charcoal,

$$\log \phi_2 = -\frac{15,000}{T} + 11.00 \qquad (6\text{-}13)$$

for metallurgical coke,

$$\log \phi_2 = -\frac{15,000}{T} + 9.98 \qquad (6\text{-}14)$$

and for electrode graphite,

$$\log \phi_2 = -\frac{15,000}{T} + 8.75 \qquad (6\text{-}15)$$

In Chapter 1, it has been already stated that the mechanism proposed by Reif[37] has been supported by a number of investigations, and is the generally accepted one.[57] Since Ergun's and Rao and Jalan's analysis are based on this, the latter's approach is being accepted here as the correct one.

The rate analysis by Darken and Turkdogan, on the other hand, assumes adsorption of CO and CO_2 on carbon surface which has been contradicted by some other investigators[38]. Moreover, Rao and Jalan have shown that one of the rate equations proposed by Darken and Turkdogan could be derived from eqn. (6-3).

6-1.3 Sources of Error in Measurements

(a) Temperature measurement and control :- The temperature of the reaction furnace was maintained at a constant value by a variac and voltage stabilizer. Temperature of the reaction zone was measured while the reaction was going on. It was observed that the temperature decreased by about 5°C during the course of the reaction.

(b) Dilution of CO_2 by CO :- Flow rate of CO_2 was 2 litres (NTP)/min. A sample calculation done for reactivity measurement at 1032°C showed that only 0.7 pct. CO_2 got converted into CO. This is negligible.

(c) Accumulation of carbon monoxide inside the pellet can lower the rate appreciably. In this investigation the procedure adopted was to take graphite powder (-200, +230 mesh), press it into a pellet of approximately 1.7 cm dia. and 0.2 cm thickness, weighing approximately 0.5 gms. Then this pellet was broken into few pieces and charged into the silica crucible.

Utilizing the relationship between η and ψ[58,59,36], it is possible to calculate η approximately, where

$$\eta = \frac{\text{actual rate of reaction}}{\text{intrinsic rate of chemical reaction step}} \qquad (6\text{-}16)$$

and

$$\eta = \left(\frac{L_c^2 \, RT}{De \; p_{CO_2,s}}\right) \dot{n}_{CO_2} \qquad (6\text{-}17)$$

where $L_c = \frac{\text{(volume of pellet)}}{\text{(external surface area of pellet)}}$

R = 82.06 cc. atm. $^{o}K^{-1}$ mole^{-1}

De = Effective diffusion coefficient in CO-CO_2 in pores cm^2/sec.

$p_{CO_2,s}$ = Partial pressure of CO_2 at the surface of solid = 1 atm.

$\dot{n}_{CO_2}$ = Reaction rate in g. mole/cm^3.sec.

Now, the pieces may be assumed as tiny disks. Hence

L_c = half thickness = 0.1 cm

$De = D \frac{\epsilon}{\tau}$

where D = Bulk diffusivity in $CO-CO_2$ gas mixture

ϵ = Porosity of the disk 0.5

τ = Tortuosity factor

= 2 (assumed).

Since the pores are several microns in size, molecular diffusion shall predominate, and D can be calculated from the kinetic theory of gases[60] at any temperature.

Using the experimental values of $\dot{F}_c$ and T, sample calculation of ψ was made at 1032°C (highest experimental temperature) and from the $n - \psi$ chart,[58] n was determined as approximately 1.

This indicates that there was negligible mass transfer resistance inside the pellet. However, possibly there was local reagent starvation inside the silica crucible because the pieces of graphite at the top visually appeared to have reacted more than those at the bottom of the crucible.

(d) The reaction of carbon with CO_2 is strongly endothermic. Thus if the rate of heat supply to the reaction site is not rapid enough, its temperature will be somewhat lower than the furnace chamber temperature. Rao and Jalan[38] have found this difference to be about 10-25°C in this range. Since they employed one large disk with very tiny pores ($\sim$ 500 Å or so), and in this investigation small broken pieces with micron size pores were used, it is not expected that the temperature difference would be so much here, but some difference cannot be ruled out.

All the effects discussed above would tend to lower the value of $\dot{F}_c$ and therefore it is believed that the actual $\dot{F}_c$ value is somewhat higher than what has been obtained. Moreover the lowering of $\dot{F}_c$ caused by these sources of error would be greater at the higher temperatures. It is very likely that these are responsible for the fact that the activation energy obtained in this investigation is lower than the literature values.

6-1.4 Comparison of Graphite Reactivity Values in Pure CO_2

As discussed above the correct $\dot{F}_c$ values in this investigation are perhaps somewhat greater if the errors could have been corrected for. When corrections for

pore diffusion were made to their data by Rao and Jalan[38] their $\dot{F}_c$ values for intrinsic chemical reactivity were found to be greater than those represented in Fig. 6.1 by factors of a few. Therefore the reactivity values would perhaps approximately agree with those determined in this investigation.

However the $\dot{F}_c$ values for electrode graphite as found by Turkdogan and Vinters[42] are an order of magnitude lower as compared to those of the present investigation. It is a little perplexing as to why similar graphite sample (electrode graphite) in their case exhibited such low reactivity. It is difficult to explain this anomaly. But one possible explanation is noted below.

Turkdogan and Vinters employed 0.5 mm particles of graphite and the particle size in this investigation was approximately 50 microns, i.e. about $\frac{1}{10}$th of theirs. If the sizes of the pores inside the particles are very small, there shall be considerable mass transfer resistance in them and the particles in effect would react only at their surfaces. Then $\dot{F}_c$ would be proportional to the specific surface area (i.e. surface area per unit volume) of the particles. For spherical particles, specific surface area is inversely proportional to the diameter of the particle. Hence,

$$\frac{(\dot{F}_c)\ \text{Turkdogan and Vinters}}{(\dot{F}_c)\ \text{this investigation}} \simeq \frac{0.05}{0.5} = \frac{1}{10}$$

Therefore it does offer an explanation for the lower rates obtained by Turkdogan and Vinters. The general conclusion drawn by the above workers that mass transfer resistance is not significant below a particle diameter of 1 cm. may be open to question.

6-1.5 Reaction of Graphite with $CO-CO_2$ Mixture

Table 5.2 presents the results of the experiments in $CO-CO_2$ mixture. Table 6.1 shows the comparison between the experimentally obtained rates and that computed from the work of others for the gas compositions and temperatures of this investigation. It can be seen that the experimentally obtained values are higher than the values extrapolated from the reactivity found by Rao and Jalan[38] and the present investigation using pure CO_2. Also they are much higher than the values obtained from Turkdogan and Vinters[42] for electrode graphite

The method of extrapolation for obtaining reactivity values in table 6.1 is based on equation (6-5). Values of k_i were calculated using equation (6-8) in the

Table 6.1 Comparison of Calculated and Experimental Values of Reactivity of Graphite in CO/CO_2 Mixtures

Expt. No.	pct.	$\dot{F}_c x10^5$, sec^{-1}, calculated from various values of reactivity of carbon					Experimental $\dot{F}_c x10^5$ sec^{-1}
		Rao and Jalan[38] (graphite)	Turkdogan et.al[42]			This investigation with pure CO_2	
			Charcoal	Met. coke	Graphite		
13	43.9	0.376	21.391	0.570	0.068	0.257	1.118
14	33.8	0.560	30.329	0.840	0.101	0.389	2.236
15	29.2	0.700	35.69	1.022	0.123	0.478	2.250

case of Rao and Jalan and equation (6-9) for the present investigation with pure CO_2.

Reactivity values in the case of Turkdogan and Vinters[42] were calculated using the following equation.

$$\dot{F}_c = \frac{\phi_2 \left[(p_{CO_2})^{\frac{1}{2}} - (p_{CO_2\,e})^{\frac{1}{2}}\right]}{\left[1 + p_{CO}/\phi_{CO}\right]60} \text{ sec}^{-1} \qquad (6\text{-}19)$$

ϕ_2 for the three types of carbon were calculated using equations (6-13), (6-14) and (6-15). ϕ_{CO} for graphite and coke were derived from the equation[36]

$$\log \phi_{CO} = -\frac{5940}{T} + 3.46 \qquad (6\text{-}20)$$

The value of ϕ_{CO} for charcoal is larger by a factor of 4 as obtained from the ϕ_{CO} Vs $\frac{1}{T}$ plot of Darken and Turkdogan[36].

The reasons for the enhanced rates in this investigation using CO-CO_2 gas mixture may be as follows:

(1) The sample was heated and cooled slowly to and from the reaction temperature in order to protect the CSZ tube from cracking due to thermal shock. Some reaction would have taken place during this time which was not accounted for.

(2) Time lag in registering the EMF of the CO-CO_2 mixture by the CSZ tube. Zero reaction time was taken as the time when the CSZ tube started indicating.

None of these could be clearly established because sufficient number of trials could not be given due to lack of time.

6-2 REACTIONS IN MIXTURES OF IRON OXIDE POWDER AND GRAPHITE POWDER

The main objectives behind the investigation of reactions in powder mixtures ofiron oxide and graphite were:

(a) to compare the data obtained by techniques employed here with those by other investigators, especially Otsuka and Kunii[40].

(b) to compare the data of powder mixtures with those of iron oxide pellet and graphite powder kept in operation.

Three sets of experiments were conducted, viz.,

I. With powder mixtures without pressing

II. With mixtures of iron oxide and graphite powder pressed into pellet using a pressure of 200 p.s.i.

III. With mixtures of micro-pellets of iron oxide ($\sim$ 2 mm. dia.) and graphite powder

In these experiments also the size of the graphite particles was in the sieve range (-200, +230 mesh) as in all other investigations.

The first two sets of experiments were carried out at three different temperatures. Only two experiments were done in the third set.

The results of the first two sets shall be discussed first and those of the third set shall be discussed next.

The experimental conditions for all the three sets are presented in table 5.1. A weight ratio of C/O equal to 1.50 was taken. This was equivalent to a mole ratio of about 2. Therefore excess graphite was present to ensure presence of enough graphite towards the end. Otsuka and Kunii[40] did not take this precaution, and hence their results towards the end of the reduction period are subject to doubt.

6-2.1 Discussion of Experimental Errors

The overall reaction is endothermic and is fairly rapid (more or less completed in 40-50 minutes). Therefore a temperature drop of 15 to 20°C was noted during each experiment. The temperatures mentioned in table 5.1 represents average values.

Table 5.2 gives the total weight losses calculated through the computer program as discussed in Section 5-1.1, and also the weight losses measured after the experiments

were over. Except for the experiment M-5, the calculated weight losses were approximately 10 to 20 pct. greater than the experimental ones. From this an idea may be obtained about the overall accuracy of the flow rate and gas composition measurements. However it is to be kept in mind that the experimental weight losses also had some errors due to the difficulty of pulling the sample out from the reaction chamber fast.

Section 4-1.3 has already presented the results of the performance testing of the solid electrolyte cell set-up using H_2/H_2O gas mixture. The errors were within 5 pct. in the gas composition. However in the experiments on powder mixtures where the solid oxide electrolyte cell was employed to monitor the CO/CO_2 ratio in the gas, there was sometime lag in measurement because of the finite dead volume of the reaction chamber etc. This normally would tend to give higher percentages of CO_2 in the gas resulting into larger calculated values of oxygen loss and percentage reduction. A larger weight of the mixture should yield a higher flow rate of the product gas and hence less time lag and less error. This is what happened for example in experiment M-4. This also indicates that flow rate measurements were fairly good.

6-2.2 Discussion of the Results

Results of these experiments are given in Appendix AIII. Figures 6.3 and 6.4 show the plots of pct. CO, $-\dot{W}_c$ and $-\dot{W}_o$ Vs. pct. reduction for two of the experiments.

In Chapter 1, Section (1-4), findings of Otsuka and Kunii[40] have been presented and discussed. The results of this investigation, for example, those shown in Figs. 6.3 and 6.4, are of similar nature. Therefore a detailed discussion is not warranted. Only the important points would be reiterated below.

It can be seen from the Figures 6.3 and 6.4 that the two-stage behaviour is very much predominant with two peaks occurring at the two stages of reduction. The first peak occurs at about 10 pct. reduction and the second peak at about 50 pct. reduction. This is identical to the findings of Otsuka and Kunii reproduced in Fig. 1.3. The magnitude of the second peak is much larger compared to that of the first one.

The variation of gas composition with pct. reduction are also shown in Figs.6.3 and 6.4. Along with them the equilibrium gas composition curves corresponding to the following stagewise reduction have also been presented.

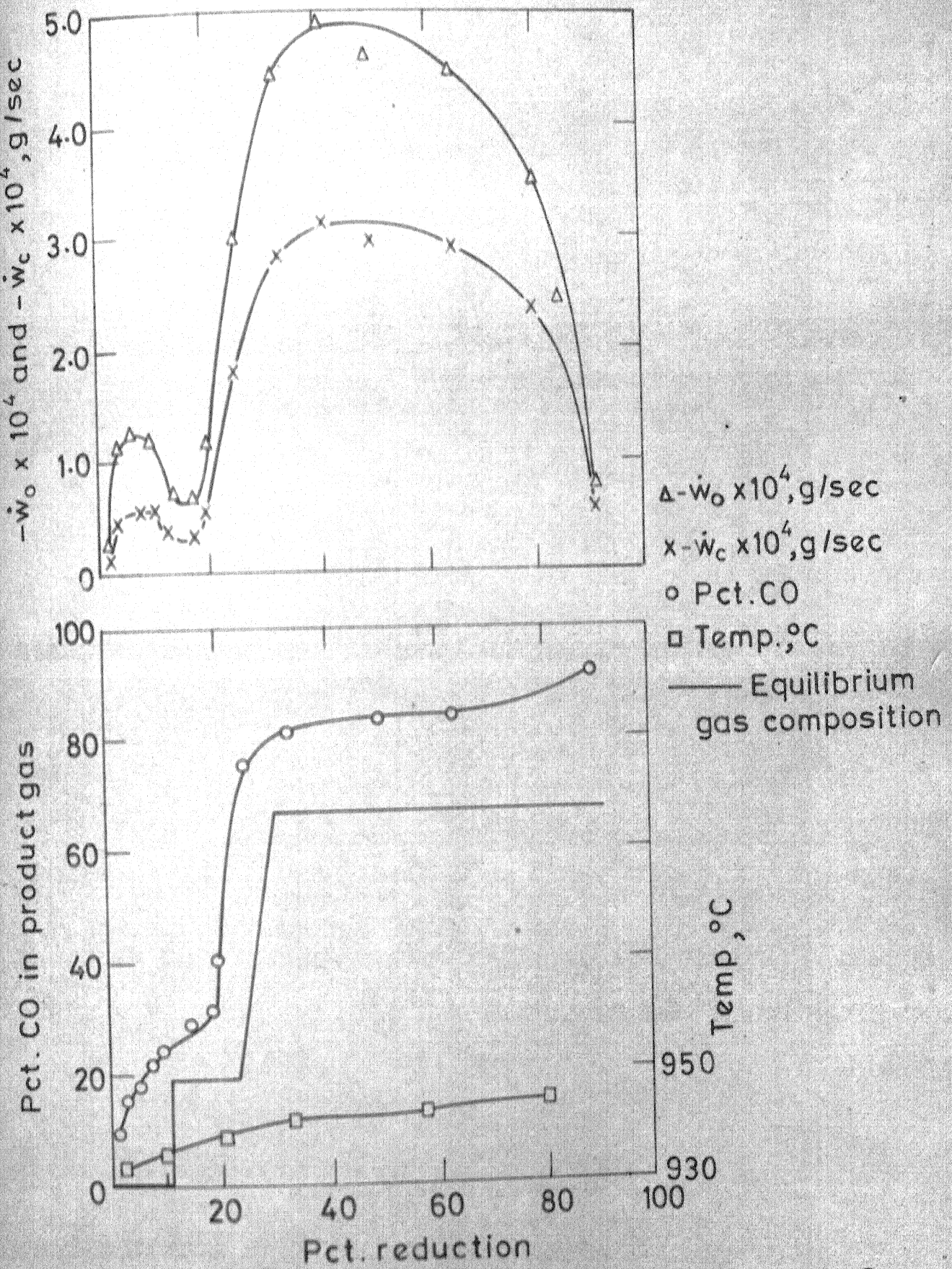

6.3 $-\dot{w}_o$, $-\dot{w}_c$ AND COMPOSITION OF THE PRODUCT GAS AS FUNCTION OF Pct. REDUCTION OF THE OXIDE FOR EXPERIMENT M-4

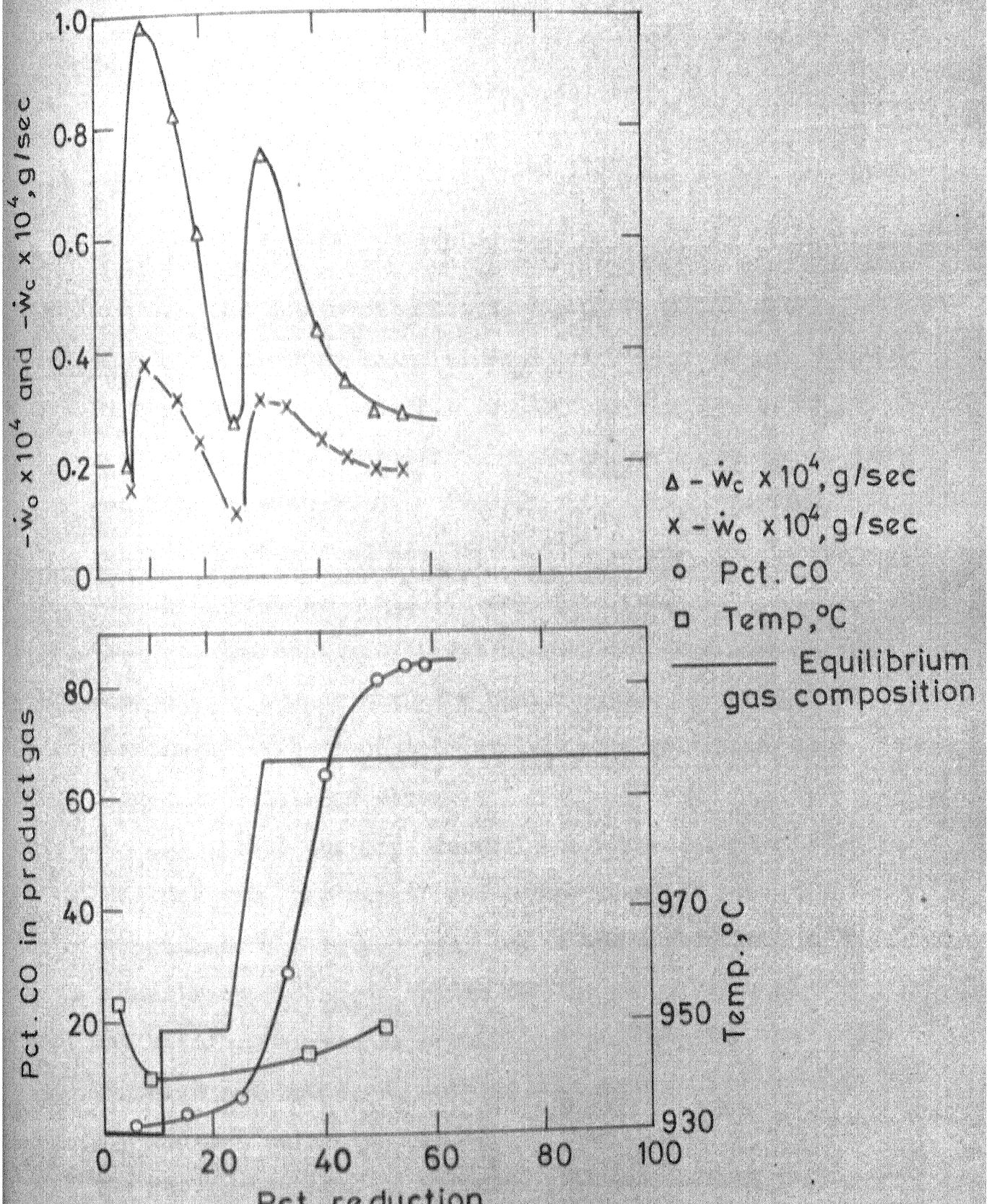

G. 6.4 $-\dot{w}_o$, $-\dot{w}_c$, TEMPERATURE AND Pct. CO IN PRODUCT GAS AS FUNCTION OF Pct. REDUCTION

$$3Fe_2O_3(s) + CO(g) = 2Fe_3O_4(s) + CO_2(g) \quad (1\text{-}4)$$

$$Fe_3O_4(s) + CO(g) = 3FeO(s) + CO_2(g) \quad (1\text{-}5)$$

$$FeO(s) + CO(g) = Fe(s) + CO_2(g) \quad (1\text{-}6)$$

The basis of plotting the equilibrium curve is that complete conversion of Fe_2O_3 into Fe_3O_4 corresponds to 11 pct. reduction and that into FeO corresponds to approximately 33 pct. reduction. Gas compositions in equilibrium coexistence with Fe_2O_3 - Fe_3O_4, Fe_3O_4 - Fe_YO, Fe_XO-Fe were noted from Ghosh and St. Pierre[61], because the latter had critically assessed all literature values.

The approximate matching of the experimental gas composition curves with the equilibrium ones further confirm that the reduction of Fe_2O_3 took place in three stages as mentioned above.

Since the experimental gas composition deviated somewhat from the actual gas compositions in some of the experiments due to some time lag it was decided to use $\dot{W}_c$ values rather than $\dot{W}_o$ values for the calculation of activation energy. As both CO and CO_2 have the same number of moles of carbon, $\dot{W}_c$ depends only on the flow rate of gas and not on the composition of the gas. However, if the gas composition is erroneous, it will affect the

percentage reduction. The percentage reduction obtained for experiment no. M-4 for which the gas composition is in good agreement with that of the equilibrium gas composition, is about 94 pct. This is the order of reduction expected when the flow of gases almost ceases. Thus the high percentage of reduction obtained in the case of experiments M-2 (119 pct.) and experiment M-5 (140 pct.) are perhaps due to the somewhat erroneous gas composition used for calculating $\dot{W}_o$.

From the above discussions it can be concluded that there was no appreciable error in the measurement of flow rates during the present investigations. Since the weights were not the same for all samples $-\dot{W}_c$ was converted into $\dot{F}_c$ by dividing by weight of graphite (eqn. 5-1).

Figure 6.5 presents the plot of log $\dot{F}_c$ Vs $\frac{1}{T}$. The activation energy obtained for the first stage is 73 Kcals/mole without pressing and 71 Kcals/mole with pressing. These are in good agreement with the 75 Kcals/mole obtained by Otsuka and Kunii.

Activation energy calculated for the second stage was 55 Kcals/mole for mixtures not pressed and 33.5 Kcals/mole for pressed pellets.

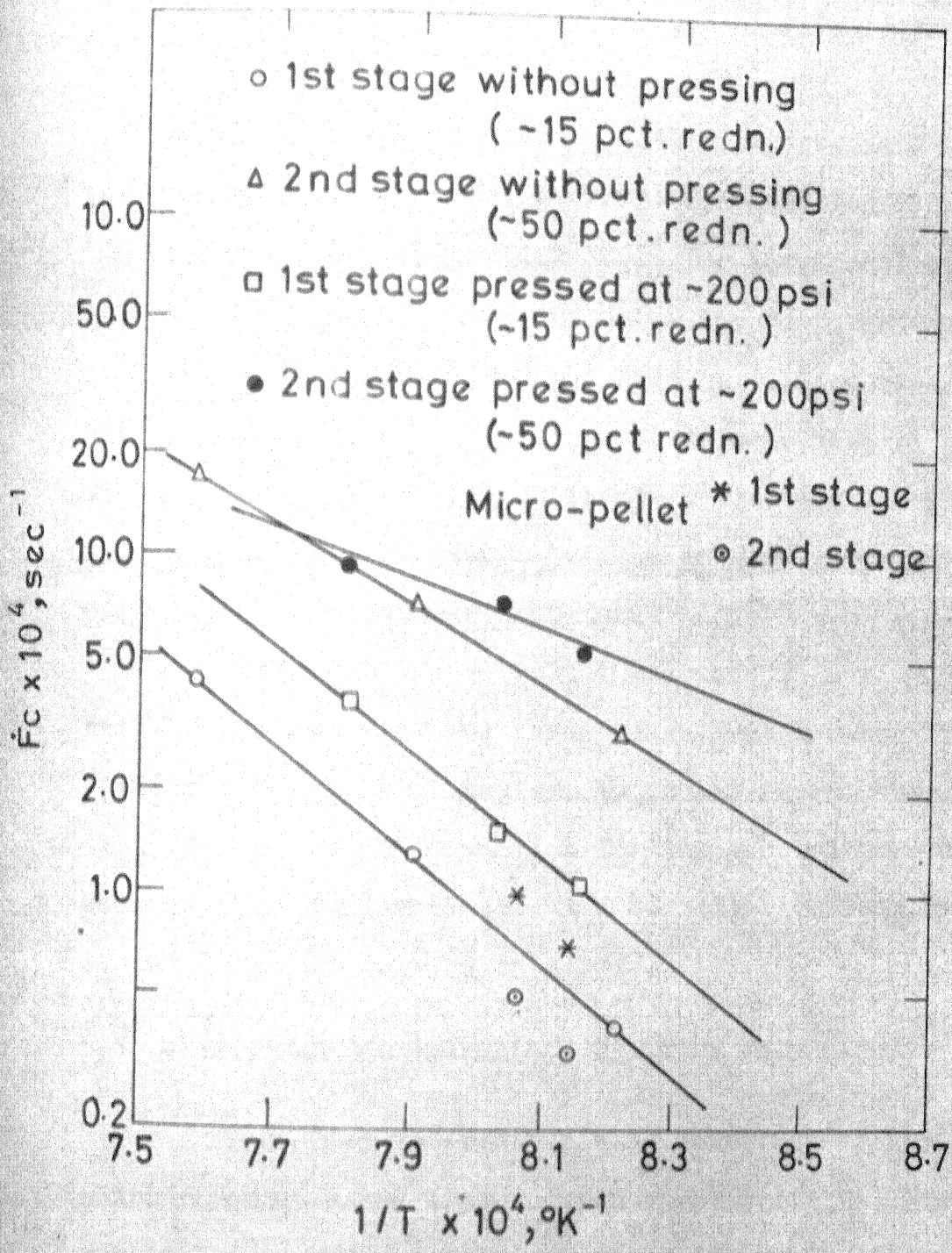

IG. 6.5 ARRHENIUS TYPE PLOT OF $\dot{F}c$ Vs. TEMPERATURE FOR MIXTURE OF Fe_2O_3 AND GRAPHITE PARTICLES

These behaviour patterns are also consistent with the findings of Otsuka and Kunii, who observed a lowering of activation energy in the second stage.

Otsuka and Kunii's results were explained (Section 1-4) by assuming that the gasification reaction ($C + CO_2 = 2CO$) is the rate controlling one. The large activation energy in the first stage is one of the confirmations for this contention. The enhanced rate as well as lowering of activation energy in the second stage were held to be due to the catalysis of the gasification reaction by reduced metallic iron. The results of the present investigation also lead to the same conclusions.

Pressing of the powder mixture did not affect the activation energy in the first stage, but lowered it from 55 Kcals/mole to 33.5 Kcals/mole in the second stage. This is an additional confirmation for the mechanism proposed, because pressing presumably led to better contact between Fe and C and hence more catalysis.

6-3 MIXTURE OF MICRO-PELLETS OF OXIDE AND GRAPHITE POWDER

Only two experiments were performed in this set, which confirmed the expected behaviour pattern. The results are shown in Appendix AIV. Figure 6.4 shows the variation of pct. CO, $-\dot{W}_c$ and $-\dot{W}_o$ against pct. reduction for one of the experiments.

The two stage reduction discussed in Section (6-2) is evident in this case as well. However, the rate in the second stage is lower than that in the first stage. As the iron oxide was in pellet form the surface of contact between reduced iron and graphite powder was very much lower. Thus the catalysing effect was very much reduced. Also the CO-content of the gas was about 70 to 80 pct., which lowered the $C-CO_2$ reaction rate considerably. This confirms that the higher rates obtained in the second stage in the experiments on powder mixture of oxide and graphite was due to the catalysing effect of the $C-CO_2$ reaction by reduced iron.

The activation energy could not be determined. However, the points corresponding to the $\dot{F}_c$ values of the two experiments shown in the log $\dot{F}_c$ Vs. 1/T plot show the comparative rates. The values corresponding to the first stage reasonably agree with those corresponding to the first stage in the powder mixture experiments, whereas those for the second stage are much lower than the corresponding second stage values in the case of powder mixture.

The above findings help us to confirm the following conclusions:

1) Reduction is controlled by $C-CO_2$ reaction

2) There is no significant catalysing effect in the first stage

3) In the second stage the reaction rate depends on the extent of catalysing effect on the $C-CO_2$ reaction by reduced metallic iron.

CHAPTER 7

DISCUSSION OF THE RESULTS ON REACTION OF IRON OXIDES PELLET WITH GRAPHITE POWDER KEPT IN SEPARATION

The literature survey (Chapter 1) revealed that informations regarding the reduction of iron oxides by carbon were lacking in some respects. Investigations have been made with powder mixtures of the two reactants. As discussed in Chapters 1 and 6, these studies have established that the gasification reaction, which is chemically controlled by and large, controls the rate of the overall reaction. However a powder mixture of iron oxide and carbon does not simulate the nature of dispersion of the reactants as encountered in the rotary kiln process of sponge iron making. Also catalysis by reduced iron complicates the interpretations.

Therefore this investigation on reaction of iron oxide pellet with graphite powder was undertaken. The oxide and graphite were kept in separation because intimate contact such as in pellets of powder mixtures, is not present in a rotary kiln.

The influence of the distance of separation between the reactants as well as of temperature on the rate of reaction were studied in the present investigation. The separation of the reactants allowed us to avoid any catalysis presumably by reduced iron through contact.

There was no external gas flow during the reaction. The empty volume of the reaction cell (Sec. 2-1.3 and Fig. 2.2) was kept small (approx. 3 cc). Also the outlet from the cell was fairly restricted, because it was a very narrow hole (0.75 mm i.d.). Both these precautions helped in lowering the influence of the surrounding atmosphere on the reaction.

The composition of the product gas as well as its flow rate were measured. By suitable calculation procedure (Sec. 4-2) it was possible to find out the instantaneous rates of oxygen and carbon loss as well as the cumulative rates of the same as a function of time. Cross-checking of these calculated values was possible by weighing of the oxide and graphite separately before and after the reaction. The distance of separation between the oxide and graphite also could be varied for determining its influence on the reaction rates.

The results of these investigations are presented in Appendix AI. Experimental conditions for all the experiments are shown in table 4.3.

7-1 REPRODUCIBILITY AND ERRORS OF MEASUREMENT

7-1.1 Errors in Temperature Measurement

The original arrangement for measurement of temperature was as shown in Figure 2.6. It was found that the Pt/10 pct. Rh wire was breaking off very often. Thus the measurement of temperature inside the reaction chamber could not be continued for most of the experiments. Excepting for experiments 7 and 9 (table 4.3), there was no insitu temperature measurement. In separate experiments without the CSZ tube, the temperatures were measured both inside and outside the reaction chamber, keeping all the other parameters the same. This showed that the temperature inside the reaction chamber was 6°C or so lower than that outside the chamber. This difference between the temperature inside and outside the reaction chamber was used for correcting the reaction temperature. An accuracy of ± 2°C can be claimed for the temperature control.

The temperature inside the reaction cell containing Fe_2O_3 and C could not be measured. Investigations on powder mixtures of Fe_2O_3 and C revealed a temperature drop of about 15°C as a result of the endothermic reaction. In pellet-graphite reaction the rates are smaller by an order of magnitude. Hence the temperature inside the cell

is expected to be only a few degrees centigrade lower compared to the temperature measured by thermocouple.

7-1.2 Errors in the Determination of Gas Composition

The reaction cell had an inner volume of about 3 cc only at the maximum distance of separation. The only outlet for the product gases was through the 0.75 mm i.d. alumina tube provided at the centre of the lid of the cell. As the CSZ tube was seated on the alumina tube outlet (Figure 2.5), the EMF corresponding to the gas composition was monitored as soon as the gas came out. As the volume of the reaction cell was small compared to the gas evolution rate (about 5 cc per minute) there could not be any appreciable time lag in measurement.

As mentioned in Sec. 6-2.1 and as shown in table 4.1, the calibration of solid oxide electrolyte cell by H_2/H_2O mixture showed that the measured ratios were in agreement with those expected within 5 pct.

7-1.3 Errors in Flow Measurement

It was inferred in Sec. 6-2.1 that the capillary flowmeters used for measuring flow rates of the product gas ($CO + CO_2$) were giving good results. Capillary No. 1 was employed for measuring flow rates in the pellet-graphite system.

7-1.4 Overall Reproducibility and Measurement Accuracy

By conducting a number of experiments initially, the reproducibility of the system was established. Figure 7.1 show comparison of Δh Vs. Pct. reduction curves for experiments 17, 21 and 22 conducted at about the same temperature of reaction (956°C). As the zero time selected for monitoring the Δh and EMF values was arbitrarily chosen in each experiment on the basis of qualitative judgement, there is some lateral displacement in the values plotted for the initial periods. It can be seen that there is fairly good agreement at the steady state region. The cumulative weight losses of oxygen and carbon calculated by numerical integration of instantaneous rates (Sec. 4-2.5) were matched with the experimentally measured weight losses. For a number of experiments the difference between the calculated and the experimental weight losses were within 5 to 10 pct., as may be seen from table 4.5. Therefore it may be stated that the rate measurements had accuracies of 5 to 10 pct. This is considered to be fairly good.

7-2 VARIATION OF RATES, GAS COMPOSITION AND TEMPERATURE WITH PROGRESS OF REACTION

Measured parameters such as Δh of flowmeter and EMF of solid oxide electrolyte cell were found to vary with

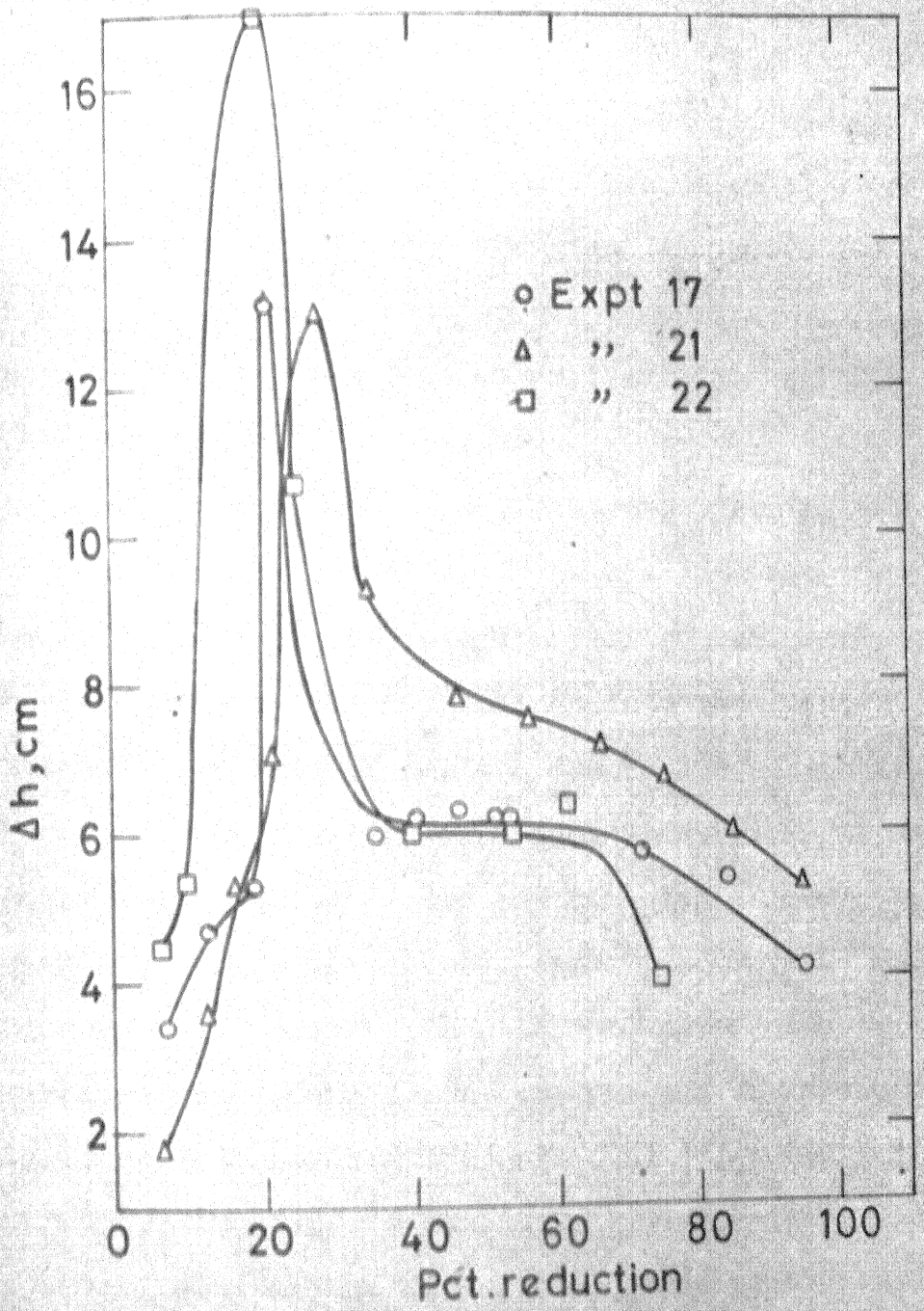

FIG. 7.1 Δ h, Vs. Pct. REDUCTION FOR EXPERIMENTS 17, 21 & 22

the progress of reaction (Figure 4.2). It was decided that for interpretation purposes pct. reduction is a better index of the extent of reaction than time. Figures 7.2 to 7.7 show $-\dot{W}_c$, $-\dot{W}_o$, gas composition and temperature as functions of pct. reduction for porous as well as dense pellets at various distances of separation.

Due to the nature of the experimental technique chosen it was not possible to have a constant temperature from the beginning of reactions to the end of reactions. The introduction of the CSZ tube into the reaction chamber demanded slow rate of heating due to its sensitivity towards thermal shock. Heating from room temperature at which the sample was introduced into the reaction chamber, to the reaction temperature (steady state temperature) was done in about 20 to 25 hours. Thus it was unavoidable that some reactions took place during the process of heating. However its extent was not significant. This slow heating also did not render the experiments strictly isothermal. Temperature varied to some extent during the course of the reaction as may be noted in Figures 7.2 to 7.7. Experiments conducted at higher temperatures (above 1000°C) suffered more from such errors. At low temperatures the reactions were extremely slow and took very long time to yield appreciable extent of reduction. This is what happened in experiment 19

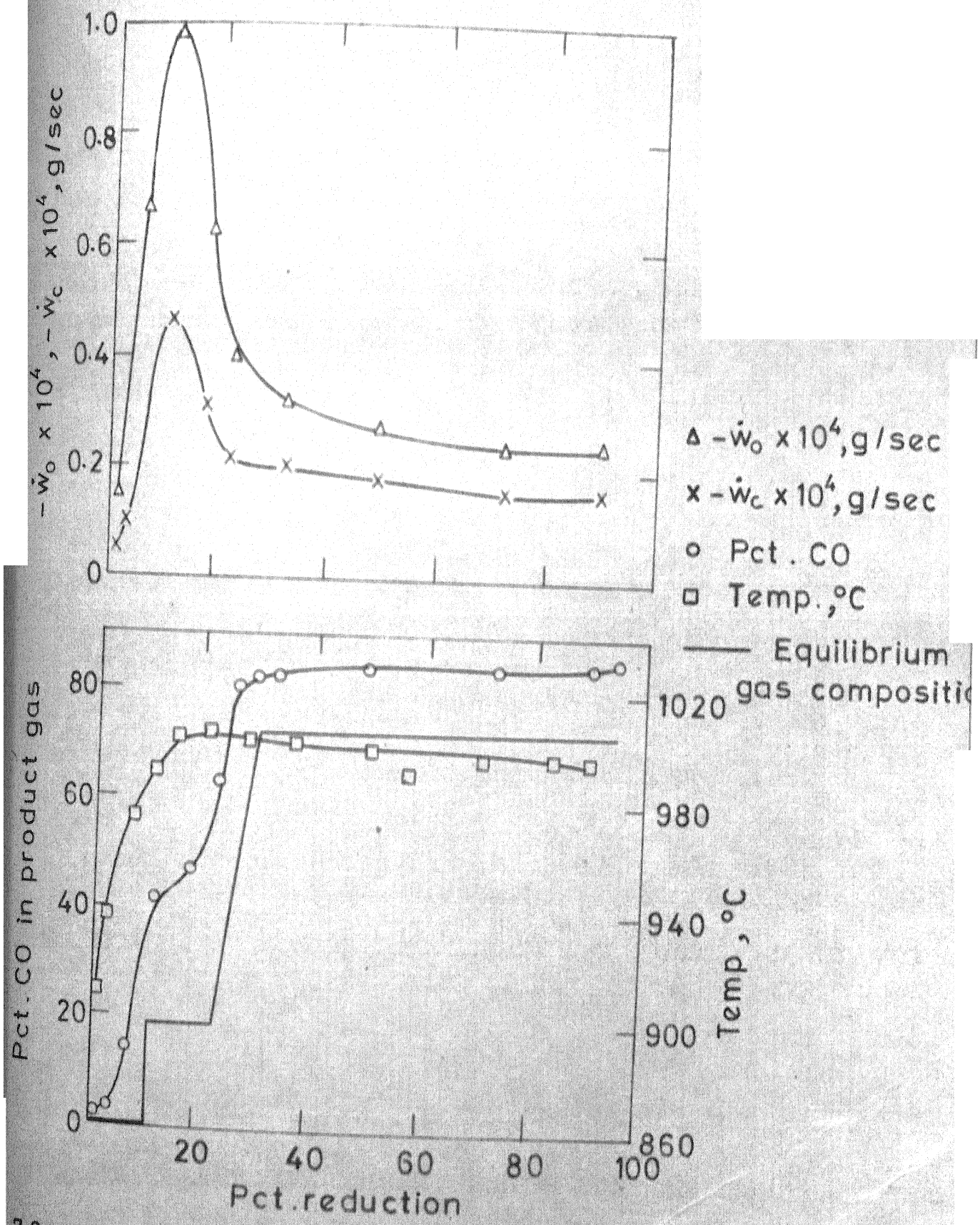

7.2 $-\dot{w}_o$, $-\dot{w}_c$, TEMPERATURE AND COMPOSITION OF THE PRODUCT GAS AS FUNCTION OF Pct. REDUC-

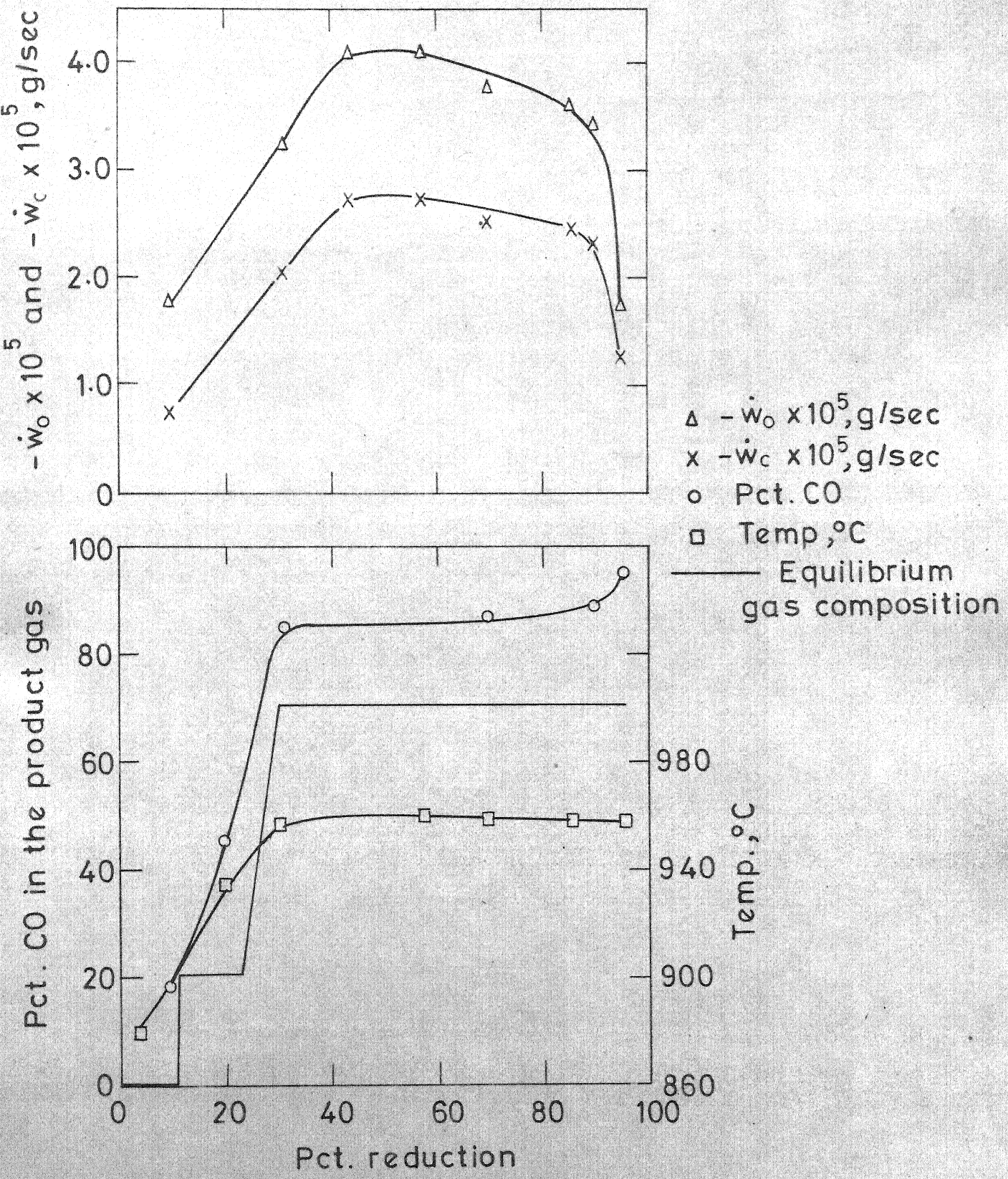

FIG. 7.4 $-\dot{w}_o$, $-\dot{w}_c$, TEMPERATURE AND COMPOSITION OF PRODUCT GAS AS FUNCTION OF Pct. REDUCTION FOR EXPERIMENT. 23

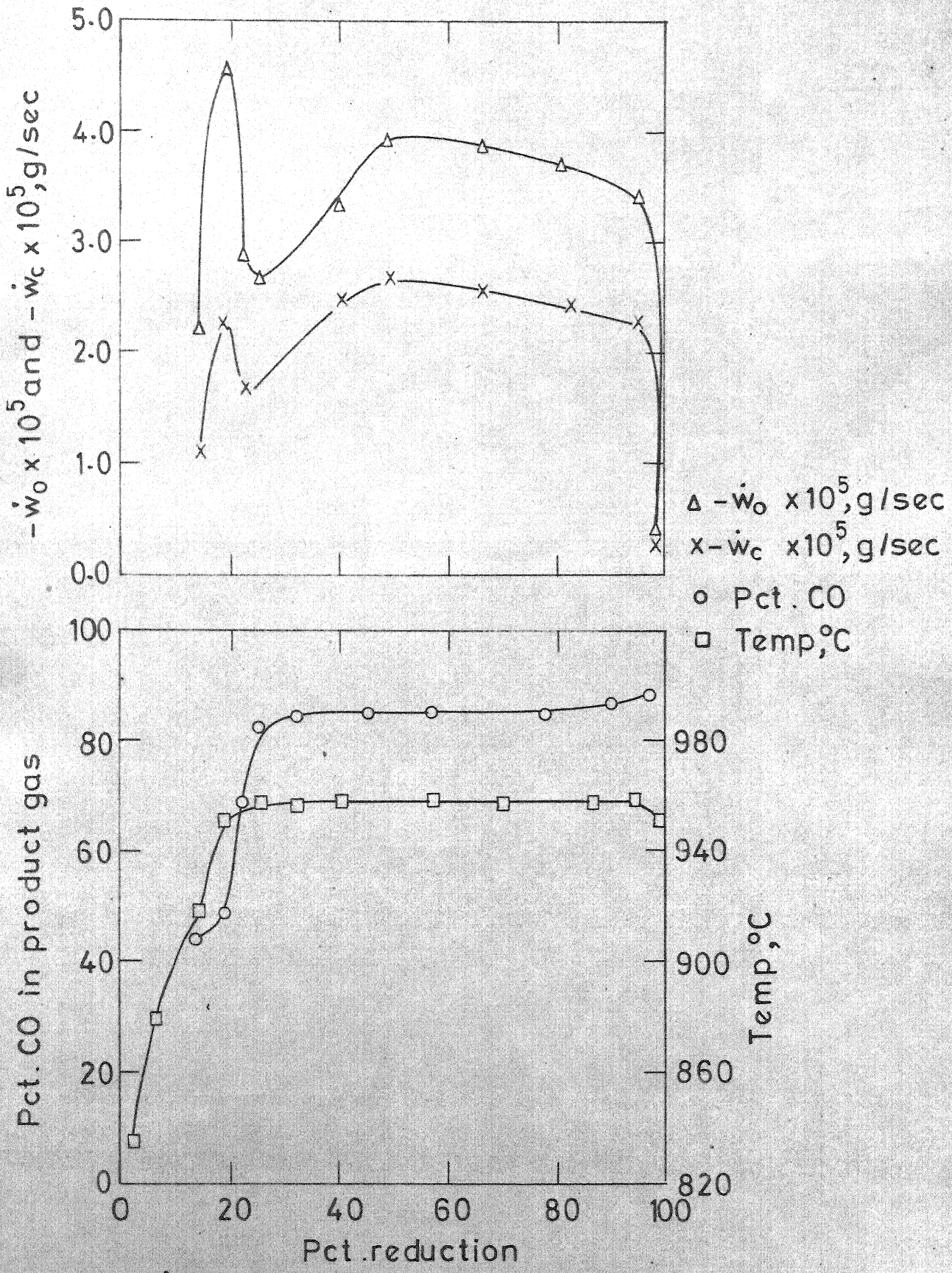

FIG. 7.5 $-\dot{w}_o$, $-\dot{w}_c$, TEMPERATURE AND COMPOSITION OF PRODUCT GAS AS FUNCTION OF Pct. REDUCTION FOR EXPERIMENT 24

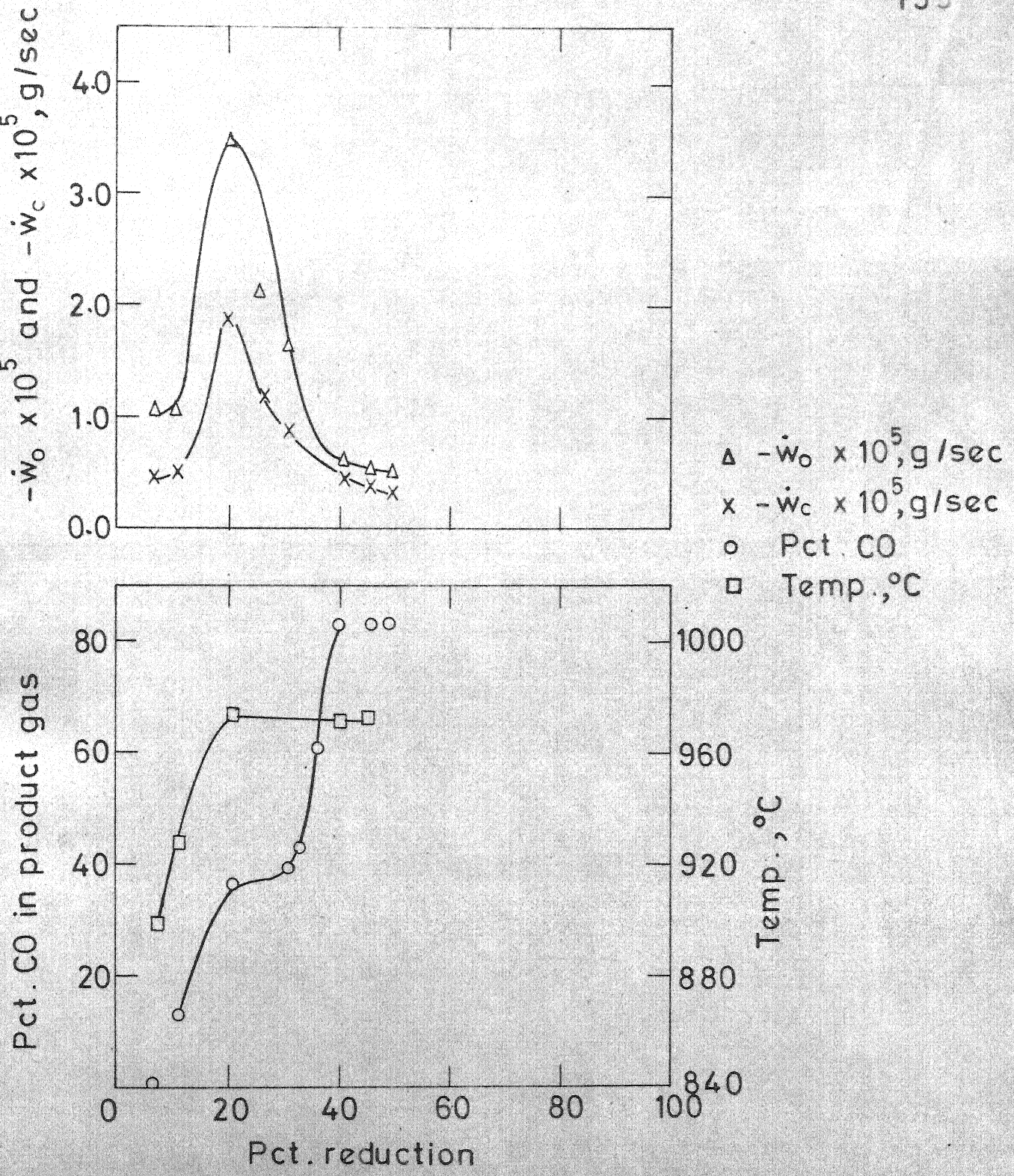

FIG. 7.6 $-\dot{w}_o$, $-\dot{w}_c$, TEMPERATURE AND COMPOSITION OF PRODUCT GAS AS FUNCTION OF Pct. REDUCTION FOR EXPERIMENT 27 (Dense pellet).

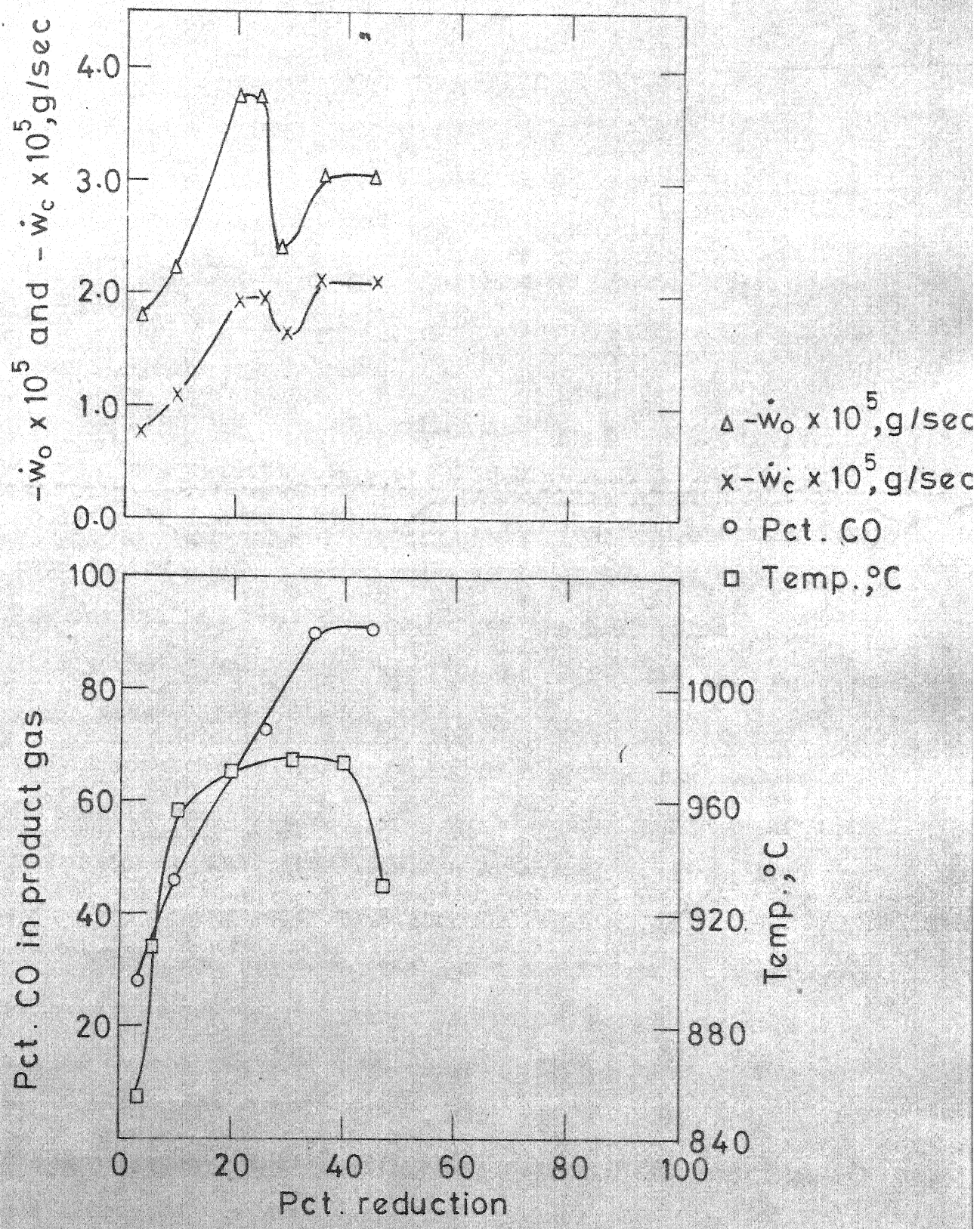

FIG. 7.7 $-\dot{w}_o$, $-\dot{w}_c$, TEMPERATURE AND COMPOSITION OF PRODUCT GAS AS FUNCTION OF Pct. REDUCTION FOR EXPERIMENT 28 (Dense pellet)

(table 4.3). Thus it was decided to do most of the studies at an intermediate temperature of about 950°C. Experiments 17, 21, 22, 23 and 24 were conducted at around this temperature. The reproducibility of these experiments has been demonstrated by Figure 7.1.

For the sake of explanation the plots of $-\dot{W}_c$ and $-\dot{W}_o$ Vs. pct. reduction may be divided into four regions as shown in Figure 7.3. In region I the reaction starts and the rate increases till a maximum rate is reached at the peak. The rate of reaction decreases from the peak value to a steady state value in region II. In region III the reactions reach steady state. Temperature and gas composition also remain constant in this region. As the reaction continues further there is scarcity of oxygen available for gasification to continue. The rate decreases drastically. This is indicated as region IV in Figure 7.3.

Figure 7.8 shows the gas compositions in coexistance with various condensed phases in the iron-carbon-oxygen system over a range of temperature. It has been reproduced from Ghosh and St. Pierre[61], because the latter checked the consistency of all available standard literature data and presented the most appropriate values.

Table 7.1 also presents the equilibrium gas compositions for all the experiments both for $CO-C-CO_2$

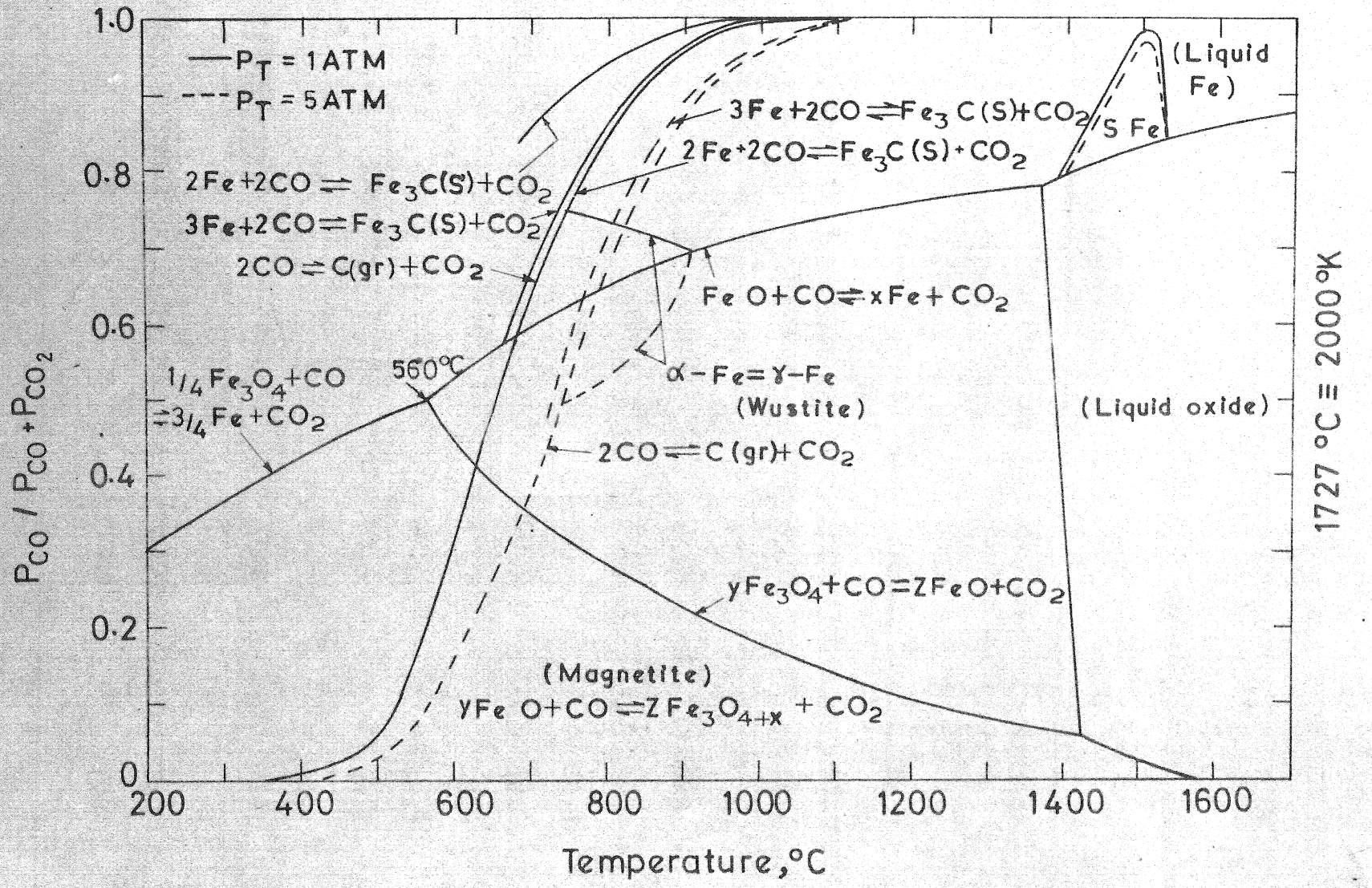

FIG. 7.8 IRON - CARBON - OXYGEN EQUILIBRIUM DIAGRAM [61]

Table 7.1 Percent CO Experimental and in Equilibrium with $Fe-Fe_{0.95}O$ and $C-CO_2$ (61)

Expt. No.	Temp., °C	Equilibrium pct. CO calculated ($Fe - Fe_xO$)	pct. CO experimental	Equilibrium pct. CO calculated ($CO-C-CO_2$)
7	1001	72.0	82.6	99.5
9	1007	72.2	85.0	99.8
14	1018	72.5	87.2	99.8
17	956	70.5	84.0	98.5
18	1017	72.5	85.2	99.8
19	840	67.0	82.6	89.5
20	926	70.0	88.1	98.0
21	957	70.6	87.7	98.6
22	956	70.5	87.9	98.5
23	958	70.7	87.6	98.7
24	957	70.6	84.6	98.6
25	986	71.7	87.4	99.2
26	975	71.2	81.8	99.0
27	972	71.3	83.0	98.8
28	974	71.2	90.9	99.0

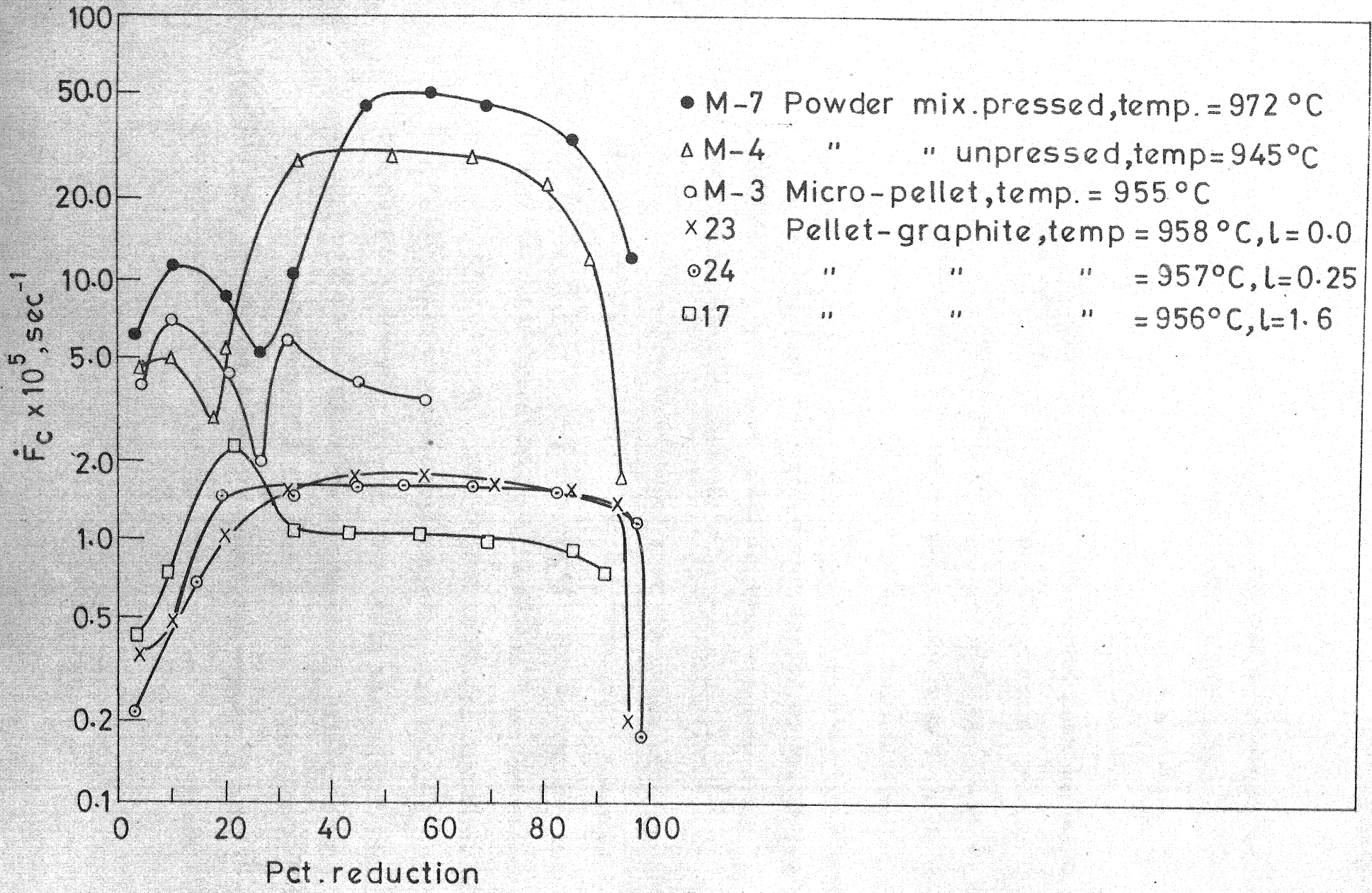

FIG. 7.9 COMPARISON OF RATES OF REACTION FOR POWDER MIXTURE PRESSED AND UNPRESSED, MICRO-PELLET-GRAPHITE MIXTURE AND PELLET-GRAPHITE IN SEPERATION AND IN CONTACT

that there was one sharp peak followed by a steady state region corresponding to wustite to iron reduction.

Thus one may note the systematic decrease of the second peak from powder mixture to micropellets to Fe_2O_3 pellet. Total elimination of the second peak was achieved by separation of the pellet from the graphite powder physically. Otsuka and Kunii[40] as well as Chapter 6 of this thesis explained the second peak observed in the powder mixture studies by catalytic action of reduced iron on the gasification reaction. The data shown in Figure 7.9 confirm it. The extent of catalysis would depend on the amount of contact between reduced metallic iron and carbon. In powder mixture the contact would be most extensive.

It may also be noted that the reaction rates in powder mixture were about 5 to 6 times larger compared to those in the pellet-graphite system even during the initial stages when catalytic action of metallic iron was presumably absent. Experiments 23 and 24 for which the distances of separation between pellet and graphite were 0.0 and 0.25 cm respectively showed a decreased rate in the initial stages as compared to the rates in experiment 17 (distance of separation = 1.6 cm) for the same stages of reduction. Thus one may be tempted to believe that the volume of the product gases exposed to the reactants has some effect on

the rate in the initial stages of reduction. A discussion on this shall be taken up later.

7-3 BEHAVIOUR PATTERN IN THE STEADY-STATE REGION

Tables in Appendix AI and Figures 7.2 to 7.7 show that the constant rate i.e. the steady state (Region III in Figure 7.3 for example) was accompanied by steady gas composition and temperature. Since the behaviour is most uniform here, an effort would be made first to interpret the behaviour in this region.

As mentioned earlier (Secs. 5-3 and 6-2.2), $\dot{F}_c$ (Rate of fractional loss of weight of carbon, in sec^{-1}) has been used for comparison of rates of gasification. Since the rate of gasification of carbon is proportional to its weight approximately[36], $\dot{F}_c$ rather than $\dot{W}_c$ (which varies with the weight of graphite), is considered to be a better index for comparison of rates. Also as discussed in Sec. 6-2.2, $\dot{F}_c$ is a parameter of more fundamental interest than $\dot{F}_o$ since the gasification reaction rather than reduction reaction is likely to control the rate of the overall reaction.

7-3.1 Activation Energy

Figure 7.10 shows the plot of log $\dot{F}_c$ Vs. $\frac{1}{T}$ for the steady state. Distances of separation between the pellet and graphite powder were the same for all the data points included. The straight line was obtained by least square fitting of the data points. The value of activation energy obtained is 75 Kcal/g mole.

The gas compositions were slightly different from experiment to experiment (84-89 pct. CO). However, this should not affect the activation energy much. The three data points clustered together at about 956°C ($\frac{1}{T} = 8.14 \times 10^{-4}$) had also different gas compositions (84-88 pct. CO). As can be seen this variation did not lead to much difference in $\dot{F}_c$.

The activation energy for gasification of carbon by CO_2 as obtained from literature is in the range of 60-90 Kcals/mole.[36,38,40] The activation energy obtained for the present investigation using powder mixtures of oxide and graphite, in the absence of catalytic effect was found to be within 70-75 Kcals/mole (Sec. 6-2.2). Therefore the value is consistent with control of rate by the gasification reaction, which is chemically controlled.

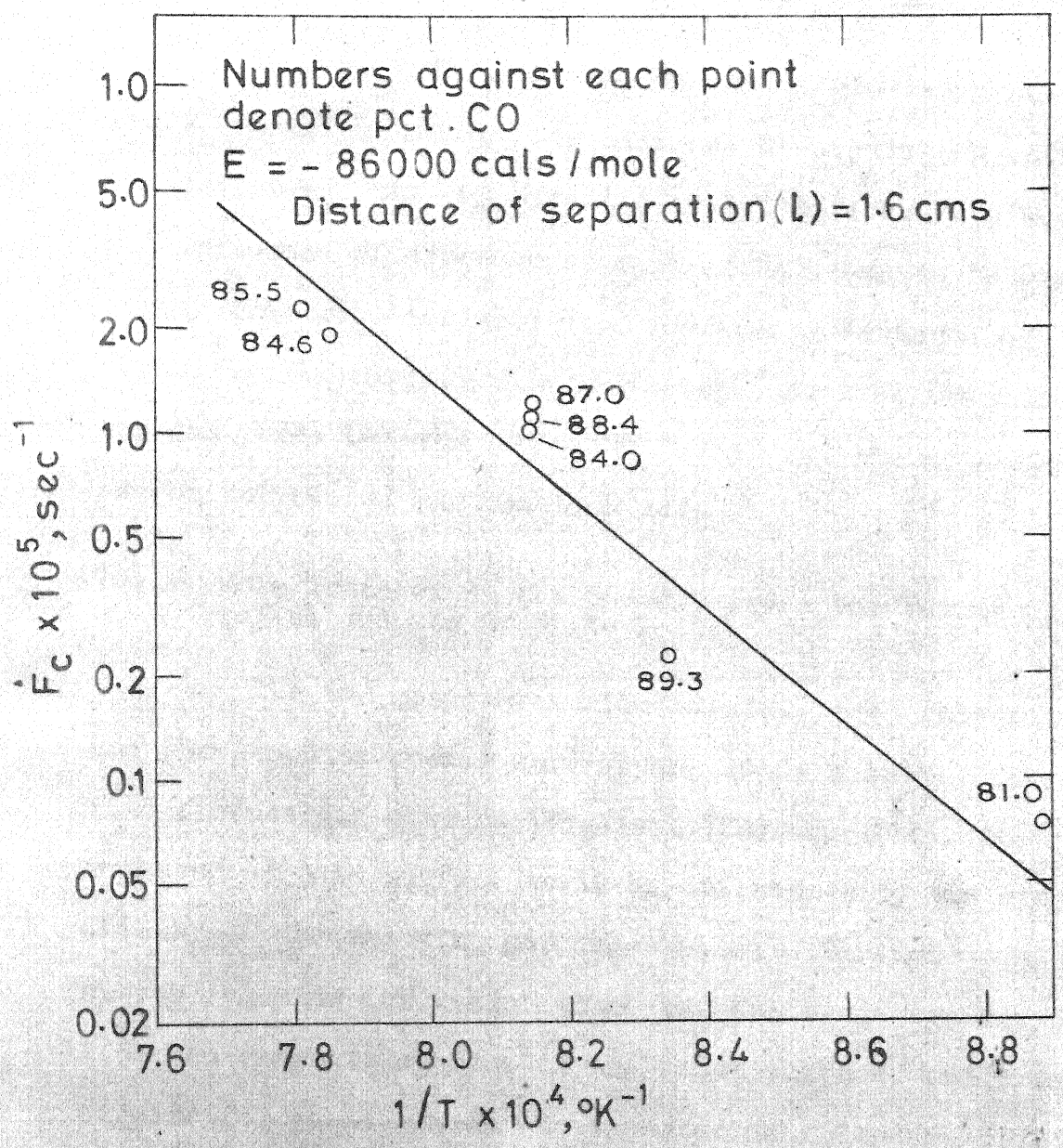

FIG. 7.10 LOG $\dot{F}_c$ Vs. 1/T LEAST SQUARE LINE

7-4 INFLUENCE OF DISTANCE OF SEPARATION ON REACTION RATE

Figure 7.11 shows the variation of steady state $\dot{F}_c$ and $\dot{F}_a$ as a function of the distance of separation between the pellet and the graphite (1) at 957°C (i.e. 1230°K). The influence of distance of separation seems to be significant. The rate decreased with increasing distance of separation linearly. This indicates that mass transfer in the gas phase between the oxide pellet and the graphite powder influenced the reaction rate.

7-4.1 Mass Transfer in the Space Between the Ferric Oxide Pellet and the Graphite Powder

The two reacting surfaces, viz., the oxide pellet and the graphite powder were separated by a space filled with product gas mixture (Figure 7.12a; page 174). The rate of reaction at each surface would be influenced by the availability of the reacting gaseous species. Through this space, carbon monoxide for reduction of the oxide was transferred from the graphite surface to the oxide surface, while carbon dioxide for gasification was transferred in the reverse direction i.e. from the oxide surface to the graphite surface. Besides molecular diffusion, natural convection is expected in this gas space.

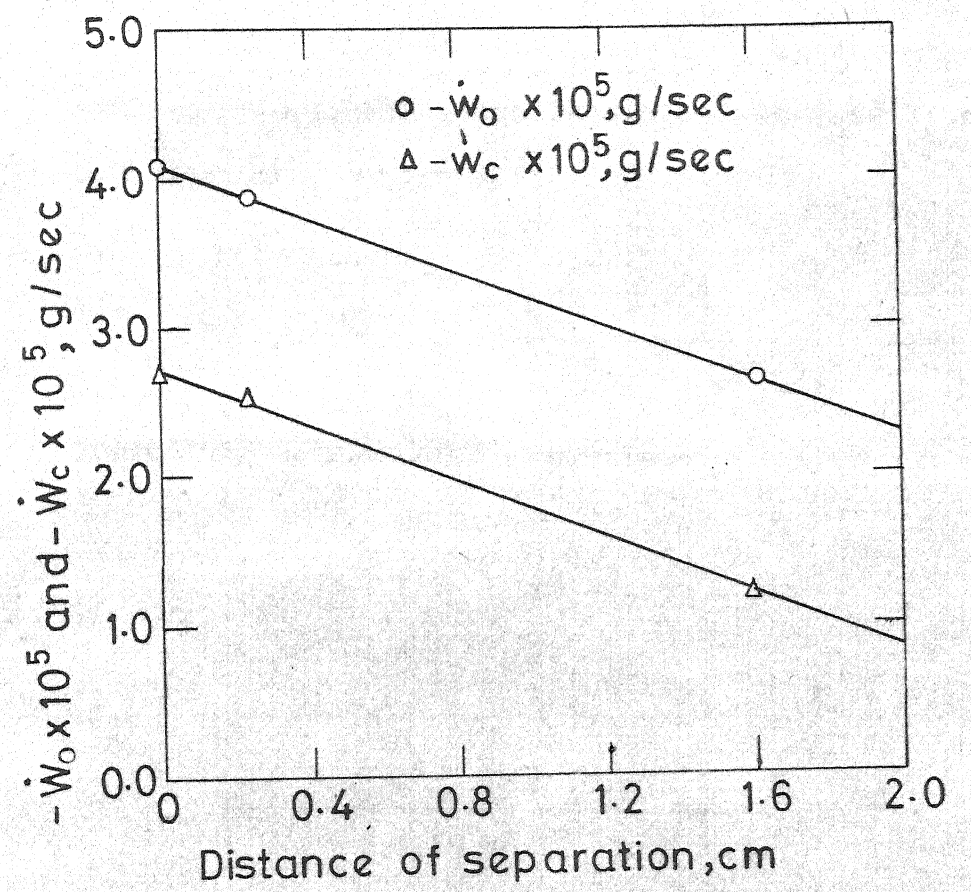

FIG.7·11 $-\dot{W}_o$ AND $-\dot{W}_c$ AT 44 Pct. REDUCTION AS A FUNCTION OF DISTANCE OF SEPARATION (Expts. 23, 24 & 17).

7-4.2 Rate of Counter Diffusion of CO and CO_2 in the Gas Space

The type of flow prevailing in the space between the pellet and the graphite can be assessed by calculating the Reynold's number (Re)

$$Re = \frac{\rho V d}{\mu} = \frac{\frac{\rho Q}{\pi/4\, d^2} \cdot d}{\mu}$$

where d = I.D. of the crucible = 1.5 cm

Q = 0.1 cc/sec.

$\rho = 0.3 \times 10^{-3}$ gm/cc

$\mu = 450 \times 10^{-6}$ poise

or,

$$Re = \frac{0.3 \times 10^{-3} \times 4/ \times 0.1}{4.50 \times 10^{-4} \times 1.5} < 1$$

This is an approximate assessment, but definitely shows that laminar flow prevails. Reduction of the oxide by CO is equimolar counter-current whereas the gasification reaction involves unequal molar fluxes of the reacting CO_2 and the product CO gases. At the steady-state, diffusion and convection arising from unequal counter fluxes would lead to the following equation.(62)

$$J_{iz} = -\frac{D_i}{RT} \cdot \frac{dp_i}{dz} + \frac{p_i}{P_T} \cdot \sum J_{iz} \qquad (7\text{-}1)$$

where Z is the vertical co-ordinate,

D_i = Diffusivity of the i^{th} species, $cm^2\ sec^{-1}$,

P_T = Total pressure, atm.,

R = 82.06 cc atm./gm.mole. °K,

and J_{iz} = Flux of the i^{th} species in z-direction in gm. moles/sec. cm^2 due to the combined effect of diffusion and convection arising from unequal counterflux.

Let $J_{iz} = J_{CO_2}$, $\sum J_{iz} = J_{CO_2} + J_{CO}$

and X_{CO_2} = Mole fraction of CO_2 in the gas

$X^{ex}_{CO_2}$ = Mole fraction of CO_2 in the exit gas.

Noting that P_T is equal to 1 atm.,

$$X_{CO_2} = p_{CO_2} \tag{7-2}$$

Also $D_{CO} = D_{CO_2} = D$ because it is a binary gas mixture.

Hence, $$J_{CO_2} = -\frac{D}{RT} \cdot \frac{d\, p_{CO_2}}{dz} + p_{CO_2}(J_{CO_2} + J_{CO}) \tag{7-3}$$

Again, $$\frac{-\dot{n}_c}{-\dot{n}_o} = \frac{X_{CO} + (1 - X_{CO})}{X_{CO} + 2(1 - X_{CO})}$$

$$= \frac{1}{2 - X_{CO}} = \frac{1}{1 + X_{CO_2}} \tag{7-4}$$

Now, $J_{CO_2} \propto -\dot{n}_c$ and $J_{CO} \propto -\dot{n}_o$ and also J_{CO} is negative with respect to J_{CO_2}. Therefore,

$$\frac{J_{CO}}{J_{CO_2}} = \frac{1 + X^{ex}_{CO_2}}{1} \tag{7-5}$$

or, $$J_{CO} + J_{CO_2} = (1 - 1 - X_{CO_2})J_{CO_2}$$

$$= - X_{CO_2} \cdot J_{CO_2} \tag{7-6}$$

Combining eqns. (7-3) and (7-6)

$$\frac{d\, p_{CO_2}}{(1 + p_{CO_2} \cdot X^{ex}_{CO_2})} = - \frac{RT}{D} \cdot J_{CO_2} \cdot dz \tag{7-7}$$

At the steady state, J_{CO_2} is a constant. Integrating within the following boundary conditions (Figure 7-12a), viz.

At the bottom surface of the oxide pellet,

$$z = 0, \quad p_{CO_2} = p^{o}_{CO_2} \tag{7-8a}$$

and at the top surface of graphite,

$$z = l, \quad p_{CO_2} = p^{l}_{CO_2} \tag{7-8b}$$

one obtains,

$$\frac{2.3}{X^{ex}_{CO_2}} \log \frac{1 + p^{l}_{CO_2} \cdot X^{ex}_{CO_2}}{1 + p^{o}_{CO_2} \cdot X^{ex}_{CO_2}} = \frac{RT}{D} \cdot J_{CO_2} \cdot l \tag{7-9}$$

Rewriting equation (7-9)

$$J_{CO_2} = \frac{2.3}{X^{ex}_{CO_2}} \cdot \frac{D}{RTl} \cdot \log \frac{1 + p^{l}_{CO_2} \cdot X^{ex}_{CO_2}}{1 + p^{o}_{CO_2} \cdot X^{ex}_{CO_2}} \qquad (7\text{-}10)$$

Assuming that, $p^{l}_{CO_2} = p_{CO_2}$ in equilibrium with carbon and $p^{o}_{CO_2} = p_{CO_2}$ in equilibrium with Fe - Fe_xO, with the following data of experiment 17, viz.

$T = 1229°K$, $D = 1.756\ cm^2/sec$, $d = 1.52\ cm$

$l = 1.6\ cm$, $-\dot{W}_c = 1.628 \times 10^{-5}\ gm/sec$

$-\dot{W}_o = 2.518 \times 10^{-5}\ gm/sec$, $p^{o}_{CO_2} = 0.295\ atm.$,

$p^{l}_{CO_2} = 0.015\ atm$, and $X^{ex}_{CO_2} = 0.16$

equation (7-10) yields:

$$J_{CO_2} = 0.313 \times 10^{-5}\ moles/sec.cm^2$$

$$-\dot{n}_c = J_{CO_2} \times \frac{\pi}{4} d^2$$

$$-\dot{W}_c = 12 \times (-\dot{n}_c) = 12 \times J_{CO_2} \times \frac{\pi}{4} d^2$$

$$= 6.872 \times 10^{-5}\ gms/sec. \qquad (7\text{-}11)$$

The above value of $-\dot{W}_c$ is expected if equilibrium is assumed to prevail at z = 0 and z = 1. In this case the value of $(p^{o}_{CO_2} - p^{l}_{CO_2})$ would be 0.28 atm. Now it can be approximated that:

$$-\dot{W}_c \propto (p^o_{CO_2} - p^1_{CO_2})$$

Then the actual value of $(p^o_{CO_2} - p^1_{CO_2})$ at the steady-state would be given as:

$$(p^o_{CO_2} - p^1_{CO_2})_{actual} = \frac{-\dot{W}_c(Exptl.)}{-\dot{W}_c(Calcd.)} \times 0.28 = 0.076$$

If equimolal counter-current diffusion were the case, then

$$J_{CO_2} = \frac{D}{RT} \cdot \frac{p^o_{CO_2} - p^1_{CO_2}}{l} \qquad (7\text{-}12)$$

and under the assumption of equilibria at both surfaces $-\dot{W}_c$ may be calculated as 4.69×10^{-5} gm/sec. This value is lower than that obtained using eqns. (7-10) and (7-11) by about 50 pct. This is because the eqn. (7-12) ignores the convection term. The value predicted by eqn. (7-10) may be taken as the more realistic one.

In addition to the convection arising out of the nonequality of fluxes of CO and CO_2, another source of convection is expected. Carbon dioxide is heavier than carbon monoxide. Also the CO_2-content of the gas layer near the bottom surface of the pellet is the highest. This would tend to set up convection loop similar to the ones that arise during induction stirring or thermal convection. However it is being ignored in this analysis because of the fact that this convection would be damped considerably due to space restrictions.

7-5 MASS TRANSFER AND CHEMICAL REACTION INSIDE THE OXIDE PELLET AT STEADY-STATE

Layerwise oxidation test of the partially reduced oxide pellets (table 4.6) indicated by and large porous pellet type reduction.

Since the reduction is porous pellet type, the reducing gas (CO) would diffuse through the oxide pellet. While it diffuses it would go on reacting with the oxide producing CO_2. Therefore a concentration gradient in CO and CO_2 would exist inside the pellet. Figure 7-12b depicts the situation. Let the concentration of CO and CO_2 at the bottom surface of the pellet be C^o_{CO} and $C^o_{CO_2}$ for CO and CO_2 respectively. The top layer of the pellet showed very little oxygen loss. Hence the concentrations there can be assumed to be those in equilibrium with Fe and wustite viz. C^e_{CO} and $C^e_{CO_2}$.

The pellet is exposed to gas only at the bottom face, other surfaces being approximately sealed. Therefore the mass transfer geometry corresponds to that of a flat disc sealed on all sides except at one face. At the steady-state,

$$D_e \cdot \nabla^2 C_i + R_i = 0 \qquad (7\text{-}13)$$

where $D_e = \frac{D\varepsilon}{\tau}$

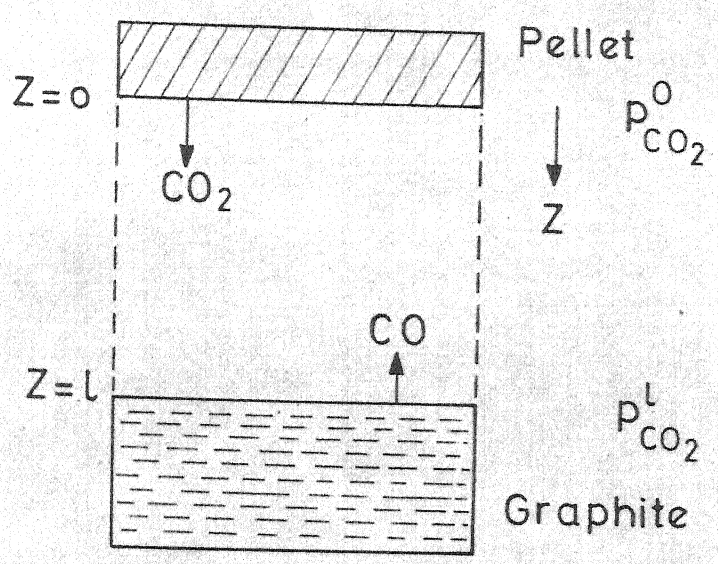

FIG.7.12(a) MASS TRANSFER IN THE GAS SPACE

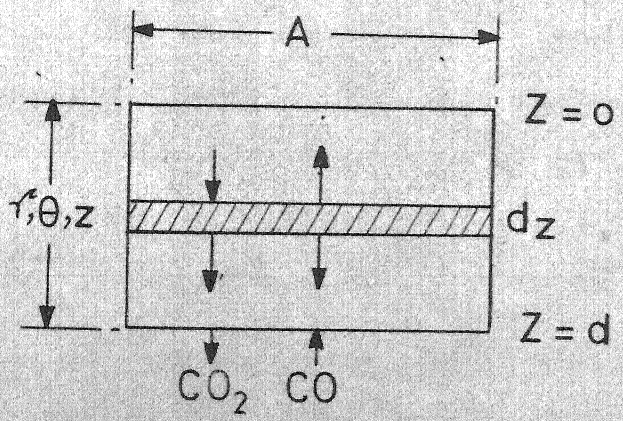

FIG.7.12(b) MASS TRANSFER IN THE PELLET

R_i = Rate of generation of species i in gm.moles/cc.sec.

and C_i = Concentration in gm.moles/cc

$$= \frac{p_i}{RT}$$

Now, for the geometry sketched in Figure 7-12b, eqn. (7-13) can be simplified as:

$$D_e \cdot \frac{d^2C}{dz^2} + R_{CO_2} = 0 \qquad (7\text{-}14)$$

where C refers to concentration of carbon dioxide as the i^{th} species. For solving this equation, a knowledge of the rate of chemical reaction:

$$Fe_xO(S) + CO(g) = XFe(S) + CO_2(g) \qquad (1\text{-}6)$$

is required. Bickenese and Clarke[21] proposed the following equation based on their experimental findings on reduction of granules of wustite with mixture of CO and CO_2.

$$\frac{[1 - (1-f)^{1/3}]}{t} = [4.3e^{-13,800/RT}] \times [\frac{C_e - C}{C_e}] \qquad (1\text{-}10)$$

A discussion on this has already been made in Chapter 1. Out of all literature reports, the rate equation (1-10) is the most appropriate one to the author's knowledge for the present situation for the following reasons.

(1) Bickenese and Clarke used small particle sizes of oxide of the order of -30 + 40 to -12 + 16 mesh. They did not find any influence of particle size on reduction rate because of sufficient porosity. Therefore it is expected to give the chemically controlled rate of reaction of gases with individual grains in the pellet.

(2) The temperature range and gas composition range covered is similar to that of the present investigation.

(3) The eqn. (1-10) deals with reduction of wustite to iron just as in the steady state here. Equation (1-10) shows that the kinetics is first order reversible with respect to carbon dioxide.

Equation (7-14) has been solved in the literature[63] and the solution presented as:

$$\eta = \frac{\tanh \phi_L}{\phi_L} \qquad (7\text{-}15)$$

where η = effectiveness factor

$$= \frac{\text{actual rate for the whole pellet}}{\text{rate evaluated at the bottom surface conditions}}$$

$$= \frac{r_p}{r_S} \qquad (7\text{-}16)$$

and $$\phi_L = L\left(\frac{k_1(K_e + 1)}{K_e} \cdot \frac{\rho_S}{D_e}\right) \qquad (7\text{-}17)$$

where $L = \frac{V}{A}$ = pellet thickness, cm

ρ_S = density of solid oxide, gms/cc

K_e = equilibrium constant

k_1 = forward reaction rate constant for eqn. (1-6), gm.moles/sec. (gm. of oxide) $(C_e - C)$

and r = local rate per unit mass of oxide, gm. mole O/ sec. (gm. of oxide)

$= f(C, T)$

$r_p = \eta r_S = \eta f(C_S)$ at constant temperature

$$r_S = k_1\left(\frac{p^e_{CO_2} - p^o_{CO_2}}{RT}\right), \text{ gm. mole } CO_2/\text{sec. (gm. of oxide)}$$

$p^e_{CO_2}$ = partial pressure of CO_2 in equilibrium with Fe_xO - Fe, atm.

η may be obtained from η Vs. ϕ_L curves[63] also instead of calculating from eqn. (7-15). D_e was calculated using the following relation[63]

$$\frac{1}{D_e} = \frac{1}{D_{e,M}} + \frac{1}{(D_k)_{CO_2}} \qquad (7\text{-}18)$$

$$D_{e,M} = \frac{1}{D_{CO_2} \times \frac{\varepsilon}{\tau}} \qquad (7\text{-}19)$$

ε and τ may be assumed to be 0.5 and 2 respectively for the present situation. D_{CO_2} may be obtained using the relation given by Bird et al.[64]

$$D_{CO_2} = 0.0018583 \frac{T^{3/2} \left(\frac{1}{M_{CO_2}} + \frac{1}{M_{CO}}\right)^{1/2}}{P_T \, \sigma^2_{CO,CO_2} \, \Omega_{D_{CO,CO_2}}} \qquad (7\text{-}20)$$

where, M = molecular weight

σ = Lennard-Jones parameter, in Angstrom

$\Omega_{D_{CO,CO_2}}$ = dimensionless function of the temperature and of the intermolecular potential field

$(D_K)_{CO_2}$ = Knudsen diffusivity[63]

$$= 9.70 \times 10^3 \cdot a\left(\frac{T}{M_{CO_2}}\right)^{1/2} \qquad (7\text{-}21)$$

For experiment 17

$T = 1229°K$, $\quad -\dot{W}_o = 2.518 \times 10^{-5}$ gm/sec.

$L = 0.29$ cm, $\quad W_p$ = wt. of pellet

$= 1.9162$ gm.

$$K_e = \frac{p^e_{CO_2}}{p^e_{CO}} = \frac{0.295}{0.705}$$

$$= 0.4184,$$

$$D_e = 0.404 \text{ cm}^2/\text{sec},$$

and $\quad \rho_S = 3.0$ g/cc

k_1 in eqn. (7-17) was determined to be 2.9 3 gm. moles/sec. (gm of oxide) pct. unit $(C_e - C)$ using data of Bickenese and Clarke[21]. The calculation procedure is given in Appendix AV. Using equation (7-17) the value of ϕ_L was obtained as 2.54 for experiment 17 for which the data are given above. Effectiveness factor (η) for this case was 0.392, using equation (7-15) and taking a value of 0.995 for tanh ϕ_L.[63]

$$r_p = -\dot{W}_o \cdot \frac{1}{16} \cdot \frac{1}{W_p} \qquad (7\text{-}22)$$

$$= 2.518 \times 10^{-5} \times \frac{1}{16} \times \frac{1}{1.9172}$$

$$= 0.082 \times 10^{-5} \text{ gm.mole O/sec. (gm. oxide)}$$

Then, $p^e_{CO_2} - p^o_{CO_2} = \frac{r_S \cdot RT}{k_1}$

$$= \frac{0.21 \times 10^{-5} \times 82 \times 1229}{2.953}$$

$$= 0.069 \text{ atm.}$$

Assuming $p_{CO_2} = p^e_{CO_2}$ at the top surface of the pellet

$p_{CO} = p^e_{CO}$ at the top surface.

$= 0.705$ atm.

Therefore $p^o_{CO} = 0.705 + 0.069$

$= 0.774$ atm. at the bottom surface of the pellet.

Now, $p_{CO}^{1} = 0.774 + 0.076$

$= 0.850$ atm. at the graphite surface.

and $p_{CO}^{ex} = 0.774 + \frac{0.076}{2}$

$= 0.812$ atm. at the exit end of the alumina tube.

as the alumina tube was placed mid-way between the oxide pellet and graphite powder. For experiment 17 the calculated exit gas composition matched well with the experimentally determined value of $p_{CO_2} = 0.84$ in the product gas at steady state. Table 7.2 shows the calculated and experimental values of p_{CO} for a number of experiments. The agreement between the two gas compositions are fairly good. It may be noted that the exact location of the exit end of the alumina tube was difficult to assess. Thus there could be some error in the calculated gas composition on this account.

7-6 MASS TRANSFER IN GRAPHITE POWDER

The analysis here is similar to what has already been carried out in Sec. 7-5. This is a case of diffusion in pores coupled with chemical reaction. The effectiveness

Table 7.2 Calculated Values of k_1, K_e, ϕ_L, η, r_p, $p^e_{CO}-p^o_{CO}$, p^{ex}_{CO} and Experimental Values of $-\dot{W}_o$ and p_{CO}

Expt. No.	k_1 gm. moles per sec. per gm. of oxide	K_e	ϕ_L	η	$-\dot{W}_o$ gm/sec. (Experimental)	r_p gm.mole O per sec. per gm. of oxide	$p^e_{CO}-p^o_{CO}$ atm.	p^{ex}_{CO}, calculated, atm.	p_{CO} experimental, atm.
7	4.07	0.389	6.05	0.165	3.210	0.051	0.080	0.840	0.84
9	4.22	0.385	5.85	0.170	3.720	0.062	0.090	0.850	0.86
17	3.05	0.418	2.54	0.392	2.518	0.082	0.069	0.812	0.84
20	2.54	0.429	2.38	0.418	0.529	0.018	0.016	0.756	0.89
22	3.05	0.418	2.58	0.386	2.340	0.080	0.069	0.812	0.88

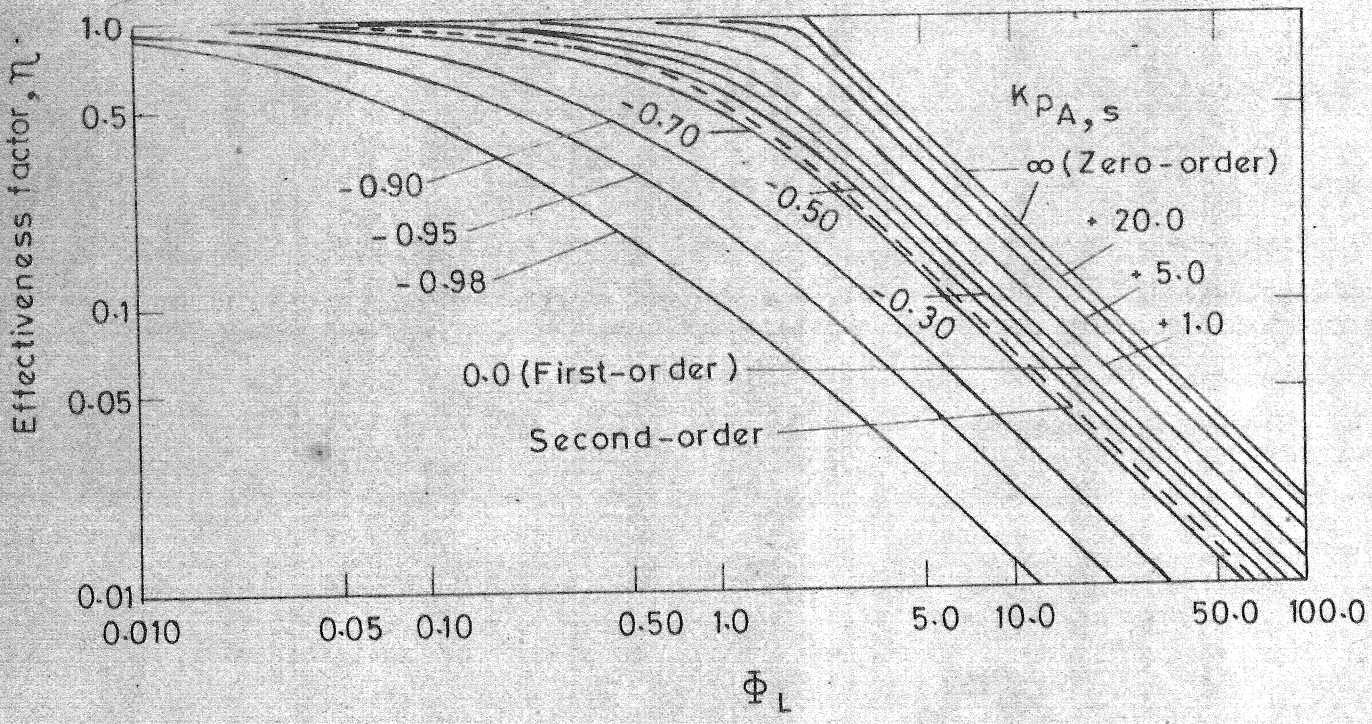

Fig. 7·13 EFFECTIVENESS FACTOR, η, AS A FUNCTION OF MODULAS Φ_L [65]

factor (η) and the modulus (ϕ_L) have similar significance here as in Sec. 7-5. However, the reaction mechanisms and thus the rate equations for the two cases are different. For the reduction of iron oxide, a first order reversible rate equation was applicable. The gasification reaction on the other hand obeys the Langmuir-Hinshelwood kinetics for which the rate expression was discussed in Chapters 1 and 6 (eqn. (6-1)). Roberts and Satterfield[65] have defined the dimensionless modulus (ϕ_L) applicable for this situation as:

$$\phi_L = \left(\frac{L^2}{D_e \cdot C^1_{CO_2}}\right) \times \frac{\text{observed reaction rate}}{\text{gross graphite volume}} \qquad (7\text{-}23)$$

where L = thickness of the graphite bed, cm.

$$C^1_{CO_2} = \frac{p^1_{CO_2}}{RT}$$

= concentration of CO_2 at the surface, gm. moles/cc

As can be seen from Figure 7.13 reproduced here from Roberts and Satterfield[65], η is quite sensitive to the value of $Kp^1_{CO_2}$, where

$$K = \text{Absorption coefficient} = \frac{\left(I_3 - \frac{D_{CO_2}}{D_{CO}} \cdot I_2 \nu_{CO}\right)}{\omega} \qquad (7\text{-}24)$$

ν_{CO} = Stoichiometric coefficient

= 2

and $$\omega = 1 + \frac{D_{CO_2}}{D_{CO}} \cdot p^1_{CO_2} \cdot I_2 \cdot \nu_{CO}$$

The values of L and ε at the beginning of the experiments did not remain the same up to the end. Thickness of graphite bed was measured before the reaction was started and after the reaction was over. The average of the two thicknesses was taken as L.

D_e used for deriving ϕ_L was obtained in the same way as in Sec. 7-5. The influence of Knudsen diffusion is negligible. For molecular diffusion, $(D_{CO_2} / D_{CO}) = 1$. $p^1_{CO_2}$ (i.e. the concentration of CO_2 at the top surface of graphite) was estimated by subtracting the difference $(p^{ex}_{CO_2} - p^1_{CO_2})$ obtained by mass transfer analysis in the gas space (Sec. 7-4) from the measured value of $p^{ex}_{CO_2}$. Table 7.3 shows the values of $p^1_{CO_2}$, D, D_e, $Kp^1_{CO_2}$, ϕ_L and η for different temperatures and stages of reduction. The experiments for which η values have been presented were all conducted at different steady state temperatures.

Too much reliance cannot be given to the mass transfer analysis given here. η is quite sensitive to errors in gas composition, L, D_e and Kp_{CO_2}. The values of L and ε would contain errors. Also the tortuosity factor

Table 7.3 Values of $p^1_{CO_2}$, D, D_e, $K^1_{p_{CO_2}}$, ϕ_L and η for Different Temperatures and Stages of Reduction

Expt. No.	Position	Temp. °K	$-\dot{W}_c \times 10^{-5}$ g/sec.	$p^1_{CO_2}$ atm.	$K^1_{p_{CO_2}}$ atm.	ϕ_L	η	D $cm^2/sec.$	D_e cm^2/sec
	Region III	1274	2.00	0.132	0.941	0.6153	0.30	1.858	0.426
7	Peak	1263	4.70	0.547	0.791	0.4113	0.65	1.839	0.422
	Region I	1246	2.72	0.817	0.989	0.1603	0.25	1.796	0.413
	Region III	1280	2.43	0.112	0.925	0.870	0.28	1.883	0.431
9	Peak	1260	3.82	0.502	0.980	0.330	0.21	1.830	0.420
	Region I	1246	3.22	0.587	0.986	0.239	0.22	1.796	0.413
	Region III	1229	1.63	0.122	0.973	0.550	0.22	1.756	0.404
17	Peak	1227	3.57	0.275	0.985	0.637	0.13	1.756	0.404
	Region I	1201	1.14	0.562	0.989	0.100	0.31	1.690	0.390
	Region III	1199	0.361	0.080	0.980	0.191	0.33	1.686	0.390
20	Peak	1200	1.16	0.447	0.993	0.116	0.25	1.686	0.390
	Region I	1170	0.64	0.455	0.996	0.064	0.30	1.618	0.375

for all calculations were taken as 2, which is a simplification.

Looking at table 7.3 it may be stated that the mass transfer inside graphite seems to offer some resistance to the gasification process. However η was approximately the same for the steady state at various temperatures. Therefore it should not affect the value of activation energy appreciably. This is consistent with the high value of activation energy representative of a chemically controlled reaction (Sec. 7-3.1).

7-7 EXPLANATION OF THE SHAPE OF $-\dot{W}_c$ Vs. PCT. REDUCTION CURVES

Figure 7.3 show that $-\dot{W}_c$ and $-\dot{W}_o$ when plotted against pct. reduction can be divided into four regions. In the beginning the rate is low. Then rate increases with progress of reaction till it reaches a peak and then decreases again. After that the rate remains constant for a reasonably long period. Towards the end it drops. So far the discussion primarily centered around the steady state region (region III). In this section attempts would be made to explain the overall shape.

On the basis of the earlier discussions it would be assumed that the rate is controlled by that of the gasification step. The rate of the gasification reaction

depends strongly on the temperature and gas composition. Both of these vary during the progress of the reaction.

The calculation procedure for $\dot{F}_c$ in pure CO_2 has already been discussed in Sec. 6-1.2. The reacting gas in the pellet-graphite system was rich in CO and thus the rate equations for calculating $\dot{F}_c$ had to be modified. Using equations (6-1), (6-3) and (6-6)[38] the following rate expression was obtained for $\dot{F}_c$ in a CO/CO_2 gas mixture.

$$\dot{F}_c = \frac{I_3 \, k_i \, p_{CO_2}}{1 + I_2 \, p_{CO} + I_3 \, p_{CO_2}} \text{ sec}^{-1} \qquad (7\text{-}25)$$

The values of I_2 and I_3 may be computed from Figure 6.2. Calculations of $\dot{F}_c$ in CO/CO_2 mixture from own reactivity data in pure CO_2 were based on eqn. (7-25).

For gaification of carbon in a CO rich gas, Turkdogan and Vinters[42] gave the rate equation as:

$$\dot{F}_c = \phi_1 \frac{[(p_{CO_2}) - (p^e_{CO_2})]}{(1 + p_{CO}/\phi_{CO})60} \qquad (7\text{-}26)$$

The temperature dependences of ϕ_1 have been found to be as follows.

(i) Coconut Charcoal

$$\log \phi_1 = -\frac{13{,}200}{T} + 9.68 \qquad (7\text{-}27)$$

(ii) Metallurgical Coke

$$\log \phi_1 = -\frac{13,200}{T} + 8.60 \qquad (7\text{-}28)$$

(iii) Electrode Graphite

$$\log \phi_1 = -\frac{13,200}{T} + 7.68 \qquad (7\text{-}29)$$

ϕ_{CO} may be calculated from the following equation[42]

$$\log \phi_{CO} = -\frac{5,940}{T} + 3.46 \qquad (7\text{-}30)$$

for graphite and coke. The value of ϕ_{CO} for charcoal was more by a factor $\simeq$ 4.[42] Thus the temperature dependence of ϕ_{CO} for charcoal was obtained as:

$$\log \phi_{CO} = -\frac{5,940}{T} + 4.06 \qquad (7\text{-}31)$$

$\dot{F}_c$ values calculated on the basis of the above equations along with the experimentally measured values in pellet-graphite system are presented in table 7.4.

In order to take care of the differences amongst the various graphite samples, all $\dot{W}_c$ values were normalized with respect to those at the steady states. Let γ denote this ratio. Then

$$\gamma = \frac{\dot{W}_c \text{ at any percentage reduction}}{\dot{W}_c \text{ at the steady state}} \qquad (7\text{-}32)$$

Table 7.4 Comparison of $\dot{F}_c$ Values Calculated Using Eqns. 7-25 and 7-26 and Obtained Experimentally

Expt. No.	Stage and pct. reduction	Temp. °C	pct. CO	$\dot{F}_c \times 10^5$, sec^{-1}, calculated from various values of reactivity of carbon					Experimental $\dot{F}_c \times 10^5$, sec^{-1}
				Rao et. al[38] graphite	Turkdogan et al[42] Charcoal	Turkdogan et al[42] Met. coke	Turkdogan et al[42] Graphite	CO_2-C reactivity of this work	
	I								
	1.5	826	19.0	0.002	1.031	0.025	0.003	0.014	0.137
	4.7	878	48.6	0.008	1.773	0.041	0.005	0.021	0.290
	7.3	897	50.7	0.021	3.056	0.073	0.008	0.036	0.415
	II								
	11.8	927	51.5	0.082	7.422	0.183	0.022	0.086	0.750
20	18.7	925	51.3	0.075	10.944	0.173	0.021	0.082	0.650
	21.9	927	63.5	0.051	4.641	0.111	0.014	0.053	0.477
	III								
	27.2	926	88.1	0.012	0.988	0.023	0.003	0.012	0.230
	33.1	927	89.3	0.011	0.674	0.016	0.002	0.011	0.246
	I								
	4.4	908	40.9	0.052	6.152	0.152	0.018	0.075	0.506
	9.0	928	40.2	0.014	11.511	0.294	0.036	0.141	0.735
	12.0	937	39.8	0.207	15.120	0.393	0.047	0.186	0.862
	15.3	945	40.3	0.293	18.559	0.488	0.059	0.229	0.968
	II								
	20.9	954	68.7	0.134	8.168	0.199	0.024	0.093	2.306
	26.8	955	82.7	0.066	3.869	0.092	0.011	0.044	1.021
17	32.1	958	83.7	0.069	3.904	0.093	0.011	0.045	1.071
	III								
	34.7	956	84.0	0.063	3.611	0.086	0.010	0.042	1.052
	53.3	956	84.0	0.062	3.369	0.081	0.010	0.042	1.052

Continue...

Table 7.4 (Continued)

Expt. No.	Stage and pct. reduction	Temp. °C	pct. CO	$\dot{F}_c \times 10^5$, sec^{-1}, calculated from various values of reactivity of carbon				Experimental $\dot{F}_c \times 10^5$, sec^{-1}
				Rao et. al[38] Graphite	Turkdogan et al[42] Charcoal	Turkdogan et al[42] Met. coke	Turkdogan et al[42] Graphite	CO_2-C reactivity of this work	
	I								
	2.7	907	19.1	0.142	14.456	0.412	0.049	0.021	0.668
	6.0	921	30.0	0.152	14.173	0.381	0.046	0.178	0.843
	9.8	930	34.5	0.188	15.140	0.394	0.047	0.189	1.018
	II								
	18.6	944	56.5	0.145	10.045	0.249	0.030	0.116	3.171
22	23.9	950	76.5	0.135	4.923	0.112	0.014	0.056	1.849
	26.9	952	86.3	0.044	2.653	0.063	0.008	0.031	1.170
	III								
	44.9	956	87.9	0.045	2.567	0.061	0.007	0.030	1.014
	52.8	957	88.4	0.045	2.289	0.055	0.007	0.029	1.030
	I								
	1.8	937	2.4	3.845	80.727	4.688	0.564	3.452	0.584
	3.3	956	3.2	6.557	116.636	6.478	0.779	4.339	1.051
	6.8	973	14.5	3.616	98.740	3.623	0.435	1.836	2.648
	II								
	11.7	990	41.5	1.970	64.264	1.662	0.200	1.145	4.575
7	18.6	1004	47.5	2.776	67.350	1.907	0.229	0.889	2.998
	23.1	1004	63.1	1.506	39.140	1.044	0.126	0.482	2.103
	III								
	32.9	1001	82.6	0.483	14.032	0.355	0.043	0.162	2.000
	49.4	999	84.1	0.398	12.300	0.303	0.036	0.137	1.740
	I								
	1.2	920	1.9	2.273	56.777	3.358	0.404	2.700	0.288
	2.8	930	2.4	2.884	68.885	3.929	0.473	2.899	0.431
	2.9	943	4.8	2.860	78.897	3.807	0.457	2.328	0.602
	9.0	973	37.5	1.120	42.928	1.207	0.495	0.658	3.080
	II								
	13.3	987	46.0	1.450	46.795	0.978	0.118	0.596	3.654
9	22.3	1009	76.4	0.526	14.456	0.368	0.044	0.296	2.487
	26.7	1008	80.4	0.758	19.298	0.493	0.059	0.229	2.391
	III								
	42.9	1007	85.0	0.995	23.454	0.606	0.073	0.161	2.324
	48.8	1007	85.5	0.506	13.200	0.336	0.040	0.156	2.305

Table 7.5 present γ values obtained by calculations using eqns. (7-26) to (7-31) for the three types of carbon investigated by Turkdogan and Vinters and using eqn. (7-25) for the k_i values obtained by Rao and Jalan as well as this investigation in pure CO_2.

Table 7.5 shows that so far as γ for the peaks are concerned, experimental values match with those calculated in some experiments, whereas in some others the calculated γ is greater than the experimental values by a factor of 2 or 3.

Figure 7.14 presents $\dot{F}_c$ calculated by the various methods as described above and experimental $\dot{F}_c$. It is clear that the qualitative natures of the curves predicted by calculations agree well with the natures of the curves found experimentally. There is quantitative disagreement, an aspect which shall be taken up later.

Table 7.3 presents values of the effectivensss factors (η) for reaction of graphite with CO_2. No clear cut pattern of difference between η at peaks and η at steady states could be found. Therefore partial mass transfer limitations in graphite would not as such account for differences in rates at peak and at steady state.

Again referring back to table 7.5 the calculated γ values for the stage I are 3 to 7 times greater as

Table 7.5 Comparison of γ Values Calculated Using Equations (7-25) and (7-26) and Obtained Experimentally

Expt. No.	Position on the F_c Vs. pct. reduction curve	Temp. °C	Pct. CO	Calculated					Experimental
				Turkdogan and Vinters			Rao and Jalan	From reactivity values in this investigation	
				Charcoal	Met. coke	Graphite			
7	Region I	973	14.51	8.030	11.95	12.08	9.08	13.40	1.52
	Peak	990	41.49	5.22	5.48	5.55	4.95	8.35	2.63
9	Region I	973	37.50	3.25	3.59	12.37	2.21	4.22	1.34
	Peak	987	46.00	3.55	2.91	2.95	2.86	3.82	1.59
17	Region I	928	40.17	3.42	3.63	3.6	2.15	3.40	0.70
	Peak	954	68.73	2.42	2.45	2.4	2.14	2.23	2.19
20	Region I	897	50.73	4.53	4.56	4.21	2.00	3.25	1.69
	Peak	927	51.52	11.01	11.43	11.57	7.81	7.83	3.05
22	Region I	930	34.5	6.61	7.16	7.23	4.17	6.45	0.99
	Peak	944	56.53	4.39	4.52	4.61	3.22	3.96	3.08

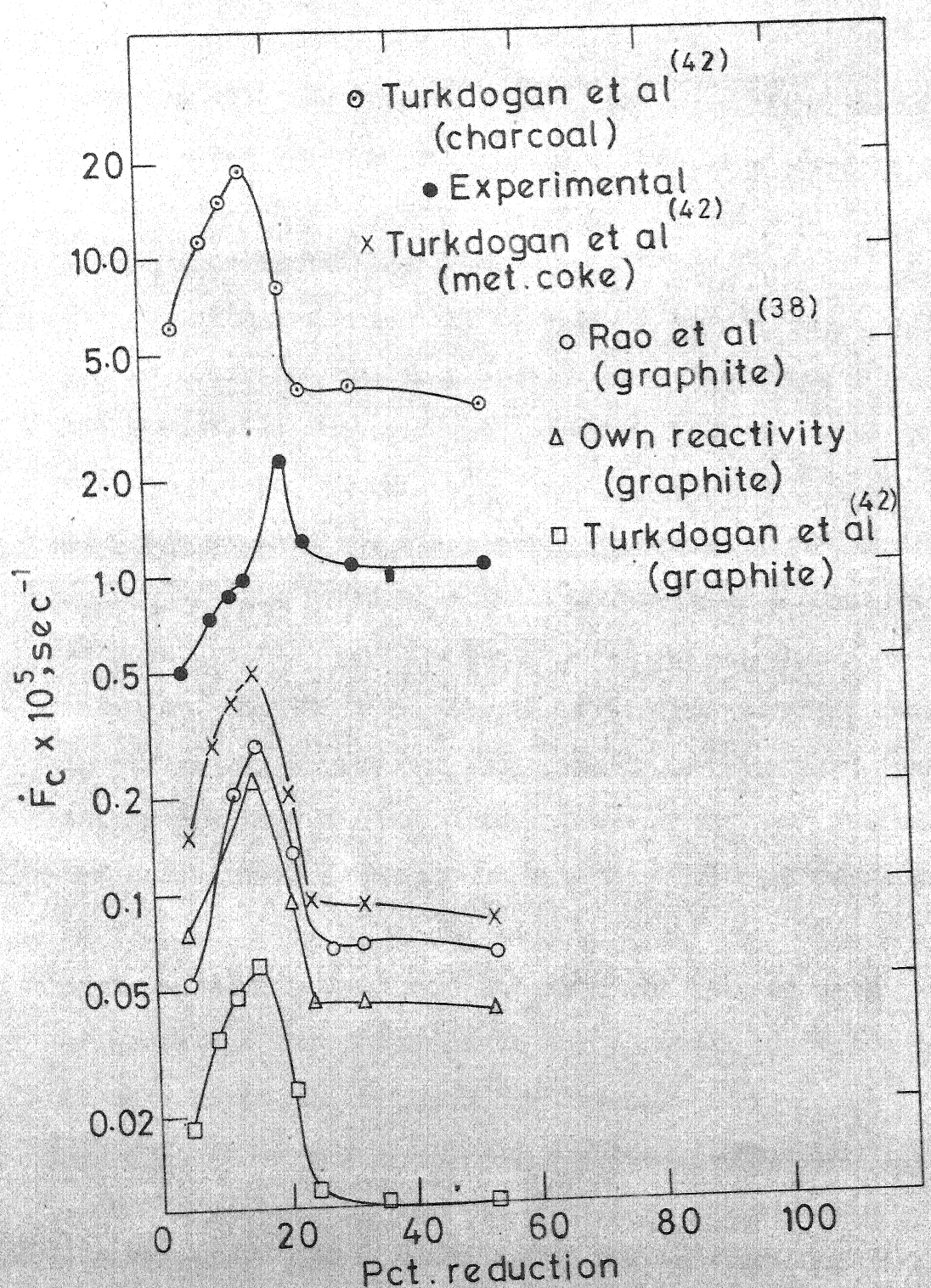

FIG. 7.14 COMPARISON OF CALCULATED AND EXPERIMENTAL $\dot{F}_c$ FOR EXPERIMENT 17

compared with the experimental values. In other words the actual rates observed during the initial periods are much lower compared to those expected on the basis of extrapolation from the steady state.

The low rates in the initial periods are partly due to lower temperatures prevailing there. However this has been taken into account in calculation of rates by various models, therefore in calculation of γ. Hence it does not explain the discrepancy mentioned above.

While heating up the assembly to the experimental temperature the reaction chamber was being flushed with nitrogen. So it is conceivable that some nitrogen remained in the gas space between the graphite and the oxide pellet during the initial period thus diluting CO_2 and lowering the rate. However sample calculations made assuming mixing in the gas space to be instantaneous revealed that nitrogen aught to have been purged out in a few minutes by the flow of gases out through the exit tube. Hence it does not seem to be responsible for this discrepancy.

Therefore the reason for this discrepancy lies probably in the errors associated with extrapolation over a wide range of gas composition employing equations (7-25) and (7-26).

Region IV shows a drooping rate. This is close to 100 pct. reduction. Hence most probably oxide reduction step is slow here and starts to exert its influence.

7-8 COMPARISON OF THE RATE OF REACTION WITH THE CARBON GASIFICATION RATE CALCULATED FROM LITERATURE

An attempt was made to compare the rates obtained in pellet-graphite reaction with the gasification rate calculated by the method discussed in the last section (Sec. 7-7). In principle, this can be done since the gasification step was found to primarily control the rate of overall reaction. Table 7.4 presents the calculated and experimental $\dot{F}_c$ for various experiments. Figure 7.14 shows the comparison for experiment 17.

Charcoal is too reactive as compared to the other types of carbon. No wonder it predicts a much higher rate than experimentally observed. However it is to be noted that the experimental values of $\dot{F}_c$ for pellet-graphite reaction are about an order of magnitude larger as compared to the gasification rates at the steady-state predicted from the reactivity data of Rao and Jalan as well as of this investigation.

The reliability of experiments on pellet-graphite reaction has been checked already. As Figure 7.1 reveal, the results could be reproduced with reasonable accuracy

when the same experimental conditions were maintained. The calculated and experimental weight losses of oxygen and carbon (table 4.5) also exhibit good agreement. γ for experimental and calculated $\dot{F}_c$ match well for the peak in experiments 17 and 22 as can be seen from table 7.5. From all these it may be assumed that the experimental determination of $\dot{F}_c$ and $\dot{F}_o$ have not suffered from much error.

Graphite analysis (Sec. 5-3) showed that there was very little impurity in it. Thus the influence of catalysis on the gasification reaction may be ruled out. Secondly the high activation energy (75 kcal/mole) obtained for the steady state (Sec. 7-3.1) is typical of a non-catalysed gasification reaction.

Therefore it appears that the discrepancies have perhaps been caused by the following sources.

(a) Graphite reactivity value: Because of the unlikely low activation energy obtained for graphite reactivity (-32,300 kcal/mole) in this investigation not much reliance can be put on them. As discussed in Sec. 6-1 there could be errors in the literature values also.

(b) Extrapolation formulae: The formulae used for extrapolation were obtained for gasification in pure CO_2 except in the case of Turkdogan et al. Thus, extrapolation to the actual co-rich gas compositions are very likely to

cause errors. This is substantiated by the fact that the discrepancies are less for the initial period, when the product gases were richer in CO_2.

7-9 COMPARISON OF POROUS PELLET REDUCTION WITH POWDER MIXTURE AND DENSE PELLET REDUCTION

The influence of mass transfer on the rate of reaction has already been illustrated in Sections 7-4 to 7-6. The analysis showed that mass transfer in the gas phase, in the oxide pellet as well as in the graphite powder have some influence on the reaction. The extent of the influence of mass transfer on the reaction rate was also revealed from the results of experiments conducted with varying distances of separation as may be seen in Figure 7.10 for the steady state (Region III).

The increase in the rate of reaction in the steady state corresponding to reduction of wustite into Fe (Region III) with decreasing distances of separation has been shown in Figures 7.9 and 7.11. This pointed out that mass transfer in the gas space has an influence on the rate of reaction (Sec. 7-4). Thus the increased rates in the second stage of reduction in powder mixture studies (Figure 7.9) does not seem to be only due to catalysis but also due to enhanced mass transfer.

Figure 7.9 also shows that the reaction rate in the first stage ($Fe_2O_3 \longrightarrow FeO$) increased with increasing separation of the two reactants. The mass transfer conditions were better for experiments 23 and 24 for which the distances of separation were 0.0 and 0.25 cm respectively. However, Figure 7.9 shows that the rates in the initial stages were more for experiment 17 where the distance of separation was 1.6 cm. Also Figure 7.15 shows that the gas composition and temperature variations predicted the presence of peak in experiments 23 and 24 whereas the experimental observations (Figures 7.4 and 7.5) do not depict the same. These discrepancies have not been understood properly. It may be that the empty volume in the reaction cell has something to do with this anomaly. On the other hand the increase in the volume of the empty space was about 10 times (25 cc) in the case of powder mixture studies as compared to the empty space in the case of pellet-graphite system (2.5 cc) at the maximum distance of separation. The increase in the rates in the first stage for powder mixture studies as seen from Figure 7.9 is about 10 times more as compared to that for pellet-graphite studies. Thus it appears that the volume of the empty space has an effect on the rate in the first stage of reduction.

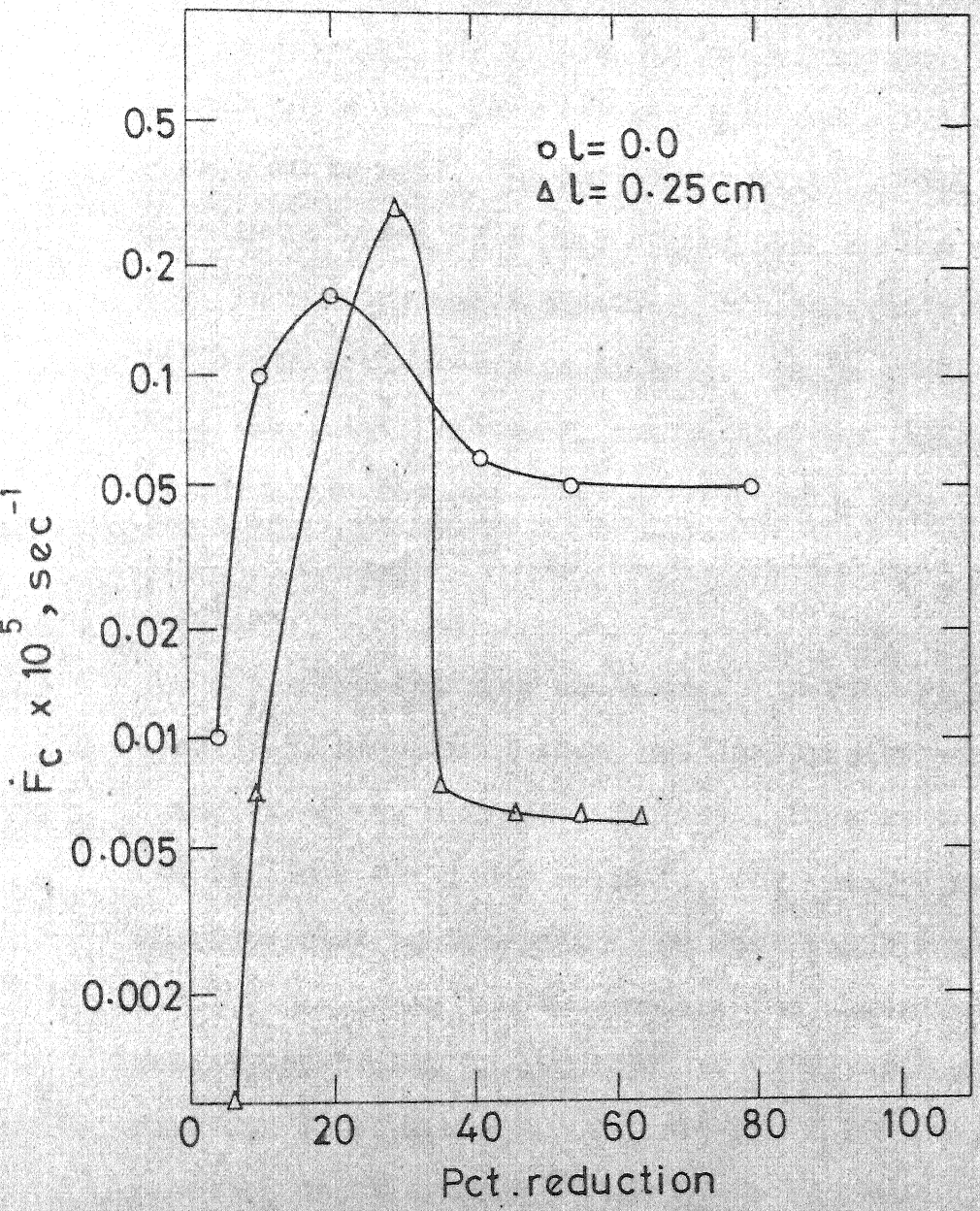

FIG. 7.15 $\dot{F}_c$ CALCULATED USING EQUATION (7-25) AT 957°C FOR DISTANCES OF SEPARATION OF 0.0 & 0.25 cm.

The shape of the $\dot{F}_c$ Vs. pct. reduction curves in Figure 7.9 shows that there is a marked difference between the pellet-graphite system and powder mixture system. In the former there is a peak in the first stage followed by a lower steady state rate. In the powder mixture studies the first peak is followed by a much higher peak in the second stage. With increasing contact between the reactants, from micro-pellet to powder mixture pressed, the rate also increased. Thus the total absence of the enhancement of the rate in the second stage for pellet-graphite studies was the absence of contact catalysis by reduced iron on the gasification reaction.

Mass transfer analysis for porous pellet reduction (Sec. 7-5) shows that there was some resistance to the transfer of gas across the pellet. This is consistent with the findings for dense pellets. The results on dense pellets are presented in Appendix AI as well as in Figures 7.6 and 7.7. Even though the temperature for experiment 27 on dense pellet was higher by about 15°C (972°C) as compared to the reaction temperature for experiment 17 (957°C), the rate of reaction in experiment 27 was lower by about 1.5 times as compared to the rate in region III for experiment 17. Also the gas composition for experiment 27 showed a higher CO content at all stages of reduction. All these differences

can be attributed to larger resistance to transfer of gases inside a dense pellet as compared to a porous pellet.

In Figure 7.7 the rate in region III (steady state) is more as compared to region III in Figure 7.6. The distance of separation for experiment 28 (Figure 7.7) was 0.0 whereas that for experiment 27 (Figure 7.6) was 1.25 cm. As can be seen from table 4.3 the thickness of the pellet was 0.468 cm. Because of the increased thickness of the dense pellet as compared to the porous pellets as well as the increase in volume due to reduction, the pellet exerted some pressure over the graphite surface during the $Fe_xO \rightarrow Fe$ stage of reduction. This happened because of the limited space inside the reaction cell for the expansion of the pellet. Thus the gasification reaction was catalysed by the reduced iron, which was responsible for the increased rate in this region.

7-10 SOME PREDICTIONS ON SPONGE IRON MAKING IN ROTARY KILN BASED ON THE FINDINGS OF THIS INVESTIGATION

In sponge iron making by the rotary kiln process iron ore pieces or pellets are fed with small pieces of solid carbonaceous reductant. The kiln is rotated slowly enhancing heat and mass transfer as well as inducing the charges to move from the entrance to exit. The contact

between ore and reductant is loose. Part of the interior of the kiln is empty space where CO, generated by gasification reaction as well as fuel fed into the kiln, are burnt to generate the necessary heat. Therefore conversion of CO into CO_2 takes place both via reduction of iron ore as well as combustion in the gas space. This, as well as, the fact that the bed of solids in a rotary kiln is much deeper as compared to the laboratory investigation, makes the two situation somewhat different, kinetically speaking. Even then it is possible to make a number of predictions regarding the kinetics of the rotary kiln process of sponge iron making from the findings of this investigation and the general understanding of iron ore reduction. These are noted below.

(1) The reduction of the ore would be stagewise, viz. hematite $\rightarrow$ magnetite $\rightarrow$ wustite $\rightarrow$ iron.

(2) Gasification reaction is expected to control the reduction rate.

(3) Mass transfer inside the ore, and in the bed of solids would also influence the rate significantly.

(4) Catalysis by reduced iron is not expected to be significant. Therefore the last stage of reduction (i.e. wustite $\rightarrow$ iron) would be slow. It ought to be pretty difficult to reduce the oxide when percentage reduction exceeds 90-95.

(5) Rates can be enhanced by increasing the reactivity of the solid reductant, decreasing the particle size of the solid reductant and by feeding porous iron ore pellets. However decrease of particle size of the reductant beyond a certain point may start adversely affecting the rate because of increase of mass transfer resistance in the graphite bed. Therefore an optimum size of the reductant is to be chosen.

(6) If somehow composite pellets of ore and reductant can be used, the rate of the process can be enhanced by an order of magnitude.

CHAPTER 8

SUMMARY AND CONCLUSIONS

Investigations were made on rates of reaction of porous and dense pellets of iron oxide with graphite powder. The distance of separation between the oxide pellet and graphite powder was varied from 0 to 1.6 cm. Temperature of reaction ranged from 880°C to 1007°C. Auxilliary investigations with powder mixtures of the two reactants as well as with mixture of graphite powder and tiny pellets of oxide were undertaken to verify the literature findings as well as to help in the interpretation of the main results. Reactivity of graphite which was the reductant in all the experiments were determined in pure CO_2 as well as in mixtures of CO and CO_2. Partially reduced pellets were examined by oxidation test for identifying the various phases present.

The flowrate and composition (CO/CO_2 ratio) of the product gas were measured at intervals of time by capillary flowmeter and a solid electrolyte oxygen sensor respectively. These were then processed by computer to obtain gas composition, instantaneous and cumulative weight losses of oxygen and carbon and pct. reduction at intervals of time. The calculated weight losses agreed with the experimentally

measured weight losses within 10 pct. Interpretations are based on the experimental results, theoretical analysis of mass transfer and calculations of rates of gasification reaction in various CO/CO_2 mixtures according to the equations given in literature. The following conclusions may be drawn from the present investigation.

1. The results on powder mixture and micropellet-graphite mixture showed a two stage behaviour. For powder mixtures, the first stage was characterised by high activation energy (73 kcals/mole). The activation energy for the second stage was only 33.5 kcals/mole. Also the rates in the second stage were found to be much higher than those in the first stage.

2. Rate in the second stage was found to increase with increasing contact between the reactants. From micropellet-graphite mixture to pressed powder mixtures of oxide and graphite the increase was of the order of a magnitude. These confirm the conclusion arrived by other investigation that reduced iron acts as catalyst in the second stage.

3. From the nature of variation of gas composition with pct. reduction, it may be concluded that the reduction proceeds stagewise, viz. $Fe_2O_3 \rightarrow Fe_3O_4 \rightarrow Fe_xO \rightarrow Fe$, in all cases.

4. The rate versus pct. reduction curves for the oxide pellet-graphite powder in separation exhibit four regions. There was a sharp peak corresponding to about 20 pct. reduction. The rate reached a steady state at pct. reduction beyond about 30 pct.

5. Activation energy obtained at the steady state is 75 kcals/mole indicating control by the gasification step and absence of any significant catalysis.

6. The rate in the steady state was found to increase with decreasing distance of separation between the two reactants oxide and graphite. It could be explained by partial mass transfer control.

7. Mass transfer analysis revealed significant mass transfer resistance in all phases, viz. in graphite bed, in the oxide pellet and in the intervening gas space. However the variation with temperature was not significant. Therefore it did not influence the activation energy. The calculated exit gas composition matched well with the experimental values.

8. Using equations cited in the literature and reactivity values for graphite in pure CO_2 both from literature as well as this investigation, calculations were made about the rates of gasification in mixtures of CO and CO_2. Qualitative agreement with the experimental

values were obtained. However, there was quantitative disagreement. This was attributed to errors in extrapolating reactivity values from pure CO_2 to gas mixture rich in CO.

9. It appears that mass transfer aspects in connection with graphite reactivity studies have not been properly understood yet.

CHAPTER 9

SUGGESTIONS FOR FUTURE WORK

The present investigation has brought out some useful conclusions on the factors affecting the reduction of iron oxide by carbon. The following investigations are suggested for the future.

(1) The effect of change of geometry on the reaction rates. It will be interesting to see what happens if the pellet was kept at the bottom and graphite at the top. Also if the reacting gases made to move parallel to a horizontal axis rather than a vertical axis.

(2) Effect of porosity of oxide pellet and graphite powder on the overall rate.

(3) Kinetics of reduction of iron oxide in a $CO-CO_2$ gas mixture.

(4) Gasification rate of graphite in a $CO-CO_2$ gas mixture.

(5) Investigations may also be taken up using different types of carbon and ores of iron oxide.

(6) Theoretical models based on the experimental evidences may be made and model studies of the rotary kiln may be undertaken.

(7) Effect of the volume of gases on the rate of reduction in the 1^{st} stage (haematite to wustite) may be investigated further.

LIST OF REFERENCES

1. J.R. Miller: Trans. I.I.M., Silver Jubilee Symp. (1972).

2. A. Lahiri: Trans. I.I.M., 21, No. 2, (1968), 33.

3. W.F. Cartwright: Proceedings of the ISI Conference on Alternative Routes to Steel, London Hilton, May 5/6, (1971), 33.

4. B.L. Sengupta, A.B. Chatterjea, G.P. Mathur and V.A. Altekar: Paper presented at the International Conference on Science and Technology of Sponge Iron and Its Conversion to Steel, Feb. 19/22, (1973); Engineering World, 3, No. 2, (1973), 67.

5. U.N. Bhrany: Ibid, Engineering World, 3, No. 2, (1973), 121.

6. Science and Technology Plan 1974-79, Draft, Vol. II, National Committee on Science and Technology, August (1973), 170.

7. A.B. Chatterjea: private communications, (1975).

8. Y.K. Rao: Met. Trans. AIME, 2, (1971), 1439.

9. W. Baukloh and R. Durrer, Arch. Eisenhuttenw, 4, (1963), 455.

10. V. Arkharov, V.N. Bogoslovskii, M.G. Zhuravaleva and Q.I. Chufarov: Zh. Fiz. Khim. 29, No. 2, (1955), 272.

11. T.S. Yun: Trans. ASM, 54, (1961), 129.

12. A. Prasad and R.H. Tupkary: International Conference on the Science and Technology of Iron and Steel, Tokyo, Japan, (1970), 249.

13. J. Yarwood: Ch. 3, High Vacuum Technique, Chapman and Hall Ltd., London (1961).

14. B. Baldwin: J.I.S.I., London, 179, (1955), 30.

15. F.S. Manning and W.O. Philbrook: Ch. 17, Blast Furnace Theory and Practice (Julius H. Strassburger Ed.), Gordon and Breach, New York, (1969).

16. L. Von Bogdandy and H.J. Engell: Ch. 2, The Reduction of Iron Ores, Springer Verlog, Berlin Heidelberg, New York, (1971).

17. E.T. Turkdogan and J.V. Vinters; Met. Trans. 2, (1971), 3175.

18. B. Stalhane and T. Malmberg: Jernkantorsts Ann; 114, (1930), 1.

19. N.D. Smith and W.M. McKewan: The Blast Furnace, Coke Oven, and Raw Materials Conference, Detroit, (1962).

20. S.E. Khalafalla, C.W. Schultz and T.N. Rushton: U.S. Bureau of Mines Report of Investigations, 6699, (1965).

21. E. Bicknese and R. Clark: Trans. IMS-AIME, 236, (1966), 2.

22. R.D. Walker and D.L. Carpenter: J.I.S.I., 208, (1970), 67.

23. E. Kawasaki, J. Sanscrainte and T.S. Walsh: A.I.Ch.E. Journal, 8, No. 1, (1962), 48.

24. S.E. Khalafalla and P.L. Weston: Jr. Trans. AIME, 239, (1967), 1494.

25. N.J. Themelis and W.H. Gauvin: Trans. Met. Soc. AIME, 227, (1963), 290.

26. W.M. McKewan: The Chipman Conference, M.I.T. Press, U.S.A., (1962), 141.

27. N.A. Warner: Trans. Met. Soc. AIME, 230, (1964), 163.

28. R.G. Olsson and W.M. McKewan: U.S. Steel Corporation, Fundamental Research Laboratory, Monroville Pa., Private Communications.

29. R.H. Spitzer, F.S. Manning and W.O. Philbrook: Trans. Met. Soc. AIME, 236, (1966), 726.

30. N. Wakao and J.M. Smith: Ind. Eng. Chem. Fundamentals, 3, (1964), 123.

31. H.U. Ross: Private Communications, (1972).

32. G.I. Chufarow: Zhur. Fiz. Khim., 28, (1954), 490.

33. M. Kurchatov; Fiz-Khim. Osnovy Proizv. Stali, Akad. Nauk SSR, Inst. Met., Shestoi, Konf, Moscow, (1961), 417.

34. J.B. Lewis: Ch. 4, Modern Aspects of Graphite Technology (L.C.F. Blackman Ed.), Academic Press, London, (1970).

35. P.L. Walker, Jr., M. Shelef and R.A. Anderson: Chemistry and Physics of Carbon (P.L. Walker Ed.), Marcel Dekker, Inc., New York, 4, (1968), 287.

36. L.S. Darken and E.T. Turkdogan: Heterogeneous Kinetics at Elevated Temperatures (G.R. Belton, W.L. Worrel, Eds.), Plenum Press, New York, (1970), 25.

37. A.E. Reif: J. Phys. Chem., 56, (1952), 778.

38. Y.K. Rao and B.P. Jalan: Met. Trans., 3, (1972), 2465.

39. Y.K. Rao and B.P. Jalan: Blast Furnace Technology Science and Practice (Julian Szekely Ed.), Marcel Dekker, Inc., New York, (1972).

40. Ken-Ichi Otsuka and Diazo Kunii: Journal of Chemical Engineering of Japan, 2, No. 1, (1969), 46.

41. P.C. Ghosh and S.N. Tiwari: J.I.S.I., London, 208, (1970), 255.

42. E.T. Turkdogan and J.V. Vinters: Carbon, 7, (1969), 101; Carbon, 8, (1970), 39.

43. W.A. Bone, L. Reeve and H.L. Saunders: J.I.S.I., London, No. 1, (1930), 35.

44. H.L. Saunders and E.J. Tress: J.I.S.I., London, 157, (1947), 215.

45. P.L. Walker, J.F. Rakszawski and G.R. Imperial: J. Phys. Chem., 63, (1959), 133.

46. T.H. Etsel and S.N. Flengas: Met. Trans. 3, (1972), 27.

47. W.M. Boorstein, R.A. Rapp and G.R. St. Pierre: High Temperature Electrochemical Research, The Ohio State Research Foundation, U.S.A., Dec. (1971).

48. H.S. Spacil: Metal Progress, 96(5), (1969), 106.

49. Motoaki Sato: Research Techniques for High Pressure and High Temperature, (Geue C. Ulmer Ed.), Springer-Verlag, New York, (1971).

50. S. Basu: Ph.D. Thesis, Department of Metallurgical Engineering, Indian Institute of Technology Kanpur, India, (1972).

51. G.P. Baxter and J.E. Lansing: J. American Chemical Society, 42, (1920), 419.

52. C.D. Hodgman, R.C. Weast and S.M. Selby: Eds., Handbook of Chemistry and Physics, The Chemical Rubber Publishing Co., Cleveland, Ohio, U.S.A., (1961).

53. J.F. Elliot and M. Gleisser: Thermochemistry for Steelmaking, Vol. I, Addison-Wesley Publishing Co., Inc., (1960).

54. R.B. Bird, W.E. Stewart and E.N. Lightfoot, Ch. 1, Transport Phenomena, John Wiley and Sons, Inc., New York, (1962).

55. R.B. Bird, W.E. Stewart and E.N. Lightfoot: Ch. 1, Transport Phenomena, John Wiley and Sons, Inc., New York, (1962).

56. S. Ergun: J. Phys. Chem., 60, (1956), 480.

57. A.E. Reif: J. Phys. Chem., 56, (1952), 785; J. Phys. Chem., 56, (1952), 778.

58. C. Chu and O.A. Hougen: Chem. Eng. Sci., 17, (1962), 167.

59. C. Wagner: Z. Phys. Chem., A193, (1943), 1.

60. R.B. Bird, W.E. Stewart and E.N. Lightfoot: Ch. 16, Transport Phenomena, John Wiley and Sons, Inc., New York, (1962).

61. A. Ghosh and G.R. St. Pierre: Indian Journal of Technology, 8, (1970), 79.

62. R.B. Bird, W.E. Stewart and E.N. Lightfoot: Ch. 17, Transport Phenomena, John Wiley and Sons, Inc., New York, (1962).

63. J.M. Smith: Ch. 11, Chemical Engineering Kinetics, McGraw Hill Book Co., New York, 2nd ed., (1970).

64. R.B. Bird, W.E. Stewart and E.N. Lightfoot, Ch. 16, Transport Phenomena, John Wiley and Sons, Inc., New York, (1962).

65. G.W. Roberts and C.N. Satterfield: Ind. Eng. Chem. Fundam., 4, (1965), 288.

APPENDIX - AI

EXPERIMENTAL RESULTS ON IRON OXIDE PELLET-GRAPHITE POWDER REACTION

Experiment No. 7

ΔW_c(calcd.) = 0.7183 gms ΔW_o(calcd.) = 1.187 gms

ΔW_c(expt.) = 0.6346 gms ΔW_o(expt.) = 1.170 gms

Time of reaction, min.	Temp. of CSZ cell, °C	EMF of CSZ cell, volts (uncor.)	Δh of capillary flow-meter, cms.	Pct. CO in the product gas	$-\dot{W}_c \times 10^4$ gm/sec	$-\dot{W}_o \times 10^4$ gm/sec	Pct. reduc-tion
5	910	0.607	1.1	1.57	0.033	0.087	0.45
15	919	0.607	1.3	1.78	0.039	0.103	0.98
25	937	0.609	2.0	2.35	0.060	0.158	1.79
35	956	0.612	3.6	3.18	0.108	0.283	3.25
35	956	0.612	3.6	3.18	0.108	0.283	3.25
45	973	0.680	9.2	14.5	0.272	0.672	6.77
55	990	0.740	16.6	41.5	0.470	0.992	11.6
65	1003	0.738	12.6	43.7	0.355	0.74	15.4
75	1004	0.745	11.0	47.5	0.308	0.627	18.5
85	1004	0.765	9.1	57.7	0.251	0.476	21.0
95	1004	0.776	7.9	63.11	0.216	0.393	23.1
105	1003	0.815	7.3	79.0	0.193	0.312	24.7
115	1003	0.820	7.5	80.7	0.198	0.315	26.3
125	1002	0.823	7.7	81.5	0.203	0.321	28.0
135	1002	0.825	7.7	82.1	0.203	0.319	29.6
145	1002	0.827	7.8	82.7	0.205	0.321	31.2
155	1001	0.827	7.8	82.6	0.205	0.321	32.9
165	1001	0.828	7.7	82.9	0.203	0.316	34.5
175	1001	0.829	7.6	83.2	0.200	0.311	36.1
195	1000	0.829	7.5	83.0	0.198	0.309	40.8
225	999	0.830	6.9	83.2	0.181	0.282	45.1
255	999	0.833	6.8	84.1	0.179	0.276	49.4
285	996	0.833	6.3	83.7	0.166	0.257	53.3
315	991	0.833	5.6	83.1	0.147	0.230	56.9
345	994	0.831	5.8	82.9	0.153	0.238	60.5
375	995	0.831	5.9	83.0	0.155	0.242	64.2
405	995	0.831	5.9	83.0	0.155	0.242	67.9
435	996	0.833	5.9	83.7	0.155	0.240	71.6
465	996	0.833	6.0	83.7	0.158	0.244	75.3
495	996	0.833	6.0	83.7	0.158	0.244	79.1
525	996	0.833	6.0	83.7	0.158	0.244	82.8
555	993	0.834	6.0	83.7	0.158	0.244	86.6
585	995	0.839	6.2	85.2	0.162	0.248	90.4
615	997	0.842	6.4	86.2	0.167	0.254	94.3

APPENDIX AI (Continued)

Experiment No. 9

ΔW_c(calcd.) = 0.3639 gms ΔW_o(calcd.) = 0.6259 gms

ΔW_c(expt.) = 0.4120 gms ΔW_o(expt.) = 0.6650 gms

Time of reaction, min.	Temp. of CSZ cell, °C	EMF of CSZ cell, volts (uncor.)	Δh of capillary flow-meter, cms.	Pct. CO in the product gas	$-\dot{W}_c \times 10^5$ gm/sec	$-\dot{W}_o \times 10^5$ gm/sec	Pct. reduc-tion
5	895	0.600	0.80	1.10	0.241	0.639	0.349
15	908	0.605	1.00	1.47	0.301	0.796	0.769
25	920	0.610	1.00	1.92	0.301	0.794	1.21
35	930	0.615	1.50	2.44	0.451	1.19	1.84
45	943	0.640	2.10	4.83	0.629	1.64	2.85
55	962	0.715	6.20	24.0	1.80	4.24	5.20
65	973	0.740	11.30	37.5	3.22	6.98	9.02
75	987	0.750	13.60	46.0	3.82	7.85	13.3
85	998	0.760	12.60	53.8	3.50	6.81	16.9
90	1003	0.770	12.20	60.0	3.35	6.25	20.1
105	1009	0.805	9.75	76.4	2.60	4.28	22.4
115	1008	0.815	9.45	79.8	2.50	4.01	24.6
125	1008	0.817	9.45	80.4	2.50	3.98	26.6
135	1007	0.815	9.35	79.6	2.48	3.97	28.8
145	1007	0.823	9.25	82.2	2.44	3.83	30.8
165	1007	0.828	9.25	83.6	2.43	3.77	36.9
195	1007	0.833	9.25	85.0	2.43	3.72	42.9
240	1007	0.835	9.20	85.5	2.41	3.68	48.8
270	1007	0.838	9.00	86.2	2.35	3.57	54.5

APPENDIX AI (Continued)

Experiment No. 14

ΔW_c(calcd.) = 0.3408 gms ΔW_o(calcd.) = 0.5634 gms

ΔW_c(expt.) = 0.3563 gms ΔW_o(expt.) = 0.5100 gms

Time of reaction, min.	Temp. of CSZ cell, °C	EMF of CSZ cell, volts (uncor.)	Δh of capillary flow-meter, cms.	Pct. CO in the product gas	$-\dot{W}_c \times 10^5$ gm/sec	$-\dot{W}_o \times 10^5$ gm/sec	Pct. reduc-tion
15	746	0.705	1.4	1.41	0.421	1.115	3.85
45	808	0.685	1.5	2.21	0.451	1.189	7.79
75	862	0.805	1.3	43.72	0.367	0.764	10.5
95	895	0.790	2.0	44.1	0.564	1.172	11.8
105	910	0.775	2.7	39.8	0.766	1.637	13.6
115	923	0.773	3.2	42.1	0.905	1.906	15.8
125	935	0.765	4.0	40.9	1.133	2.405	18.5
135	948	0.755	5.1	38.9	1.450	3.113	22.0
145	958	0.753	6.2	40.4	1.758	3.742	26.1
155	968	0.790	6.0	62.1	1.640	3.016	29.6
165	977	0.835	9.4	82.1	2.478	3.896	33.9
175	985	0.842	11.6	85.0	3.041	4.662	39.1
185	992	0.842	12.2	85.7	3.194	4.866	44.6
195	999	0.842	12.7	86.4	3.320	5.028	50.2
205	1006	0.842	13.3	87.1	3.473	5.229	56.1
215	1012	0.838	13.8	86.7	3.606	5.448	62.2
225	1016	0.838	14.2	87.1	3.708	5.584	68.5
235	1019	0.838	14.5	87.3	3.784	5.685	74.9
245	1018	0.838	14.0	87.2	3.655	5.494	81.0
255	1017	0.838	13.6	87.2	3.551	5.342	87.0
265	1019	0.838	13.5	87.3	3.523	5.293	93.0
275	1021	0.838	13.5	87.5	3.522	5.283	98.9
285	1023	0.845	12.7	89.1	3.303	4.883	104.0

APPENDIX AI (Continued)

Experiment No. 17

ΔW_c(calcd.) = 0.3458 gms ΔW_o(calcd.) = 0.5617 gms

ΔW_c(expt.) = 0.3318 gms ΔW_o(expt.) = 0.5731 gms

Time of reaction, min.	Temp. of CSZ cell, °C	EMF of CSZ cell, volts (uncor.)	Δh of capillary flow-meter, cms.	Pct. CO in the product gas	$-\dot{W}_c \times 10^5$ gm/sec	$-\dot{W}_o \times 10^5$ gm/sec	Pct. reduc-tion
5	893	0.840	2.0	46.3	0.562	1.151	1.20
15	903	0.827	2.4	41.7	0.668	1.409	2.66
25	908	0.823	2.8	40.9	0.782	1.659	4.39
35	919	0.815	3.4	39.4	0.954	2.043	6.50
45	928	0.812	4.0	40.1	1.140	2.418	9.04
55	937	0.807	4.7	39.8	1.334	2.849	12.0
65	945	0.804	5.3	40.2	1.498	3.190	15.3
75	954	0.855	13.2	68.7	3.567	6.242	20.9
85	952	0.887	7.4	81.0	1.955	3.100	24.2
95	955	0.891	6.0	82.7	1.580	2.471	26.8
105	957	0.892	6.1	83.2	1.605	2.498	29.4
115	958	0.893	6.3	83.6	1.656	2.568	32.1
125	956	0.893	6.0	83.4	1.578	2.452	34.7
135	956	0.893	6.3	83.4	1.657	2.575	37.3
145	955	0.894	6.2	83.6	1.630	2.529	40.0
155	957	0.894	6.3	83.8	1.655	2.564	42.6
165	956	0.894	6.3	83.7	1.656	2.567	45.3
175	955	0.894	6.3	83.6	1.656	2.570	48.0
185	957	0.894	6.2	83.8	1.629	2.523	50.6
195	956	0.895	6.2	84.0	1.628	2.518	53.3
205	956	0.895	6.2	84.0	1.628	2.518	55.9
215	956	0.895	6.2	84.0	1.628	2.518	58.5
225	957	0.895	6.2	84.1	1.628	2.515	61.1
235	957	0.895	6.1	84.1	1.628	2.475	63.7
245	956	0.896	6.1	84.3	1.601	2.470	66.3
255	955	0.896	5.7	84.4	1.496	2.304	68.7
265	955	0.897	5.7	84.5	1.496	2.301	71.1
285	957	0.897	5.6	84.6	1.469	2.258	78.2
315	956	0.897	5.4	84.8	1.416	2.174	84.8
345	958	0.899	4.7	86.3	1.229	1.862	90.5
375	955	0.905	4.2	86.5	1.098	1.660	95.7

APPENDIX AI (Continued)

Experiment No. 18

ΔW_c(calcd.) = 0.2958 gms ΔW_o(calcd.) = 0.5638 gms

ΔW_c(expt.) = 0.3126 gms ΔW_o(expt.) = 0.5694 gms

Time of reaction, min.	Temp. of CSZ cell, °C	EMF of CSZ cell, volts (uncor.)	Δh of capillary flow-meter, cms.	Pct. CO in the product gas	$-\dot{W}_c \times 10^5$ gm/sec	$-\dot{W}_o \times 10^5$ gm/sec	Pct. reduc-tion
15	790	0.763	0.8	10.6	0.238	0.600	0.84
45	829	0.755	1.1	13.9	0.325	0.806	2.00
75	852	0.742	1.5	13.8	0.443	1.100	3.58
105	869	0.732	1.5	13.6	0.443	1.102	5.26
135	914	0.732	3.0	21.1	0.877	2.092	8.53
155	943	0.735	6.4	28.2	1.850	4.237	10.8
165	954	0.745	10.5	35.4	3.002	6.587	13.9
175	962	0.742	9.6	35.8	2.742	6.002	16.9
185	969	0.738	9.1	35.6	2.601	5.702	19.7
195	977	0.737	9.5	36.9	2.709	5.888	22.5
205	986	0.742	9.3	41.6	2.632	5.558	25.2
215	992	0.759	9.0	51.8	2.504	4.947	27.6
225	999	0.800	7.2	72.8	1.931	3.274	29.3
235	1004	0.818	6.9	80.2	1.825	2.916	30.7
245	1008	0.825	7.1	82.9	1.869	2.919	32.2
255	1013	0.825	7.7	83.5	2.025	3.146	33.7
265	1017	0.830	8.0	85.2	2.096	3.208	35.3
275	1017	0.830	7.9	85.2	2.086	3.192	36.8
285	1019	2.830	8.1	85.4	2.122	3.241	38.4
295	1020	0.828	8.6	85.0	2.255	3.457	40.1
305	1022	0.830	8.9	85.7	2.330	3.550	41.8
315	1019	0.840	7.6	87.7	1.982	2.966	43.2
325	972	0.848	4.9	85.2	1.284	1.965	44.2
335	946	0.852	3.2	83.4	0.842	1.308	44.8
345	922	0.860	2.0	82.9	0.526	0.822	45.2
355	902	0.868	1.4	82.8	0.369	0.576	45.5

APPENDIX AI (Continued)

Experiment No. 19

ΔW_c(calcd.) = 0.1022 gms ΔW_o(calcd.) = 0.2265 gms.

ΔW_c(expt.) = 0.1198 gms ΔW_o(expt.) = 0.1724 gms.

Time of reaction, min.	Temp. of CSZ cell, °C	EMF of CSZ cell, volts (uncor.)	Δh of capillary flow-meter, cms.	Pct. CO in the product gas	$-W_c \times 10^5$ gm/sec	$-W_o \times 10^5$ gm/sec	Pct. reduc-tion
15	767	0.612	1.0	0.23	0.355	0.614	2.62
45	792	0.612	1.0	0.34	0.355	0.614	5.31
75	823	0.615	1.6	0.60	0.568	0.981	9.33
105	851	0.621	1.7	1.05	0.603	1.039	13.6
125	865	0.645	1.3	2.13	0.460	0.789	14.7
135	870	0.725	1.0	11.5	0.349	0.570	15.5
145	877	0.750	1.1	19.4	0.380	0.594	16.3
155	882	0.769	1.3	27.6	0.457	0.682	17.3
165	881	0.781	1.4	32.7	0.474	0.686	18.2
175	882	0.789	1.5	36.7	0.504	0.713	19.2
185	883	0.792	1.4	38.6	0.469	0.656	20.1
195	883	0.795	1.5	40.1	0.501	0.695	21.1
205	883	0.799	1.5	42.1	0.499	0.684	22.1
215	882	0.799	1.5	41.9	0.500	0.685	23.0
225	882	0.800	1.6	42.4	0.533	0.728	24.1
235	882	0.801	2.8	42.9	0.932	1.268	25.9
245	882	0.795	3.4	39.8	1.137	1.578	28.0
255	882	0.798	1.1	41.3	0.380	0.523	28.8
275	883	0.810	1.2	47.9	0.396	0.522	30.3
295	883	0.810	1.3	47.9	0.429	0.566	31.9
315	883	0.810	1.3	47.9	0.429	0.566	33.5
335	883	0.815	1.2	50.5	0.394	0.511	35.0
355	883	0.830	1.0	58.3	0.337	0.414	36.2
375	883	0.848	1.0	67.2	0.306	0.353	37.2
395	883	0.865	1.0	74.6	0.309	0.335	38.2
415	883	0.875	0.8	78.4	0.250	0.264	39.0
435	883	0.880	0.6	80.1	0.187	0.194	39.5
445	883	0.882	0.5	80.8	0.156	0.161	39.8
455	883	0.885	0.5	81.7	0.155	0.159	40.0
465	883	0.888	0.5	82.7	0.155	0.158	40.2
475	883	0.890	0.4	82.7	0.124	0.126	40.4

APPENDIX AI (Continued)

Experiment No. 20

ΔW_c(calcd.) = 0.1289 gms

ΔW_c(expt.) = 0.3469 gms

ΔW_o(calcd.) = 0.2250 gms

ΔW_o(expt.) = 0.5387 gms

Time of reaction, min.	Temp. of CSZ cell, °C	EMF of CSZ cell, volts (uncor.)	Δh of capillary flow-meter, cms.	Pct. CO in the product gas	$-\dot{W}_c \times 10^5$ gm/sec	$-\dot{W}_o \times 10^5$ gm/sec	Pct. reduc-tion
5	797	0.718	0.56	4.1	0.168	0.438	0.470
15	810	0.740	0.56	8.1	0.167	0.427	0.940
25	826	0.772	0.72	19.0	0.211	0.509	1.49
35	842	0.796	0.90	33.4	0.258	0.573	2.11
45	857	0.805	1.12	42.3	0.317	0.666	2.82
55	868	0.808	1.36	47.0	0.382	0.778	3.67
65	878	0.806	1.60	48.6	0.448	0.904	4.67
75	884	0.803	2.00	48.4	0.560	1.130	5.90
85	897	0.801	2.30	50.7	0.641	1.280	7.32
95	914	0.791	3.30	49.6	0.922	1.850	9.33
105	927	0.788	4.16	51.5	1.160	2.290	11.8
115	924	0.786	4.00	49.4	1.120	2.240	14.2
125	925	0.786	3.76	49.7	1.050	2.110	16.5
135	925	0.789	3.60	51.3	1.000	1.990	18.7
145	927	0.800	3.10	57.3	0.854	1.620	20.5
155	927	0.811	2.70	63.5	0.736	1.340	21.9
165	927	0.832	2.80	73.1	0.751	1.270	23.3
175	927	0.851	3.14	80.6	0.830	1.320	24.7
185	925	0.869	2.64	85.8	0.691	1.050	25.9
195	927	0.873	1.70	87.1	0.444	0.668	26.6
205	926	0.878	1.36	88.1	0.355	0.529	27.2
215	926	0.878	1.20	88.2	0.313	0.466	27.7
225	927	0.879	1.04	88.5	0.271	0.403	28.1
235	926	0.879	1.10	88.4	0.266	0.426	28.6
245	927	0.879	1.14	88.5	0.297	0.442	29.1
255	925	0.879	1.30	88.3	0.339	0.504	29.6
265	927	0.880	1.30	88.7	0.338	0.502	30.2
275	927	0.881	1.36	88.9	0.354	0.524	30.7
285	927	0.881	1.40	88.9	0.364	0.539	31.3
305	927	0.883	1.46	89.3	0.380	0.560	33.1
335	926	0.886	1.40	89.4	0.364	0.534	34.9

APPENDIX AI (Continued)

Experiment No. 21

ΔW_c(calcd.) = 0.3574 gms ΔW_o(calcd.) = 0.5668 gms

ΔW_c(expt.) = 0.3393 gms ΔW_o(expt.) = 0.5091 gms

Time of reaction, min.	Temp. of CSZ cell, °C	EMF of CSZ cell, volts (uncor.)	Δh of capillary flow-meter, cms.	Pct. CO in the product gas	$-\dot{W}_c \times 10^5$ gm/sec	$-\dot{W}_o \times 10^5$ gm/sec	Pct. reduc-tion
15	852	0.837	1.30	34.9	0.355	0.739	2.60
45	879	0.843	1.80	45.1	0.484	0.945	6.08
75	911	0.833	3.60	48.6	0.962	1.842	12.8
95	929	0.824	5.34	48.8	1.430	2.721	16.1
105	945	0.822	7.10	51.9	1.890	3.523	21.0
115	952	0.898	13.00	83.0	3.270	4.827	27.2
125	958	0.914	10.50	87.6	2.620	3.714	31.7
135	957	0.913	9.30	87.3	2.322	3.300	33.7
145	958	0.913	8.44	87.4	2.101	2.993	39.3
155	958	0.913	8.16	87.4	2.030	2.891	42.8
165	958	0.914	7.90	87.6	1.972	2.792	46.2
175	958	0.914	7.90	87.6	1.973	2.794	49.6
185	958	0.913	7.70	87.4	1.921	2.735	52.9
195	959	0.914	7.66	87.7	1.914	2.701	56.1
205	960	0.914	7.60	87.7	1.892	2.682	59.4
215	959	0.914	7.50	87.7	1.871	2.650	62.6
225	956	0.914	7.36	87.4	1.830	2.613	65.7
235	959	0.915	7.14	87.9	1.780	2.512	68.8
245	957	0.914	6.96	87.5	1.730	2.461	71.7
255	959	0.916	6.84	88.1	1.701	2.402	74.6
265	958	0.915	6.50	87.8	1.622	2.292	77.4
275	958	0.915	6.40	87.6	1.590	2.261	80.2
285	956	0.915	6.30	87.6	1.571	2.232	82.8
295	958	0.915	6.16	87.8	1.532	2.173	85.5
305	957	0.915	6.60	87.7	1.490	2.124	88.0
315	957	0.915	5.90	87.7	1.470	2.082	90.5
325	956	0.915	5.66	87.6	1.410	2.001	92.9
335	956	0.915	5.40	87.6	1.350	1.912	95.3
345	956	0.915	5.30	87.6	1.323	1.873	97.5

APPENDIX AI (Continued)

Experiment No. 22

ΔW_c(calcd.) = 0.2527 gms ΔW_o(calcd.) = 0.4097 gms

ΔW_c(expt.) = 0.2754 gms ΔW_o(expt.) = 0.4158 gms

Time of reaction, min.	Temp. of CSZ cell, °C	EMF of CSZ cell, volts (uncor.)	Δh of capillary flow-meter, cms.	Pct. CO in the product gas	$-\dot{W}_c \times 10^5$ gm/sec	$-\dot{W}_o \times 10^5$ gm/sec	Pct. reduc-tion
5	907	0.730	3.5	19.1	1.026	2.475	2.74
15	921	0.750	4.5	30.0	1.297	2.940	6.01
25	930	0.755	5.5	34.6	1.574	3.473	9.83
35	944	0.790	17.7	56.5	4.886	9.347	18.6
45	950	0.830	10.7	76.5	2.851	4.695	23.9
55	952	0.860	6.9	86.3	1.804	2.736	26.9
65	958	0.863	6.1	87.6	1.591	2.385	29.6
85	958	0.864	5.9	87.8	1.538	2.301	37.2
115	956	0.865	6.0	87.8	1.564	2.339	44.9
145	957	0.867	6.1	88.4	1.589	2.364	52.8
175	957	0.869	6.4	88.8	1.666	2.479	60.9
205	957	0.868	6.4	88.6	1.666	2.475	68.9
235	931	0.871	4.0	86.9	1.045	1.575	73.7

APPENDIX AI (Continued)

Experiment No. 23

ΔW_c(calcd.) = 0.3307 gms ΔW_o(calcd.) = 0.5304 gms

ΔW_c(expt.) = 0.3275 gms ΔW_o(expt.) = 0.5395 gms

Time of reaction, min.	Temp. of CSZ cell, °C	EMF of CSZ cell, volts (uncor.)	Δh of capillary flow-meter, cms.	Pct. CO in the product gas	$-\dot{W}_c \times 10^5$ gm/sec	$-\dot{W}_o \times 10^5$ gm/sec	Pct. reduc-tion
15	880	0.810	1.90	46.0	0.534	1.096	3.40
45	897	0.730	2.50	17.3	0.735	1.790	9.51
75	935	0.774	5.50	45.7	1.546	3.182	19.6
105	957	0.852	8.00	84.7	2.009	3.226	30.4
135	958	0.861	10.40	87.1	2.715	4.087	43.6
165	960	0.862	10.50	87.5	2.739	4.108	56.9
195	958	0.863	9.70	87.6	2.530	3.793	69.4
225	958	0.863	9.70	87.6	2.530	3.793	81.7
245	958	0.868	9.40	88.7	2.457	3.631	85.7
255	958	0.870	9.00	89.1	2.341	3.461	89.5
265	958	0.873	8.44	89.7	2.193	3.224	92.9
275	957	0.888	4.80	92.3	1.241	1.782	94.9
285	957	0.920	1.20	95.9	0.308	0.427	95.4

APPENDIX AI (Continued)

Experiment No. 24

ΔW_c(calcd.) = 0.3299 gms ΔW_o(calcd.) = 0.5329 gms

ΔW_c(expt.) = 0.3405 gms ΔW_o(expt.) = 0.5541 gms

Time of reaction, min.	Temp. of CSZ cell, °C	EMF of CSZ cell, volts (uncor.)	Δh of capillary flow-meter, cms.	Pct. CO in the product gas	$-\dot{W}_c \times 10^5$ gm/sec	$-\dot{W}_o \times 10^5$ gm/sec	Pct. reduc-tion
15	835	0.830	1.2	50.8	0.335	0.666	2.12
45	879	0.809	2.1	50.5	0.586	1.167	6.00
75	918	0.780	3.8	44.5	1.070	2.218	13.9
95	951	0.770	8.0	47.5	2.242	4.557	18.7
105	956	0.809	6.1	68.6	1.648	2.886	22.0
115	957	0.842	6.4	81.7	1.688	2.663	24.9
125	957	0.850	7.5	84.1	1.970	3.043	28.3
135	955	0.851	8.6	84.6	2.258	3.487	32.1
145	956	0.851	9.1	84.3	2.389	3.685	36.2
155	957	0.851	9.5	84.5	2.493	3.387	40.4
165	957	0.852	9.6	84.5	2.519	3.877	44.7
175	959	0.852	9.8	84.9	2.570	3.943	49.0
185	956	0.852	9.6	84.4	2.519	3.882	53.3
195	958	0.853	9.4	84.9	2.465	3.781	57.4
205	958	0.852	9.5	84.8	2.492	3.827	61.7
215	958	0.852	9.6	84.8	2.518	3.867	65.9
225	957	0.852	9.5	84.6	2.492	3.831	70.1
235	958	0.852	9.4	84.8	2.465	3.787	74.3
245	958	0.853	9.0	85.0	2.359	3.615	78.3
255	959	0.853	9.2	85.1	2.411	3.691	82.4
285	957	0.855	9.2	85.5	2.410	3.679	86.4
275	958	0.858	8.8	86.3	2.301	3.486	90.3
285	959	0.858	8.7	86.6	2.274	3.438	94.0
295	960	0.868	7.2	88.8	1.874	2.776	96.8
305	959	0.900	1.3	93.9	0.335	0.473	97.4
315	951	0.923	1.1	96.0	0.282	0.391	97.8

APPENDIX AI (Continued)

Experiment No. 25

ΔW_c(calcd.) = 0.3606 gms ΔW_o(calcd.) = 0.5910 gms

ΔW_c(expt.) = 0.3338 gms ΔW_o(expt.) = 0.5359 gms

Time of reaction, min.	Temp. of CSZ cell, °C	EMF of CSZ cell, volts (uncor.)	Δh of capillary flow-meter, cms.	Pct. CO in the product gas	$-\dot{W}_c \times 10^5$ gm/sec	$-\dot{W}_o \times 10^5$ gm/sec	Pct. reduc-tion
15	821	0.708	1.0	4.55	0.299	0.780	2.80
45	866	0.695	2.0	6.05	0.598	1.546	7.75
75	907	0.788	2.4	46.5	0.674	1.379	12.9
105	948	0.760	6.0	41.5	1.698	3.589	24.2
135	973	0.846	9.6	84.8	2.518	3.867	37.3
165	981	0.850	11.6	86.7	3.032	4.582	51.9
195	989	0.857	11.2	87.6	2.922	4.378	66.0
225	986	0.851	10.6	87.4	2.766	4.155	79.3
255	986	0.851	10.2	87.4	2.662	3.999	92.1
285	985	0.858	9.6	88.8	2.498	3.705	103.4
305	986.	0.895	1.65	94.5	0.412	0.579	104.3
315	975	0.920	0.6	96.4	0.154	0.213	104.5

Experiment No. 26

ΔW_c(calcd.) = 0.3364 gms ΔW_o(calcd.) = 0.5392 gms

ΔW_c(expt.) = 0.3931 gms ΔW_o(expt.) = 0.7953 gms

Time of reaction, min.	Temp. of CSZ cell, °C	EMF of CSZ cell, volts (uncor.)	Δh of capillary flow-meter, cms.	Pct. CO in the product gas	$-\dot{W}_c \times 10^5$ gm/sec	$-\dot{W}_o \times 10^5$ gm/sec	Pct. reduc-tion
15	974	0.795	6.2	65.8	1.684	3.013	6.00
45	973	0.830	5.8	79.9	1.535	2.458	10.6
75	974	0.832	5.8	80.7	1.533	2.437	15.2
105	974	0.832	5.8	80.7	1.533	2.437	19.7
135	974	0.832	5.8	80.7	1.533	2.437	24.3
165	975	0.832	6.3	80.9	1.665	2.644	29.2
195	975	0.835	7.0	81.8	1.846	2.909	34.6
225	975	0.835	7.5	81.8	1.978	3.117	40.4
255	976	0.840	8.3	83.5	2.182	3.391	46.7
285	976	0.842	9.0	84.1	2.364	3.655	53.1
315	920	0.852	2.8	79.9	0.471	1.186	55.4
335	870	0.873	0.6	80.1	0.159	0.254	55.5

APPENDIX AI (Continued)

Experiment No. 27

ΔW_c(calcd.) = 0.2683 gms ΔW_o(calcd.) = 0.5478 gms

ΔW_c(expt.) = 0.2471 gms ΔW_o(expt.) = 0.4327 gms

Time of reaction, min.	Temp. of CSZ cell, °C	EMF of CSZ cell, volts (uncor.)	Δh of capillary flow-meter, cms.	Pct. CO in the product gas	$-\dot{W}_c \times 10^5$ gm/sec	$-\dot{W}_o \times 10^5$ gm/sec	Pct. reduc-tion
15	843	0.505	1.8	0.00	0.510	1.165	2.37
45	892	0.570	3.2	0.01	0.905	2.063	6.53
75	927	0.700	3.6	13.3	1.000	2.134	11.0
105	945	0.715	4.2	20.4	1.154	2.371	16.2
125	974	0.740	13.8	36.4	3.700	6.921	20.2
135	966	0.745	7.8	36.8	2.090	3.901	22.9
145	968	0.745	8.6	37.2	2.302	4.285	25.8
155	969	0.748	7.6	38.9	2.029	3.739	28.4
165	968	0.749	6.7	39.1	1.788	3.290	30.6
175	971	0.757	6.3	43.6	1.669	2.984	32.6
185	971	0.772	5.8	51.0	1.518	2.587	34.3
195	972	0.792	5.1	60.8	1.313	2.089	35.8
205	973	0.813	4.7	70.3	1.189	1.764	37.0
215	971	0.831	4.2	76.8	1.050	1.480	38.1
225	971	0.845	3.9	81.3	0.967	1.312	38.9
235	971	0.850	3.8	82.8	0.939	1.260	39.8
245	971	0.850	3.8	82.8	0.940	1.260	40.7
255	972	0.850	3.8	82.9	0.915	1.225	41.5
265	971	0.850	3.8	82.8	0.915	1.227	42.3
275	972	0.850	3.7	82.9	0.915	1.225	43.1
285	971	0.850	3.6	82.8	0.890	1.193	43.9
295	973	0.850	3.5	83.0	0.865	1.157	44.7
305	973	0.850	3.4	83.0	0.840	1.124	45.5
315	972	0.850	3.4	83.0	0.841	1.124	46.3
325	970	0.850	3.4	82.6	0.841	1.129	47.0
335	962	0.850	3.1	81.6	0.767	1.040	47.7
345	951	0.858	2.8	82.6	0.693	0.930	48.3
355	933	0.862	1.9	81.4	0.471	0.639	48.4

APPENDIX AI (Continued)

Experiment No. 28

ΔW_c(calcd.) = 0.3177 gms ΔW_o(calcd.) = 0.5415 gms

ΔW_c(expt.) = 0.3182 gms ΔW_o(expt.) = 0.5451 gms

Time of reaction, min.	Temp. of CSZ cell, °C	EMF of CSZ cell, volts (uncor.)	Δh of capillary flow-meter, cms.	Pct. CO in the product gas	$-\dot{W}_c \times 10^5$ gm/sec	$-\dot{W}_o \times 10^5$ gm/sec	Pct. reduc-tion
15	856	0.785	2.6	28.5	0.767	1.764	2.79
45	909	0.767	2.6	33.1	0.762	1.704	5.52
75	957	0.770	4.2	46.5	1.204	2.477	9.40
105	962	0.780	5.3	52.7	1.504	2.969	14.3
135	971	0.780	6.8	54.9	1.923	3.739	20.2
155	972	0.788	7.0	58.9	1.965	3.715	22.1
165	971	0.798	7.2	63.4	2.006	3.672	24.1
175	971	0.820	6.6	72.7	1.808	3.084	25.7
185	972	0.848	5.2	82.3	1.399	2.307	26.8
195	972	0.867	6.0	87.1	1.600	2.420	28.2
205	973	0.880	6.5	89.8	1.724	2.547	29.5
215	975	0.881	6.8	90.1	1.803	2.655	30.9
225	975	0.883	7.0	90.5	1.865	2.738	32.4
240	976	0.886	7.6	91.0	2.011	2.938	33.9
250	975	0.887	8.0	90.1	2.117	3.089	35.5
260	975	0.887	7.9	91.0	2.091	3.052	37.2
270	974	0.886	7.9	90.9	2.091	3.058	38.8
280	974	0.886	7.9	90.9	2.091	3.058	40.4
290	975	0.886	8.0	90.9	2.117	3.094	42.0
300	974	0.887	8.0	91.0	2.117	3.091	43.7
310	973	0.887	7.9	90.9	2.091	3.055	45.3
320	973	0.887	8.0	90.9	2.117	3.093	46.9
330	957	0.890	3.4	90.4	0.901	1.323	47.6
340	939	0.898	0.7	90.5	0.185	0.272	47.8

APPENDIX - AII

COMPUTER PROGRAMME

```
      C       ABRAHAM- CALCULATION CO' CO2' INSTANTANEOUS RATES AND
      C       INTEGRATED WEIGHT LOSS AND PCT REDUCTION
      C       INPUT.TIME-MIN,TEMP-DEG.CEN.,V-VOLTS,DELH-CM.LIQ,
      C       SIGN OF VOLTAGE POSITIVE
      C
      C       OUTPUT. TIME-MIN,TEMP-DEG.K,CO-FRATION CO,RWC-CARBON
              LOSS RATE GMS/SEC, POL-PCT OXYGEN LOSS,TC-TOTAL CARBON
      C       GMS,    RWO-OXYGEN LOSS RATE,GMS/SEC,WCT-TOTAL CARBON
              LOSS,CALCD,GMS,WCE-TOTAL CARBON LOSS EXPTAL,GMS
1             DIMENSION TIME(150),TEMP(150),V(150),DELH(150),CO(150),
          1 CO2(150),Q(150),RWC(150),RWO(150),N(2),DELTS(2)
2             PRINT 14
3         14  FORMAT(1H1,15X,*TIME*,8X,*TEMP*,10X,*V*,8X,*DELH*)
4             DO  10  I=1,77
5             READ   12,TIME(I),TEMP(I),V(I),DELH(I)
6         12  FORMAT (4F10.0)
7             PRINT 16 ,TIME(I),TEMP(I),V(I),DELH(I)
10        16  FORMAT (10X, 4F12.4)
11        10  CONTINUE
      C
      C       CALCULATION OF GAS COMPOSITION
      C
12            DO20I=1,77
13            T = TEMP(I) +273.0
14            IF (V(I)-1.0) 24,24,26
15        24  VC=1.12974*V(I)-0.059408
16            GO TO 28
17        26  VC=.9875*V(I)
20        28  DEN=9.152*T
21            G=-85020,0+41.4*(T-1200.)
22            U=G/DEN
23            W=92240.0*VC/DEN
24            C=-0.5*ALOG(0.2045)
25            Z=U+W+C
26            RATIO=10.0**Z
27            CO2(I)=1.0/(1.0+RATIO)
30            CO(I)=1.0-CO2(I)
      C
      C       CALCULATION  OF  INSTANTANEOUS  RATES
      C
```

```
31            A1=1.80E-04*CO(I)/(CO(I)+1.36*CO2(I))
32            A2=1.52E-04*CO2(I)/(CO2(I)+0.73*CO(I))
33            VIS=A1+A2
34            A=8.552E-7
35            Q(I)=A*DELH(I)/VIS
36            QCO=Q(I)*CO(I)
37            QCO2=Q(I)*CO2(I)
40            RWC(I)=(QCO+QCO2)*12.0/22400.0
41         20 RWO(I)=(QCO+2.0*QCO2)*16.0/22400.0
42            PRINT 25
43         25 FORMAT(1H1),5X,*TIME*,8X,*CWC*,8X,*CWO*,8X,*PCL*,8X,*POL*,
              1 8X,*RWC*,8X,*RWO*,8X,*CO2*,8X,*CO*,8X,*TEMP*)
           C
           C        INTEGRATED  WEIGHT  LOSS,  SIMPSON  RULE
           C
44            WC=0
45            WO=0
46            N(1)=37
47            N(2)=40
50            DELTS(1)=300.0
51            DELTS(2)=900.0
52            I=1
53            DO 40 M = 1,2
54            K=N(M)-1
55            IF (K. LT. 2)  GO TO 40
56            WC=RWC(I)*DELTS(M)/3.0+WC
57            WO=RWO(I)*DELTS(M)/3.0+WO
60            DO 50 J = 2, K
61            I=I+1
62         40 AB = J/2
63            NA=AB
64            NB=NA*2
65            IF(NB.EQ.J)GO TO 100
66            WC=WC+2./3.*DELTS(M)*RWC(I)
67            WO=WO+2./3.*DELTS(M)*RWO(I)
70            GO TO 50
71        100 WC=WC+4./3.*DELTS(M)*RWC(I)
72            WO=WO+4./3.*DELTS(M)*RWO(I)
73            IJK = I+1
74            CWC=WC+1./3.*DELTS(M)*RWC(INK)
75            CWO=WO+1./3.*DELTS(M)*RWO(INK)
76            TC=.66459
77            TO=1.17594
100           PCL=CWC*100./TC
101           POL=CWO*100./TO
```

```
102          PRINT 30,TIME(I),CWC,CWO,PCL,POL,RWC(I),RWO(I),CO2(I),
             CO(I),TEMP(I)
103      30  FORMAT(/2X,10E11.4)
104       50 CONTINUE
105          I=N(M)
106          WC=WC+1./3.*DELTS(M)*RWC(I)
107          WO=WO+1./3.*DELTS(M)*RWO(I)
110       40 CONTINUE
111          WCT=WC
112          WOT=WO
113          WOE=1.17219
114          WCE=.63459
115          PRINT42,WCT,WCE,WOT,WOE
116       42 FORMAT(1H1,4X,*WCT=*,E12.4,*WCE=*,E12.4,*WOT=*,E12.4,
             *WOE=*,E12.4)
117          PRINT 44
120       44 FORMAT(5X,*TIME*,8X,*COF*,8X,*CO2F*,8X,*RWC*,8X,*RWO*,
            1 8X,*CO*,8X,*CO2*)
121          X=WCE/WCT
122          Y=WOE/WOT
123          DO70I=1,77
124          Q(I)=Q(I)*X
125          RWC(I)=Q(I)*12./22400.
126          RWO(I)=RWO(I)*Y
127          QCO2=RWO(I)*22400./16.-Q(I)
130          QCO=Q(I)-QCO2
131          COF=QCO/Q(I)
132          CO2F=QCO2/Q(I)
133          PRINT 75,TIME(I),COF,CO2F,RWC(I),RWO(I),CO(I),CO2(I)
134       75 FORMAT(/2X,7E11.4)
135       70 CONTINUE
136          STOP
137          END
         $ENTRY
```

APPENDIX - AIII

EXPERIMENTAL RESULTS ON POWDER MIXTURES OF FERRIC OXIDE AND GRAPHITE

Experiment No. M-2

Solid Oxide Electrolyte Cell Temperature = 770°C

Initial Temperature of the Reaction Zone = 1005°C

Time of reaction, min.	Temp. of reaction zone, °C	EMF of CSZ cell, volts (uncor.)	Δh of capillary flow-meter, cms.	Pct. CO in the product gas	$-\dot{W}_c \times 10^4$ gms/sec	$-\dot{W}_o \times 10^4$ gms/sec	Pct. reduc-tion
2	990	0.720	2.4	3.01	0.661	1.740	7.42
6	991	0.755	3.6	6.85	0.986	2.540	19.0
10	993	0.835	13.6	35.4	3.570	7.830	53.0
14		0.888	20.4	67.5	5.070	8.950	94.5
18	994	0.903	11.0	75.2	2.700	4.490	115.1
22		0.915	1.0	80.4	0.243	0.387	117.5
26	994	0.915	0.5	80.4	0.121	0.194	118.4
29		0.915	0.5	80.4	0.121	0.194	118.9
31		0.915	0.5	80.4	0.121	0.194	119.3

Experiment No. M-4

Solid Oxide Electrolyte Cell Temperature = 768°C

Initial Temperature of the Reaction Zone = 953°C

Time of reaction, min.	Temp. of reaction zone, °C	EMF of CSZ cell, volts (uncor.)	Δh of capillary flow-meter, cms.	Pct. CO in the product gas	$-\dot{W}_c \times 10^4$ gms/sec	$-\dot{W}_o \times 10^4$ gms/sec	Pct. reduc-tion
2	933	0.767	0.40	9.7	0.104	0.265	1.2
5		0.789	1.8	15.8	0.466	1.144	3.2
7		0.795	2.0	17.9	0.516	1.253	5.4
9		0.805	2.0	21.8	0.513	1.218	7.6
11		0.810	2.0	24.0	0.511	1.199	9.7
13		0.814	1.6	25.9	0.408	0.946	11.4
15	936	0.815	1.4	26.4	0.356	0.825	12.8
17		0.817	1.2	27.4	0.305	0.702	14.0
19		0.820	1.2	28.9	0.304	0.694	15.3
20		0.821	1.2	29.4	0.304	0.692	16.5
22		0.825	1.2	31.5	0.303	0.681	17.7
24	939	0.840	2.2	40.1	0.548	1.169	19.8
26		0.900	7.6	75.0	1.783	2.972	24.9
28	942	0.915	12.2	81.4	2.828	4.474	32.7
30	943	0.916	13.4	81.7	3.104	4.895	41.3
32		0.920	12.8	83.2	2.957	4.606	49.5
34	943	0.921	12.2	83.5	2.817	4.374	57.2
36		0.922	12.8	83.9	2.953	4.573	65.3
38		0.923	12.6	84.2	2.905	4.486	73.2
40	945	0.928	10.2	85.8	2.345	3.570	79.6
42		0.932	7.2	86.9	1.651	2.489	84.0
44		0.940	5.4	89.1	1.233	1.824	87.2
46		0.953	3.4	91.9	0.772	1.114	89.2
48		0.965	2.4	93.8	0.543	0.769	90.5
50		0.970	1.4	94.5	0.316	0.445	91.3
52		0.970	1.2	94.5	0.271	0.381	92.0
54	944	0.970	0.8	94.5	0.181	0.254	92.4
56		0.970	0.8	94.5	0.181	0.254	92.9
58		0.970	0.6	94.5	0.136	0.191	93.2
60		0.970	0.5	94.5	0.113	0.159	93.5

Experiment No. M-5

Solid Oxide Electrolyte Cell Temperature = 770°C

Initial Temperature of the Reaction Zone = 1054°C

Time of reaction, min.	Temp. of reaction zone, °C	EMF of CSZ cell, volts (uncor.)	Δh of capillary flow-meter, cms.	Pct. CO in the product gas	$-\dot{W}_c \times 10^4$ gms/sec	$-\dot{W}_o \times 10^4$ gms/sec	Pct. reduc-tion
1	1037	0.750	6.8	6.01	1.780	4.610	14.7
3		0.830	34.8	32.6	8.770	19.600	67.0
5		0.875	32.8	60.0	7.900	14.800	112.7
7		0.900	20.8	73.8	4.890	8.230	136.2
9		0.920	1.8	82.3	0.417	0.654	138.5
11	1043	0.920	0.60	82.3	0.139	0.218	139.2
14	1045	0.920	0.50	82.7	0.116	0.161	140.3

Experiment No. M-7

Solid Oxide Electrolyte Cell Temperature = 793°C

Initial Temperature of the Reaction Zone = 969°C

Time of reaction, min.	Temp. of reaction zone, °C	EMF of CSZ cell, volts (uncor.)	Δh of capillary flow-meter, cms.	Pct. CO in the product gas	$-\dot{W}_c \times 10^4$ gms/sec	$-\dot{W}_o \times 10^4$ gms/sec	Pct. reduc-tion
1		0.050	2.0	0.00	0.397	1.059	4.1
3	956	0.590	2.8	0.17	0.741	1.974	11.3
5		0.608	2.6	0.27	0.688	1.832	18.3
7		0.670	2.2	1.23	0.581	1.541	24.3
9		0.700	1.9	2.55	0.501	1.319	29.4
11	966	0.870	1.6	63.1	0.383	0.700	32.3
13		0.870	3.0	63.1	0.719	1.312	39.0
15		0.910	14.2	82.1	3.287	5.169	58.3
17		0.920	11.4	85.4	2.622	4.007	74.2
19		0.920	9.6	85.4	2.208	3.374	87.2
21		0.920	8.0	85.4	1.840	2.812	98.0
23	966	0.930	5.4	85.2	1.236	1.841	105.0
25		0.930	1.8	88.2	0.412	0.614	107.0
28	968	0.930	0.6	88.2	0.137	0.205	109.0

Experiment No. M-8

Solid Oxide Electrolyte Cell Temperature = 791°C

Initial Temperature of the Reaction Zone = 954°C

Time of reaction, min.	Temp. of reaction zone, °C	EMF of CSZ cell, volts (uncor.)	Δh of capillary flow-meter, cms.	Pct. CO in the product gas	$-\dot{W}_c \times 10^4$ gms/sec	$-\dot{W}_o \times 10^4$ gms/sec	Pct. reduc-tion
1		0.590	1.0	00.16	0.264	0.705	3.19
3		0.660	1.4	0.93	0.370	0.982	7.64
5	940	0.650	1.8	0.73	0.475	1.266	13.2
7		0.650	1.7	0773	0.449	1.194	18.7
9		0.662	1.6	0.98	0.422	1.122	23.8
11		0.685	1.4	1.72	0.369	0.977	28.2
13		0.690	1.2	1.94	0.316	0.836	31.9
15	945	0.697	1.0	2.30	0.263	0.695	35.0
17		0.700	0.8	2.47	0.211	0.555	37.6
19	946	0.707	0.9	2.92	0.237	0.623	40.4
21		0.721	1.7	4.68	0.447	1.169	46.7
23	946	0.800	7.4	22.9	1.894	4.470	65.8
25		0.870	9.0	62.6	2.159	3.955	83.8
27	947	0.890	8.0	73.2	1.883	3.181	98.4
29		0.900	7.0	77.8	1.634	2.661	110.0
31		0.909	6.4	81.4	1.484	2.346	121.0
33	949	0.915	5.6	83.5	1.293	2.007	130.0
35		0.920	2.2	85.1	0.506	0.775	138.0

Experiment No. M-9

Solid Oxide Electrolyte Cell Temperature = 784°C

Initial Temperature of the Reaction Zone = 1009°C

Time of reaction, min.	Temp. of reaction zone, °C	EMF of CSZ cell, volts (uncor.)	Δh of capillary flow-meter, cms	Pct. CO in the product gas	$-\dot{W}_c \times 10^4$ gms/sec	$-\dot{W}_o \times 10^4$ gms/sec	Pct. reduc-tion
1		0.570	7.0	0.09	1.853	4.930	12.9
3	992	0.565	6.6	0.09	1.747	4.656	26.3
5	996	0.740	8.0	5.81	2.100	5.438	43.4
7		0.855	27.0	51.7	6.600	13.050	75.4
9	1001	0.890	20.0	71.8	4.719	8.067	96.6
11		0.905	17.8	78.7	4.147	6.708	113.5
13	1003	0.920	7.0	84.3	1.614	2.490	121.0
15		0.927	3.2	86.4	0.735	1.112	123.0
18	1005	0.928	0.8	86.7	0.183	0.277	125.0

APPENDIX – AIV

EXPERIMENTAL RESULTS ON MIXTURE OF FERRIC OXIDE MICRO-PELLETS AND GRAPHITE POWDER

Experiment No. M-3

Solid Oxide Electrolyte Cell Temperature = 778°C

Initial Temperature of the Reaction Zone = 954°C

Time of reaction, min.	Temp. of reaction zone, °C	EMF of CSZ cell, volts (uncor.)	Δh of capillary flow-meter, cms.	Pct. CO in the product gas	$-\dot{W}_c \times 10^4$ gms/sec	$-\dot{W}_o \times 10^4$ gms/sec	Pct. reduc-tion
2	954	0.660	0.80	1.31	0.211	0.560	3.73
6		0.690	0.70	1.60	0.154	0.206	6.36
9		0.690	1.4	1.60	0.370	0.978	9.61
11		0.710	1.4	2.61	0.370	0.972	12.8
13	940	0.728	1.2	4.03	0.316	0.825	15.5
15		0.735	1.0	4.76	0.263	0.684	17.8
17		0.740	0.9	5.36	0.236	0.614	19.9
19		0.742	0.8	5.62	0.210	0.544	21.7
21		0.749	0.7	6.62	0.184	0.473	23.3
23		0.750	0.6	6.77	0.157	0.405	24.6
25		0.752	0.4	7.09	0.105	0.270	25.5
27		0.757	0.4	7.96	0.105	0.268	26.5
29		0.770	0.8	10.7	0.209	0.526	28.3
31		0.795	1.2	18.2	0.309	0.750	30.8
33		0.820	1.2	29.4	0.304	0.692	33.1
35		0.835	1.2	37.7	0.300	0.650	35.2
37		0.852	1.1	48.1	0.271	0.548	37.1
39	945	0.869	1.1	58.6	0.266	0.501	38.8
41		0.878	1.0	63.9	0.239	0.434	40.2
43		0.885	1.0	67.8	0.238	0.419	41.6
45		0.891	0.9	71.0	0.213	0.366	42.9
47		0.895	0.9	73.0	0.212	0.359	44.1
49		0.901	0.9	75.9	0.211	0.349	45.2
51		0.906	0.8	78.1	0.187	0.303	46.2
53		0.909	0.8	79.3	0.186	0.300	47.2
55		0.910	0.8	79.7	0.186	0.298	48.2
57	950	0.910	0.8	79.7	0.186	0.298	49.2
59		0.913	0.8	80.9	0.186	0.295	50.2
61		0.915	0.8	81.7	0.185	0.293	51.2
63		0.917	0.8	82.4	0.185	0.290	52.1
65		0.917	0.8	82.4	0.185	0.290	53.1
67		0.918	0.8	82.8	0.185	0.289	54.1
69		0.920	0.8	83.5	0.185	0.287	55.0
71		0.920	0.8	83.5	0.185	0.287	56.0
73		0.920	0.8	83.5	0.185	0.287	56.9
75		0.920	0.8	83.5	0.185	0.287	57.9

Experiment No. M-6

Solid Oxide Electrolyte Cell Temperature = 793°C

Initial Temperature of the Reaction Zone = 967°C

Time of reaction, min.	Temp. of reaction zone, °C	EMF of CSZ cell, volts (uncor.)	Δh of capillary flow-meter, cms.	Pct. CO in the product gas	$-\dot{W}_c \times 10^4$ gms/sec	$-\dot{W}_o \times 10^4$ gms/sec	Pct. reduction
1		0.772	1.4	13.3	0.363	0.904	3.30
3		0.770	1.4	12.7	0.363	0.908	6.61
5	953	0.775	2.2	14.2	0.570	1.410	11.5
7		0.775	2.0	14.2	0.518	1.280	16.3
9		0.772	1.4	13.3	0.363	0.904	19.6
11	962	0.773	1.0	13.6	0.259	0.645	22.1
13		0.778	1.0	15.1	0.259	0.638	24.4
15	964	0.780	0.9	15.7	0.232	0.572	26.4
17		0.780	0.7	15.7	0.181	0.444	28.0
19		0.780	0.6	15.7	0.155	0.381	29.4
21	965	0.782	0.5	16.4	0.129	0.316	30.6
23	965	0.782	0.5	16.4	0.129	0.316	31.8
25		0.783	0.5	16.7	0.129	0.315	32.8
27		0.808	1.6	27.1	0.406	0.937	35.7
29	966	0.818	1.4	32.2	0.353	0.789	38.6
31		0.832	1.4	40.2	0.348	0.743	41.3
33		0.850	1.2	51.1	0.293	0.582	43.5
35	965	0.865	1.2	60.2	0.289	0.538	45.4
37		0.878	1.2	67.5	0.285	0.503	47.3
39		0.885	1.2	71.2	0.283	0.486	49.0
41		0.890	1.1	73.6	0.258	0.435	50.6
43		0.895	1.1	76.0	0.257	0.425	52.2
45		0.900	1.1	78.1	0.256	0.416	53.7
47		0.905	1.1	80.1	0.255	0.408	55.2
49	965	0.910	1.1	82.0	0.254	0.400	56.6
51		0.913	1.1	83.1	0.207	0.324	57.9
53		0.913	1.1	83.1	0.207	0.324	59.1
55		0.915	0.8	83.8	0.184	0.286	60.2
58		0.920	0.8	85.4	0.184	0.281	61.9
60		0.920	0.8	85.4	0.184	0.281	63.6
64		0.921	0.8	85.7	0.183	0.280	65.7
68	966	0.923	0.8	86.5	0.183	0.277	67.7

APPENDIX AV

MASS TRANSFER ANALYSIS INSIDE THE OXIDE PELLET

This analysis is based on similar analysis available in the literature[63].

The reaction for which the analysis is made is:

$$Fe_xO + CO = xFe + CO_2$$

This is a first order reaction for which

$$r = k_1(C_e - C)$$

The geometry corresponds to flat disc exposed to reactant only from one side.

$$\therefore \quad \phi_L = L\left(\frac{k_1(K_e + 1)}{K_e} \cdot \frac{\rho_s}{D_e}\right)^{1/2}$$

where

$L = \frac{V}{A}$ = pellet thickness, cm

ρ_s = density of solid, g/cc

D_e = effective diffusivity of gases through macropores, cm^2/sec

K_e = equilibrium constant

k_1 = forward reaction rate constant, gm mole/sec

The following data from experiment 17 have been used in the calculation.

ρ_s = 3.0 g/cc; T = 1229°K

W_p = weight of pellet = 1.9172 gms

L = 0.29 cm; $-\dot{w}_o$ = 2.518×10^{-5} gm/sec.

$$D_{CO_2} = 0.0018583 \frac{T^{3/2}\left(\frac{1}{M_{CO_2}} + \frac{1}{M_{CO}}\right)^{1/2}}{P_T \, \sigma^2_{CO,CO_2} \, \Omega_{D_{CO,CO_2}}}$$

= 1.752 cm^2/sec.

$(D_K)_{CO_2}$ = Knudsen diffusivity

$$= 9.70 \times 10^3 \cdot a\left(\frac{T}{M_{CO_2}}\right)^{1/2}$$

= 5.13 cm^2/sec

M_{CO_2} = molecular wt. of CO_2, a = pore radius in cm

= 10^{-4} cm

$$\frac{1}{D_c} = \frac{1}{D_M} + \frac{1}{(D_K)_{CO_2}}$$

= 2.473 + 0.1949

= 2.6679

or, D_c = 0.4044 cm^2/sec.

k_1 was calculated from the data of Bickenese and Clarke as follows:

$$\frac{[1 - (1-f)^{1/3}]}{t} = [4.3 \exp^{(-\frac{13,800}{RT})}] \frac{1}{C_e} \frac{(C_e - C)}{60}$$

Assuming $[1 - (1-f)^{1/3}]$ to vary linearly with time,

$$\frac{[1 - (1-f)^{1/3}]}{t} = \frac{d}{dt}[1 - (1-f)^{1/3}]$$

$$= \frac{1}{3}(1-f)^{-2/3}(-\frac{df}{dt})$$

$$= \frac{1}{3}(1-f)^{-2/3} \times \frac{1}{W_o^o} \frac{dW_o}{dt}$$

where W_o = weight of oxygen left

W_o^o = initial weight of oxygen

$$f = \frac{W_o^o - W_o}{W_o^o} = 1 - \frac{W_o}{W_o^o}$$

$$k_1 = \frac{r}{C_e - C}$$

where C denotes concentration of CO_2 in g moles/cc

$$\therefore \quad k_1 = (-\frac{dW_o}{dt}) \cdot \frac{1}{16W_p} \cdot \frac{1}{C_e - C}$$

$$= -(\frac{dW_o}{dt}) \frac{1}{16W_o^o} \cdot \frac{3}{10} \cdot \frac{1}{C_e - C}$$

$$= \frac{1}{16(C_e - C)} \cdot \frac{3}{10} \frac{[1 - (1-f)^{1/3}]}{60t} \cdot 3 \cdot (1-f)^{2/3}$$

$$= \frac{3 \times 3}{10 \times 16C_e} \frac{[4.3 \exp^{(-\frac{13,800}{RT})}]}{60} \cdot (1-f)^{2/3}$$

$$4.3 \exp^{\left(-\frac{13,800}{RT}\right)} = 1.464 \times 10^{-2}$$

$$C_e = \frac{p^e_{CO_2}}{RT} = \frac{0.295}{82 \times 1229}$$

$$= 2.928 \times 10^{-6} \text{ gm.moles/cc}$$

assuming,

$$f = 0.5; \qquad (1-f)^{2/3} = 0.63$$

or,

$$k_1 = \frac{3 \times 3}{10 \times 16 \times 2.928 \times 10^{-6}} \times 1.464 \times 10^{-2} \times \frac{0.63}{60}$$

$$= 2.953 \text{ gm. moles/sec. (gm of oxide) per unit } (C_e - C)$$

or,

$$\phi_L = 0.29 \left[\frac{2.953}{0.4184} \times \frac{3.0}{0.4044}\right]^{1/2}$$

$$= 2.54$$

$$\tanh \phi_L \simeq 0.995$$

$$\eta = \frac{\tanh \phi_L}{\phi_L} \simeq \frac{0.995}{\phi_L} = 0.3920$$

where η is the effective rate per unit mass of oxide

r_p = effective rate per unit mass of oxide

$= \eta \cdot r_s$

where r_s = rate at the surface.

$$r_p = -\left(\frac{dW_o}{dt}\right)\frac{1}{16}\cdot\frac{1}{W_p}$$

$$= -\dot{W}_o \times \frac{1}{16} \times \frac{1}{W_p}$$

$$= 2.518 \times 10^{-5} \times \frac{1}{16} \times \frac{1}{1.9172}$$

$$= 0.082 \times 10^{-5} \text{ gm mole O/sec. gm oxide}$$

$$\therefore \quad r_s = \frac{r_p}{\eta} = 0.21 \times 10^{-5} \text{ gm moles per sec (gm. of oxide)}$$

Again, $r_s = K_1(C_e - C_s) = k_1\left(\frac{p^e_{CO_2} - p^o_{CO_2}}{RT}\right)$

Hence, $p^e_{CO_2} - p^o_{CO_2} = r_s \times \frac{RT}{k_1}$

$$= \frac{0.210 \times 10^{-5} \times 82 \times 1229}{2.953}$$

$$= 0.069 \text{ atm.}$$

Thus the difference in p_{CO_2} between the top and bottom surfaces of the pellet is about 7 pct.

BIOGRAPHICAL NOTE

The author was born in Muvattupuzha, Kerala State on the 19th of April 1939. After completing the high school and Intermediate Science examinations from the Kerala University, he joined the Metallurgical Engineering department of Banaras Hindu University in the year 1959. He obtained the Bachelor of Science degree in Metallurgical Engineering from B.H.U. in 1963. On completion of the Master of Science in Metallurgical Engineering also at the same university, he joined the Regional Engineering College, Durgapur as a lecturer in the year 1966. While he was at the R.E. College he worked on the agglomeration and reduction of iron ores. In January 1972 he was sponsored by the college for doing Ph.D. at I.I.T., Kanpur under the Quality Improvement Programme. He went back to the college in January 1975 where he teaches subjects in process metallurgy, in which he has specialized.